DOCTORAL DISSERTATION

Development of Balloon-Expandable Stents for Treatment of Eccentric Plaque Considering Surface Roughening

By:

Achmad Syaifudin

Under supervisor:

Katsuhiko Sasaki

Laboratory of Micro Energy Systems

Division of Human Mechanical System and Design

Graduate School of Engineering

Hokkaido University

Development of Balloon-Expandable Stents for Treatment of Eccentric Plaque Considering Surface Roughening

A thesis submitted in partial fulfillment of the requirements for the degree of Doctoral of Engineering

By:

Achmad Syaifudin

Division of Human Mechanical System and Design

Graduate School of Engineering, Hokkaido University

August 2016

Acknowledgements

First and above all, I praise God, the almighty for providing me this opportunity and granting me the capability to proceed successfully. This thesis appears in its current form due to the assistance and guidance of several people. I would therefore like to offer my sincere thanks to all of them.

Prof. Katsuhiko Sasaki, my esteemed supervisor, my cordial thanks for accepting me start from Master student and then as Doctoral student, your warm encouragement, thoughtful guidance, critical comments, and correction of the paper and thesis. Dr. Ryo Takeda sensei, I greatly appreciate your excellent assistance during thesis and manuscript completion. In my daily work, I have been blessed with friendly and cheerful of fellow students, Kohei Fukuchi san – Atsuko Takita san – Yusuke Tomizawa san, who always ready to help me in translating many letters and communicating with Japanese. To all of Micro Energy System members, thank for good commentary and question in the lab presentation, and for warm respect and attention. DIKTI (Directorate General for Higher Education of Indonesian), that provided scholarship so enable me pursuing study in Hokkaido University and finally earning a Master's and Doctoral degree.

Last but not the least, I warmly thank and appreciate my beloved and lovely sweet wife, dear Sayidah Aulia'ul Haque, for your material and spiritual support in all aspects of my life, in numerous ways. Without your supports and encouragements, I could not have finished this work. It was you who kept the fundamental of our family, I understand it was very difficult for you. Therefore, I am very satisfied upon you so can just say thanks for everything. May Allah give you all the best in the world and hereafter, and bless you as queen in our paradise. My cute princess, dear Sayidah Jihan Elkarima, for your joke and laughter that eliminates my tired and dizzy head in the late night. May Allah give you brighten and bless your future. And my handsome little prince, dear Muhammad Ali Rahman, for your cheer and cry that makes me want to always hug you. May Allah always keep and bless you in your life, and make you as one of the ranks of His lovers. Aamiin..

Achmad Syaifudin

Sapporo, June 23th, 2016

Abstract

Stent, a tiny mesh tube that well known to treat narrow or blocked artery due to plaque obstruction, remains relevant to investigate after decades of development. In the case of balloon expandable stent (BES), its development remains necessity due to having superior material properties and affordable price. Nowadays, the development of BES should adapt latest issues. The physical properties of the stent surface affect the effectiveness of vascular disease treatment. During the expanding process, the stent acquires high-level deformation that alters the surface roughness level. To improve the surface roughness changes in the treatment of eccentric plaque, applying the symmetric expansion will generate the non-uniform stress distribution, which may aggravate the fibrous cap prone to rupture. Therefore, the development of a new stent design that adapts plaque shape is necessity. Mechanical characteristic assessment of new stent design should be conducted afterwards to improve stent performance during stenting process. FEM assessment is a good choice to save the cost and time of manufacturing. As a series of new stent development, rupture analysis after stent deployment is essential to investigate plaque vulnerability and arterial tissue rupture.

All structural analysis was performed using ANSYS R15.0. To observe the effects of the plaque length on the changes in the surface roughness, two types of bare metal stents such as Palmaz and Sinusoidal stent are studied. Three different lengths of plaque, i.e. the plaque length longer than the stent, shorter than the stent, and the same length as the stent are chosen in the simulation. The material models was defined as a multilinear isotropic for the stent and the hyperelastic for the balloon, plaque, and vessel wall. The correlation between the plastic deformation and the changes in surface roughness was obtained by the intermittent pure tensile test using a specimen made of type 316NG. To develop a new stent design, a non-symmetric structural geometry of stent is derived from Sinusoidal stent type by modifying struts length, struts width, bridges, and curvature width of struts. An end ring of stent struts was also modified to eliminate the dogboning phenomenon and to reduce the ectropion angle. Two balloon types used to deploy stent, i.e. the ordinary cylindrical and the offset balloon. Positive modification results were used to construct a final non-symmetric stent design, called an Asymmetric stent. Analyses of the deformation characteristics, the surface roughness changes, and stresses within the intact arterial layer were subsequently examined. To assess the flexibility of Asymmetric stent, FEM assessments are conducted, i.e. flexibility tests on unexpanded and expanded condition. To investigate plaque vulnerability and arterial tissue rupture, Asymmetric stent is expanded inside an idealized human carotid artery, which has the eccentric plaque obstruction. The large lipid pool and the thin fibrous cap are accommodated in the model to behave the prone to rupture. The arterial tissue with the multilayer material parameters, including intima, media, and adventitia is also focused in the study.

The study found that the plaque size relative to the stent length affected the changes in the surface roughness. It was also found that the stent should have the similar length with the plaque because of the moderate change in the surface roughness. As for the surface roughness changes in treatment of the eccentric plaque, Asymmetric stent has a comparable effect with Sinusoidal stent though Asymmetric stent drives the distribution of the surface roughening as expanded by the offset balloon. From the flexibility assessment, it is found that the flexibility of both stents is comparable in both the unexpanded or expanded condition. However, the inflated-side of Asymmetric stent is more flexible than its fixed-side. Finally, the analyses demonstrated that the expansion combination between Asymmetric stent – offset balloons might increase the plaque vulnerability.

Key words: *surface roughness, Asymmetric stent, flexibility, plaque vulnerability, FEM.*

Contents

List of Figures

List of Tables

1 STENT DEVELOPMENT

1.1 INTRODUCTION

Since Puel and Ulrich Sigwart have implanted a stent into a patient in Toulouse, France in 1986 [1], the development of stent becomes serious concern by experts and practitioners. In 1987, Julio Palmaz and Richard Schatz patented their similar stent that is well known as a balloon-expandable stent. The use of these bare-metal stents helped to reduce the incident of restenosis from 30–40% in coronary surgery to 20–30% [2]. Up to now, more than 100 different stent have been designed and they are currently marketed, and in evaluation mainly in Europe. As a result of the strict FDA regulations, the number of approved stents in the USA is not quite as high, but is still substantial [3].

The development of stent is still growing. This chapter begins with a brief review of balloon-expandable stent based on its material type, mechanism of expansion, and mesh structure as a general preliminary so that the author determines the objectives of research.

1.1.1 Development on stent material

First implanted stent was balloon-expandable stent, one of metallic stent that was made from stainless steel, typically SUS316. It is a particularly corrosion-resistant material with low carbon content and additions of molybdenum and niobium, as the chemical composition [5] is shown in Table 1-1. This type of stainless steel is deformable in its fully annealed condition, having the good wear resistance, excellent machinability and the corrosion resistance. Therefore, SUS316L stainless steel becomes the standard material for balloon-expandable stents [4][6]. SUS316L stainless steel also has enough plasticity in its full-hard condition. The priority of SUS316L platforms for making stents are approved by the US Food and Drug Administration (FDA), for seven popular stent types (Biodic Ysio™, BeStent ™, CYPHER™, NIRflex ™, TAXUS™, Liberte™, and Rithron-XR) which are made from SUS316L [4].

Table 1-1: The chemical composition of SUS316L

Steel type	Chemical composition (wt. %)								
	Cr	Ni	Mn	Mo	Si	C	S	P	Fe
SUS316L	18.0	12.0	2.0	2.5	≤1.00	≤0.03	≤0.03	0.045	Bal

However, SUS316L has some weaknesses, such as the non-MRI compatible, biocompatibility, poorly visible fluoroscopic material, and the allergic reactions that found due to the release of nickel. Therefore, the researchers also focused on alternative materials as a complement of SUS316L. The

alternative materials for balloon-expandable stent are tantalum, platinum alloys, niobium alloys, and cobalt alloys.

Tantalum (*Ta*) has excellent corrosion resistance because of its highly stable surface oxide layer, which prevents the electron exchange between the metal and the adsorbed biological species. Its superiority is having excellent fluoroscopic visibility, an MRI compatible material, and known for its good biocompatibility. Due to its poor mechanical properties, the commercial availability of Ta stents is lower than SUS316L stents. Platinum alloys (*Pt–Ir* alloys consist of 90% platinum and 10% iridium), which has almost similar characteristics with tantalum, was used for the bare stents due to the excellent radiopacity and an MRI compatible material. However, because of the higher recoiling percentage, biocompatibility, and haemocompatibility, the number of *Pt–Ir* alloys stent remains limited.

Another candidate for the stent material alternative is niobium alloys. Several patents were issued regarding with this alloys. One of them is forming niobium alloys by adding zirconium (less than 5%) and tantalum (less than 20%). The alloy surprisingly allows developing new characteristic stents, which have the biocompatibility, contain no known allergens, and have the good mechanical properties. They are also visible in radiographs (MRI compatible), and identified in nuclear spin tomography [7][8]. In order to reduce the MR image artifact, tungsten (3.5%) may be added into niobium alloys [9].

There are material types that have good radial strength and return to pre-deformed shape after heated. These characteristics are essential in producing self-expanding stent. Cobalt alloys (*Co–Cr*), which conform to ASTM standards F562 and F90, have been used for self-expanding stents. These alloys have excellent radial strength because of their high elastic modulus. Therefore, it becomes an appropriate material for self-expanding stent. In addition, they are radiopaque and MRI-compatible. The main attractiveness of these alloys is the ability to make ultra-thin struts with increased strength. The thickness of the struts is a critical issue in designing a stent. However, its machinability and the plasticity properties have the limitation of the stent applications [6].

There are new alternative materials intensively developed by researchers, which are promise as the new candidate of stent materials, i.e. biodegradable material. Biodegradable materials are usually classified into two classes: biodegradable metallic material and biodegradable polymer. The biodegradable metallic materials are metallic alloys expected to corrode gradually in vivo, with an appropriate host response elicited by released corrosion product. In the present, three classes of the biodegradable metallic materials have been systematically observed, including Fe-based, Mg-based, and Zn-based materials [10].

In Fe-based biodegradable stent, the ferrous ions reduce the proliferation of smooth muscle cells in in-vitro conditions, and thus may inhibit neointimal hyperplasia. Moreover, thrombogenicity and

neointimal proliferation were reduced and no local toxicity was observed. Since the yield strength and the tensile strength of the pure Fe are theoretically almost same, these stents may fracture during the deployment. Meanwhile, Mg alloy stents may fracture because of their low ductility. These mean that the stent thickness is an important factor for these stent. These stents are radiolucent and cannot be imaged by X-rays, even intravascular ultrasound and the MRI techniques have used to visualize these stents. The mechanical properties of Mg are also poor for a coronary stent and its degradation behavior is not controllable [4]. Therefore, the usage of Fe-based and Mg-based stent is still limited. In the meantime, the metallic zinc appears to be acceptable metal for bioabsorbable stent. Zinc is widely acknowledged as an important element for the basic biological function, as it participates in the nucleic acid metabolism, the signal transduction, the apoptosis regulation, and the gene expression. It is reported for the first time that the metallic zinc shows great potential as a base material for the next generation of biodegradable stents, while it requires further development to achieve the desired mechanical properties, the corrosion resistance, and the better biocompatibility [10][11].

One concern in using biodegradable stents is the unevenness of the material remaining after the degradation process. Various cells in the body bind to the uneven surfaces and induce the complications. By using the biodegradable polymer, the biocompatible polymers are applied to the surface of the organ and the vessel. These polymers are simultaneously contoured in situ to yield a smooth layer of the polymer in contact with the tissue surface, effectively eradicating irregularities in the tissue surface. Some biodegradable polymers may be able to modulate the local delivery of the drugs and degrade safely. However, the biodegradable drug delivery systems require the steady degradation, permeability, and the moderate tensile strength [12].

From the aforementioned description (the advantages and disadvantages are summarized in Table 1-2), it seems clearly that SUS316L is still superior and the main material for balloon-expandable stent as well as Nitinol for self-expanding stent. Because of an affordable price, the author remains developing the stent made from this material type in order to improve its performance in stenting process.

Table 1-2: Material characteristics for making stent

Material	Advantages	Disadvantages
Stainless steel SUS316L	Good mechanical properties and wear resistance; excellent plasticity, machinability and corrosion resistance; provided abundant	Poor biocompatibility, non-MRI compatible, poor fluoroscopic visibility, cause allergic reactions
Tantalum (*Ta*)	Excellent corrosion resistance, MRI compatible, good fluoroscopic visibility, good biocompatibility	Poor mechanical properties

Platinum alloys (*Pt-Ir*)	Excellent corrosion resistance, MRI compatible, good fluoroscopic visibility	Poor biocompatibility and haemocompatibility, poor mechanical properties
Niobium alloys (*Nb–Ta–Zr*)	Good biocompatibility, contain no known allergens, good mechanical properties, MRI compatible	Limited in number, cost expensive.
Cobalt alloys (*Co-Cr*)	Excellent radial strength, radiopaque and MRI-compatible	Poor plasticity and machinability
Fe-based biodegradable metal	Superior radial strength	Yield strength and tensile strength are close, cause easily fracture during deployment
Mg-based biodegradable metal	Good biocompatibility	Poor mechanical and corrosion properties, degradation behavior uncontrollable
Zn-based biodegradable metal	Acting as transition metal element in human body	Poor mechanical and corrosion properties, fair biocompatibility
Biodegradable polymer	Excellent biocompatibility	Unsteady degradation, poor permeability and mechanical properties

1.1.2 Development on expanding mechanism of stent

Stent needs to be expanded inside stenosed artery to remain in the location after reaching the desired plastic deformation. The mechanism of stent expansion depends on the type of stent itself. Balloon-expandable stents are manufactured in the crimped state and are expanded to the vessel diameter by inflating a balloon. Self-expanding stents are manufactured at the vessel diameter (or slightly above) and are crimped to the smaller diameter until the intended delivery site is reached. The mechanism of self-expanding stent is deployed by removing the constraint.

There is not large difference in the behavior of the stent expansion between balloon-expandable and self-expanding stent. Therefore, the attention of researchers focused on the development of the stent due to some problems that appear after stent deployment. Several studies give an exploration of what appropriate material for the balloon, the expansion techniques, and the determination of the shape of balloon. First study concerned with the influence of balloon size was performed by Migliavacca et al. (2002). They conducted finite element method (FEM) analysis on the mechanical behavior of coronary stents and proposed a method to parameterize the influence of balloon size to stent expansion. If the end ring of struts of the expanded stent is turned out, this phenomenon is called as the dogboning effect. This effect frequently causes the over-stress on arterial layer, which may lead to

the inflammation of vessel wall [13]. Following this study, Wang et al. (2006) conducted an analysis of the transient expansion behavior and the design optimization of coronary stents by the finite element method, which were further confirmed by *in situ* observation. They found that the dogboning phenomenon can be eliminated by improving the geometry of a stent and by varying the length of balloon over stent. They highlighted that increasing the stent strut width of its end rings in conjunction with the reduction of the overlength of balloon could control the transient dogboning during the system expansion effectively. They also pointed out that it is possible to reduce the stent's foreshortening and design a zero-shortening stent by changing its link position and geometry [14]. Meanwhile, Cui et al. (2010) introduced a new parameter, namely the Ectropion angle, to describe the turning effect of the stent end in situations when the dogboning could not adequately characterize this phenomenon [15].

Regarding with the balloon, the development on balloon shape for balloon-expandable stent was initiated in 1999 by Saab from Advanced Polymers, Inc., USA. They produced many types of the high-pressure balloon, which is implemented in the stenting process. The ordinal cylindrical balloon gives less pressure to dilate the stent, which produces larger recoiling of stent after balloon removal. Variations in the balloon type and shape are important for the angioplasty and the stenting process, especially, to treat the bifurcation or tortuous stenosed artery. Another improvement for balloon performance is the use of the folded balloon to expand the stent as shown in Fig. 1-1. 'C' and 'S' folded balloon types increase the final diameter of the lumen because it dilates the stent more.

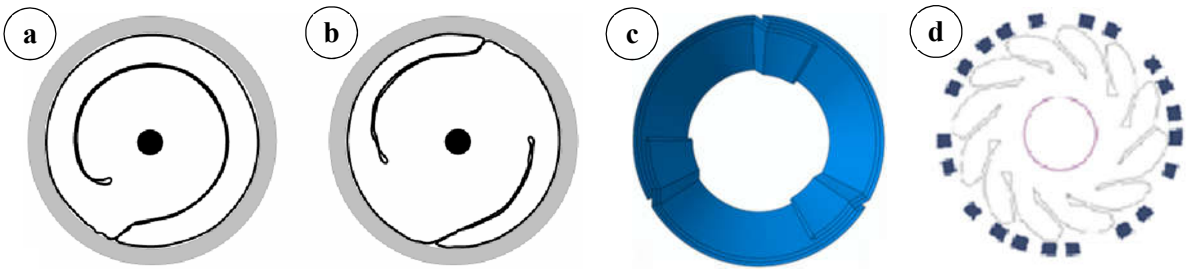

Figure 1-1: Balloon folding configuration: (a) 'C' shape, (b) 'S' shape, (c) Three-folded, (d) Multi-folded.

However, the non-uniform contact in the deployment process may contribute to the non-uniform stress distribution. This is one of the remain problem [16] for eccentric plaque obstruction. To improve the deliverability, several studies observed the optimum configuration for the folding mechanism of the balloon such as three folded, and multi-folded balloon [17][18][19][20]. Even the multi-folded balloon gives more pressure to dilate the stent; the uniform stress distribution within arterial tissue is preferable in the treatment of eccentric plaque. Therefore, utilization the asymmetric expansion of the balloon or the stent in the treatment of eccentric plaque may help to solve the problem.

Another issue with regard to the expanding balloon is how long the balloon should suppress the stent, and how many time it should be? Study in this research area is quite limited. A study conducted by Saha et al. (2013) reported that the longer duration of the stent inflation increases the minimal luminal diameter. They suggested that the minimum duration for stent inflation is 30 sec. However, after 60 sec, the minimal luminal diameter does not expand to the monogram derived expected diameter [21]. As for the quantity of inflation, Iwamoto et al. (2012) found that two-time stent balloon inflation may allow the better stent expansion regardless of the inflation time and that the two-time inflation may be equivalent to the longer inflation [22].

1.1.3 Development on stent mesh structure

The development on stent mesh configuration is necessary because it can minimize the problem such as the myointimal hyperplasia, and restenosis. Balloon-expandable stents may be subdivided into coil and tube designs. With coil stents, the strut width is generally greater than in tubular stents and this leads to the coil stents flexibility. However, the coil stent has the poor characteristics of radial strength and allows the tissue prolapse between the widely spaced wire elements. The balloon-expandable stents may be divided into *slotted tube* and *modular* designs. They are cut from a tube of metal by the laser, although some modular designs are composed of the rings of wire that are welded together. *Closed cell* slotted tube stents are close to the original concept of the *slotted tube*, while the *open cell* designs are *modular* stents. The slotted tubes of the closed cell design are inherently less flexible than the modular designs. However, the large ingenuity has been exercised in the design of articulations for these stents to provide the reasonable flexibility [23].

Effects of varying the slotted tube geometry (struts length and width) on the expansion behavior of J&J Palmaz-Schatz stent was observed by Chua et al. (2004) using ANSYS. They found that altering the stent strut configuration and number has the practical effects on the clinical use of vascular stents. If a stent consists of the same number of struts and slots, increasing the length of the slots may be better than increasing the width of the slots. Increasing the length of struts does not have a major effect on the stress distribution in slotted tube stent [24]. In a study using the rabbit iliac arteries, stents of simple design with 8 or 12 elements in each crown were implanted under the similar conditions. The injury score was 0.26 for the 12-strut design vs. 0.34 for the 8-strut. It is noticed that the injury was considerably more in the eight struts stent, because the cross-sectional polygon produced by the stent with fewer struts was more angulated and liable to produce deep arterial injury [25]. Other studies also demonstrated that the presence of more or less (stainless steel) struts in the artery wall is immaterial to the development of neointima. The neointima is the depth of injury produced by those struts (whether many or few) that leads to neointimal growth [26]. Regarding with the thickness of stent struts, the stents with thinner struts have a lower restenosis rate. The current generation of stents almost all being produced with the thinner struts than previously, particularly with

the advent of new materials, such as cobalt–chromium alloys [23].

Stent manufactures were judged by the production of a flawless surface, usually by electro-polishing. Early studies were persuasive that a smooth, polished surface reduced thrombus adhesion, and neointimal growth. Recent work also suggests that the extreme smoothness may not be the optimal surface to encourage re-endothelialisation. Moreover, the presence of more rather than less pores on the surface of the covered stents was successful to reduce the thickness of neointima in canine carotid arteries [23]. While all practitioners believe that they handle stents with care, the reality may be unclear. During the expansion process, the stents experiences plastic deformation that changes surface physical properties. This condition may increase the restenosis rate.

Some slotted tube stent, such as J&J Palmaz-Schatz stent, exhibited the poor symmetry of deployment in the case of eccentric plaque. Most of plaque obstruction is in the eccentric shape. The consequence of non-symmetric deployment may lead to restenosis due to the vessel wall inflammation. Furthermore, recent experimental studies confirm that the rupture criteria for fibrous cap, which cover lipid lumen core and healthy intimal layer, is not similar [27][28][29]. The author assumes that this difference should gain different treatment from the stent surface/part.

1.1.4 Latest issues and general background

The development of stent should adapt the latest issues, particularly with the results of clinical trials or experimental data. From the clinical trials or outcomes, in-stent restenosis (ISR) still becomes a major problem. ISR occurs due to hyperplasia of smooth muscle cells in the intimal layer of the vessel wall (so-called neointimal hyperplasia) and mural thrombus. On the molecular and cellular levels, the initial insult is vascular injury caused by both the inflation of intracoronary balloons and the metal of the stent itself [30][31][32]. Vascular stretching after the stenting process is usually considered and it contributes to the neointima formation, even in the absence of the deep injury. However, the deep injury is a more potent stimulus to the neointima formation than stretch [33]. From this point of view, the author presumes that stent development to improve expanded stent condition remains a big issue to minimize the vascular injury.

A recent simulation study confirmed that an anisotropic model should be used in the analysis of atherosclerotic artery. There are significant differences between the simulations using an isotropic and an anisotropic model. These results revealed that the usage of the isotropic models for the analysis of arteries during and after the supra-physiological loadings might be critical. This is particularly important for the analysis of stents after their insertion [34]. Moreover, recent *in vitro* experiment reported that all soft atherosclerotic components in carotid plaques exhibit non-linear behavior with both media and fibrous cap [35]. A review by Akyildiz et al. (2014) also demonstrated that the intima

tissue from atherosclerotic plaques differs greatly and depends on the plaque type. Intima tissue from early plaques is soft and isotropic, while the disease progresses intima tissue stiffness decreases, and the anisotropy and heterogeneity increase [36]. All these results suggested that the specific plaque type and more appropriate material behavior of the arterial tissue should be applied in the future rupture analysis.

1.2 OBJECTIVES

Based on the aforementioned review and latest issues, these following goals would be attempted to achieve by the author within the research works:

1. To develop analysis of the surface roughness changes on balloon-expandable stent after the balloon removal considering the plaque length.
2. To develop a new design of balloon-expandable stent for treating eccentric plaque obstruction of the human carotid artery by taking advantage of the asymmetric expansion.
3. To conduct the geometry assessment of the new stent design.
4. To observe the effect of asymmetric expansion on the plaque and arterial layer caused by the new stent design.

References

[1] Roguin, A., 2011. Historical Perspectives in Cardiology. Circulation: Cardiovascular Interventions 4, 206–209.

[2] Wikipedia, Stent. https://en.wikipedia.org/wiki/Stent#cite_note-11. (Accessed 22th January 2016).

[3] Stoeckel, D. et al., 2002. A survey of stent designs. Minimal Invasive Therapy Allied Technology 11, 137–47.

[4] Mani, G. et al., 2007. Coronary stents: A materials perspective. Biomaterials 28, 1689–1710.

[5] Stoychev, D. et al., 2002. Chemical composition and corrosion resistance of passive chromate films formed on stainless steels 316 L and 1.4301. Materials Chemistry and Physics 73, 252–258.

[6] Hanawa, T., 2009. Materials for metallic stents. Journal of Artificial Organs 12, 73–79.

[7] Trotzshcel et al., 2004. Alloy for use as stents. US Patent Application Publication No. 2004/0062676 A1. April 1, 2004.

[8] Li, H.Z. and Xu, Jian, 2014. MRI compatible Nb‐Ta‐Zr alloys used for vascular stents: Optimization for mechanical properties. Journal of the Mechanical Behavior of Biomedical Materials 32, 166–176.

[9] O'Brien, B. et al., 2008. Development of a new niobium-based alloy for vascular stent applications. Journal of the Mechanical Behavior of Biomedical Materials 1, 303–312.

[10] Li, H. et al., 2014. Progress of biodegradable metals. Progress in Natural Science: Materials International 24, 414–422.

[11] Bowen, P.K. et al., 2013. Zinc exhibits ideal physiological corrosion behavior for bioabsorbable stents. Advanced Materials 25, 2577–2582.

[12] Lim, I.A., 2004. Biocompatibility of stent materials. MIT Undergraduate Research Journal (MURJ) 11, 33–37.

[13] Migliavacca, F. et al., 2002. Mechanical behavior of coronary stents investigated through the finite element method. Journal of Biomechanics 35, 803–811.

[14] Wang, W.Q. et al., 2006. Analysis of the transient expansion behavior and design optimization of coronary stents by finite element method. Journal of Biomechanics 39, 21–32.

[15] Cui, F.S. et al., 2010. Effects of Balloon Length and Compliance on Vascular Stent Expansion. International Journal of Applied Mechanics 2, 681–697.

[16] Narracott, A.J. et al., 2007. Balloon folding affects the symmetry of stent deployment: experimental and computational evidence. Proceedings of the 29th Annual International Conference of the IEEE EMBS, 3069–3073.

[17] Martin, D. and Boyle, F., 2013. Finite element analysis of balloon-expandable coronary stent deployment: Influence of angioplasty balloon configuration. International Journal of Numerical Method in Biomedcal Engineering 29, 1161–1175.

[18] De Beule et al., 2008. Realistic finite element-based stent design: The impact of balloon folding. Journal of Biomechanics 41, 383–389.

[19] Gervaso, F. et al., 2008. On the effects of different strategies in modelling balloon-expandable stenting by means of finite element method. Journal of Biomechanics 41, 1206–1212.

[20] Ragkousis, G.E. et al., 2015. Computational modelling of multi-folded balloon delivery systems for coronary artery stenting: Insights into patient-specific stent malapposition. Annals of Biomedical Engineering 43, 1786–1802.

[21] Saha, M. et al., 2013. Coronary stent implantation technique: Prolonged inflation time maximizes stent expansion. Journal of Invasive Cardiology 25, 28–31.

[22] Iwamoto, Y. et al., 2012. Better stent expansion by two-time inflation of stent balloon and its responsible mechanism. Journal of Cardiology 59, 160–166.

[23] Morton, A.C. et al., 2004. The influence of physical stent parameters upon restenosis. Pathologie Biologie 52, 196–205.

[24] Chua, S.N.D. et al., 2004. Effects of varying slotted tube (stent) geometry on its expansion behavior using finite element method. Journal of Material Processing Technology 155−156, 1764–1771.

[25] Garasic, J.M. et al., 2000. Stent and artery geometry determine intimal thickening independent of arterial injury. Circulation 101, 812–8.

[26] Gunn, J. et al., 2002. Coronary artery stretch versus deep injury in the development of in-stent neointima. Heart 88, 401–5.

[27] Maher, E. et al., 2009. Tensile and compressive properties of fresh human carotid atherosclerotic plaques. Journal of Biomechanics 42, 2760–2767.

[28] Maher, E. et al., 2011. Inelasticity of human carotid atherosclerotic plaque. Annals of Biomedical Engineering 39, 2445–2455.

[29] Teng, Z. et al., 2014. Material properties of components in human carotid atherosclerotic plaques: A uniaxial extension study. Acta Biomaterialia 10, 5055–5063.

[30] Sullivan, T.M. et al., 2002. Effect of endovascular stent strut geometry on vascular injury, myointimal hyperplasia, and restenosis. Journal of Vascular Surgery 36, 143–149.

[31] Winslow, R.D. et al., 2005. Restenosis and drug-eluting stents. The Mount Sinai Journal of Medicine 72, 81–89.

[32] Mitra, A.K. and Agrawal, D.K., 2006. In stent restenosis: Bane of the stent era. Journal of Clinical Pathology 59, 232–239.

[33] Gunn, J. et al., 2002. Coronary artery stretch versus deep injury in the development of in-stent neointima. Heart 88, 401–405.

[34] Schmidt, T. et al., 2015. Influence of isotropic and anisotropic material models on the mechanical response in arterial walls as a result of supra-physiological loadings. Mechanics Research Communications 64, 29–37.

[35] Teng, Z. et al., 2014. Material properties of components in human carotid atherosclerotic plaques: A uniaxial extension study. Acta Biomaterialia 10, 5055–5063.

[36] Akyildiz, A.C. et al., 2014. Mechanical properties of human atherosclerotic intima tissue. Journal of Biomechanics 47, 773–83.

2 EFFECTS OF PLAQUE LENGTHS ON STENT SURFACE ROUGHNESS

2.1 INTRODUCTION

Stent implantation is a well-known non-surgical method to treat vascular diseases. As an object implanted in the human body, it should have certain physical properties to avoid the surface passivation, encrustation, and tissue damage. The physical properties of the stent surface, well known as surface roughness, influence the effectiveness of vascular disease treatment 0. In the deployment process, stent acquires high-level deformation that changes the magnitude of surface roughness. A considerable amount of literature has been published on the surface roughness of stent and its influence. The first serious analysis reported that the surface roughness of the micrometer strongly hinders the process of surface passivation and leads to thrombus formation, which may adhere to the vessel wall and block the blood flow [2]. Roughness of the biomaterial implant turned out to have a significant effect on thrombogenicity. An observation on the outer surface of some intravascular catheters confirmed that the surface roughness is one of the factors of thrombogenicity [3].

Materials with a smooth surface and a low coefficient of friction are more biocompatible by reducing the mechanical skinning and the shear forces at the biomaterial-tissue interface. This phenomenon has been supported by the animal studies where stents with those surface properties have been shown to produce less urethral reaction [4]. The other study showed that the grooved surfaces leads to the increase in the migration rate of endothelial cells up to 64.6% comparing with the smooth and control surfaces [5]. Furthermore, study on the effect of surface roughness of stainless steel on human vein endothelial cell conformed that the stainless steel roughness of 671.8±27.8 nm causes membrane cell injury. The injury leads to endothelial cell activation and inflammation [6]. These studies emphasize that the surface roughness of stainless steel is an indispensable surface property in the vascular stent development.

The changes in stent surface roughness have two meanings: negative and positive effect. Severe changes of surface roughness cause endothelial cells (ECs) injury/trauma. The trauma of ECs enhances smooth muscle cells (SMCs) to migrate into intimal layer. These cells will act as synthetic type cells and produce much protein (collagen and elastin) surrounding the stent struts, which is gradually leading to in-stent restenosis (ISR) and intimal hyperplasia. This phenomenon is well known as negative meaning of changes in surface roughness. Nevertheless, a certain amount of surface roughness changes may generate unique profile of stent surface and do not enhance SMCs to migrate into intimal layer (SMCs act as contractile type cells), which causes the interaction between ECs and stent surface is more stable. In this condition, migration of healthy endothelial cells will occur and help recovery of

ECs while the balloon is deflated.

Based on those facts, the control of the surface properties of stent after the deployment is extremely important. Concerning with the physical surface properties, several studies have been conducted to improve the surface roughness of stent using the acid pickling, annealing, electro polishing, and the electrochemical polishing [7][8][9]. Those methods succeed to decrease the surface roughness of stent. However, they did not consider the plastic deformation during the expanding of stent, which changes the surface condition. Many investigators also confirmed that the changes in the grain structure of the metals lead to changes in its surface roughness [10][11][12] [13][14].

2.2 BACKGROUND AND OBJECTIVE

The stent manufacturers are required to determine the allowable surface roughness of the stent before the implantation because the surface roughness changes during the stent expansion. The experiments conducted both *in vitro* and *in vivo* encounter many obstacles due to the lack of strain gauge in micro-scale observation of the expanding stent. However, the changes in the stent surface roughness during its deployment process can be observed easily using the finite element method (FEM).

There are numerous FEM simulations relating to the interaction between the expanding stent, plaque, and arterial vessel wall. However, there are few FEM simulations considering the relationship between the plastic deformations of stent and the surface roughness. In this study, therefore, observations on the relationship between the plastic strain and the surface roughness of balloon expandable stents were conducted using FEM. The FEM analysis considered various length of plaque that affects the distribution of the changes in the stent surface roughness. The results of investigation are expected to provide a better guideline for the manufacturing process of stents.

2.3 METHODS

2.3.1 Finite Element Model

ANSYS R12.1 (ANSYS Inc., Pennsylvania, USA) was used to design the geometric models presented in this work. It is a nonlinear dynamic transient finite element modeling with the presence of plaque and vessel wall. The three-dimensional finite element model consisted of two kinds of bare metal stents: “Palmaz stent” that is representative of stent type with the rigid structural geometry, and “Sinusoidal stent” that is representative of stent type with the flexible structural geometry [14]. The geometry of both models is shown in Fig. 2-1.

The material models are defined as multilinear isotropic for stent and hyperelastic for the balloon,

plaque and vessel wall. For the hyperelastic constitutive equation, 5-parameters Mooney-Rivlin was used for the plaque and vessel wall while 2-parameters Mooney-Rivlin was assigned for the material characteristic of the balloon. All of parameters, except for the material properties for stent, are taken from previous literatures as summarized in Table 2-1. As a pilot study, using the same material for the plaque design during all simulation will be useful in eliminating the effect of the fracture mechanism of plaque during the stent expansion. More sophisticated plaque structures will be discussed in next chapter.

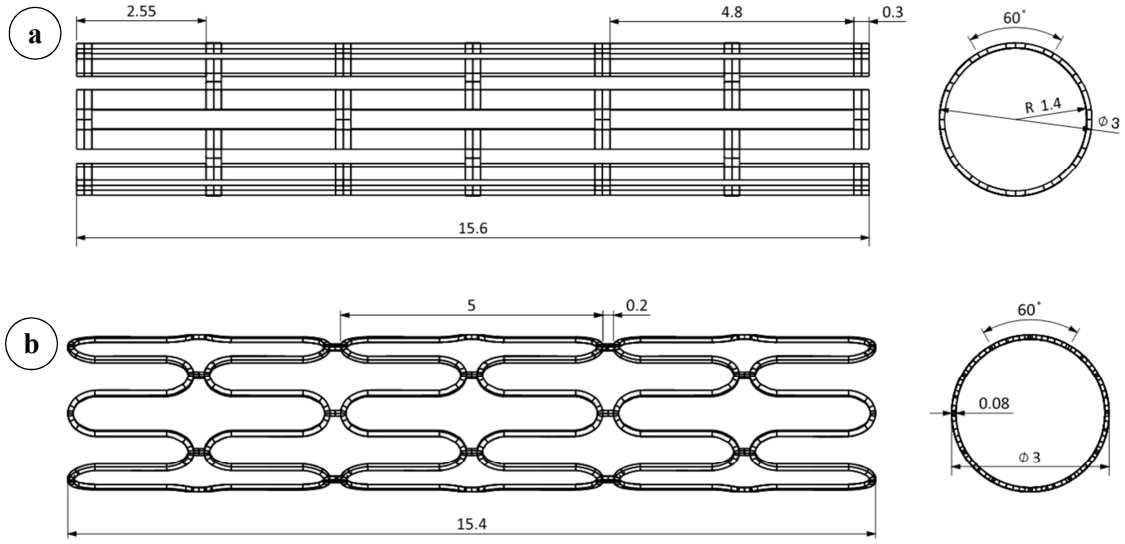

Figure 2-1: Front and side views of stents used: (a) the Palmaz as rigid stent, (b) Sinusoidal stent as flexible stent. All units in mm.

Table 2-1: Material properties used in the finite element simulation

Component	Balloon	Stent	Plaque	Vessel Wall
Material	Polyurethane	SUS316NG	Hypocellular	Carotid
Young's Modulus (GPa)	0.03447	186.67	0.00219	0.00175
Poisson's Ratio	0.495	0.33	0.495	0.495
Material Behavior	Hyperelastic	Multilinear Isotropic	Hyperelastic	Hyperelastic
Material Constant	Mooney-Rivlin (MPa): C_{10}= 1.032×10^{-7} C_{01}= 3.693×10^{-7}	Fitting stress- strain curve resulted from pure tensile test of SUS316NG.	Mooney-Rivlin (KPa): C_{10}= -802.723 C_{01}= 831.636 C_{11}= 1157.680 C_{20}= 0.000 C_{30}= 0.000	Mooney-Rivlin (KPa): C_{10}= 18.90 C_{01}= 2.75 C_{11}= 85.72 C_{20}= 590.43 C_{30}= 0.00

Compiled using data from [25] and [26].

Considering the cyclical and reflective symmetry of the model, a 1/12 model was generated for

Palmaz and Sinusoidal simulation as shown in Fig. 2-2a. The plaque is modeled in three different lengths and having equal thickness in the central radial as illustrated in Fig. 2-2b to observe its effect on the changes in the surface roughness. The balloon was located inside the stent with the outside diameter of the balloon to be equal to the inside diameter of the stent. The vessel wall and the plaque were modeled in such a way so that the plaque surface was not in contact with the stent before the inflation process. The plaque was assumed attaching on the vessel wall firmly, so there is no generated contact behavior and frictional force. The element type for meshing is used a higher order 3-D 20-node solid element that exhibits quadratic displacement behavior, which is superior in the irregular meshing and simulating the deformations of incompressible hyperelastic materials.

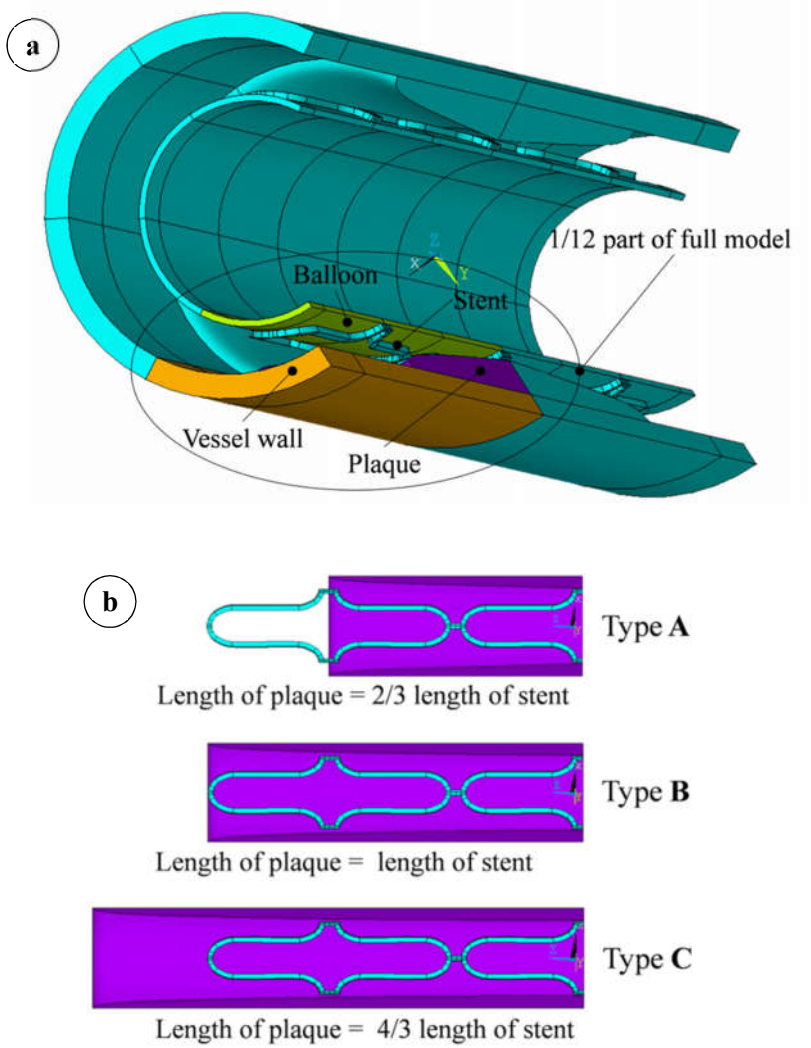

Figure 2-2: (a) Sectional view of the full model: 1/6 due to cyclical symmetry of geometry and 1/2 due to symmetry of boundary conditions. (b) Three different length of plaque compared to the length of stent.

Defining the contact properties is a decisive stage in the procedure of the nonlinear finite element modeling. For the stent simulation, the surface-to-surface contact model is the most well suited one because it covers the interference fit assembly contact. Because stent undergoes the large deformation,

flexible contact to flexible targets is the most suitable choice. A reasonable contact condition should be chosen carefully to obtain rapid converged calculation with accuracy. The normal stiffness of 0.1 for the contact between the balloon and stent, and 10 between the balloon and both plaque and vessel produce the reasonable results.

In order to achieve the better-converged result in the finite element simulation, the coefficient of friction should be defined and chosen properly. The coefficient of friction for the contact between the rubber and a metal surface without the dynamic pressure is below the value of 0.4 [15], and for stent is about 0.125 but no more than that of 0.15 [16]. Another research has reported that the friction coefficient from the experimental measurements on the living endothelial cells due to polished glass pin is around 0.06 [17]. In this investigation, the value of 0.3, 0.15, and 0.06 were assumed respectively as the coefficient of friction for the balloon, the stent, and the plaque/vessel wall.

2.3.2 Loading and Solution

Boundary conditions of the model are shown in Fig. 2-3a by the polar coordinates, where *X*, *Y* and *Z* are the radial, circumferential and longitudinal directions, respectively. On the repetitive symmetric plane (both sides of model), y direction is restrained. In the end-side of the model, the degree of freedom of balloon is restricted in all direction, while that of the vessel wall is restrained in *y* and *x* direction due to its infinite length and hyperelasticity properties. To achieve geometric symmetry, symmetry boundary conditions are applied to the cross section of the model. Both sides of the model are coupled with offset nodes coupling along the circumferential direction for cyclical/repetitive symmetry.

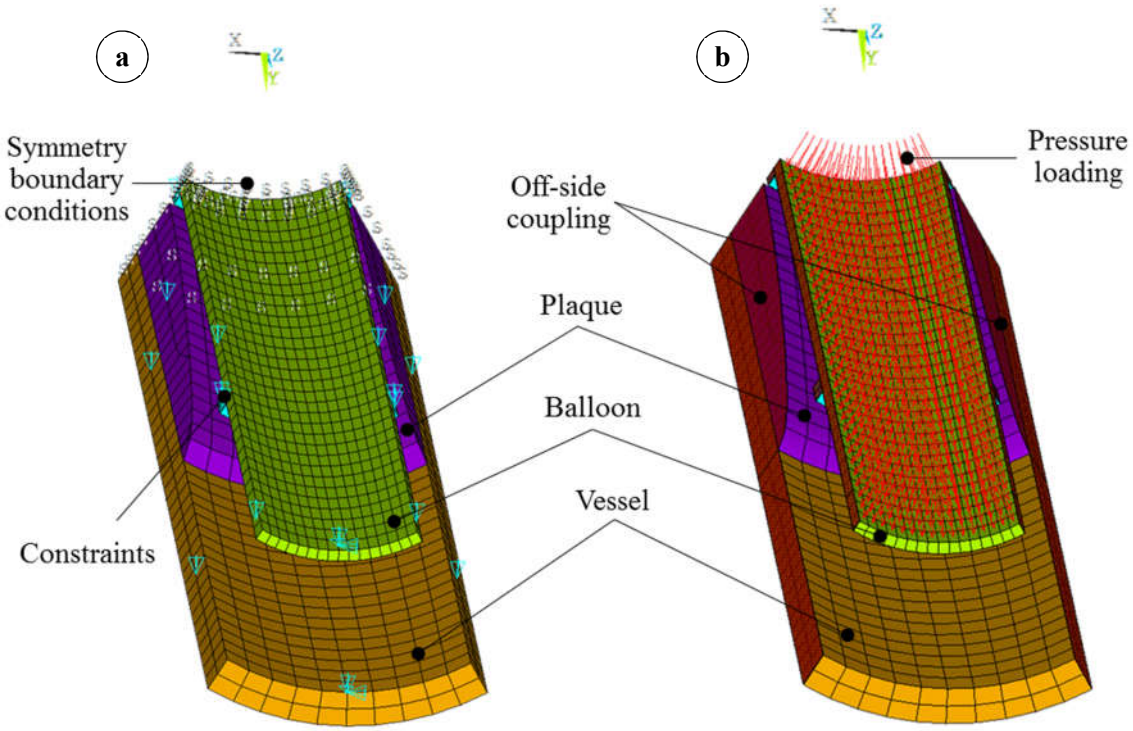

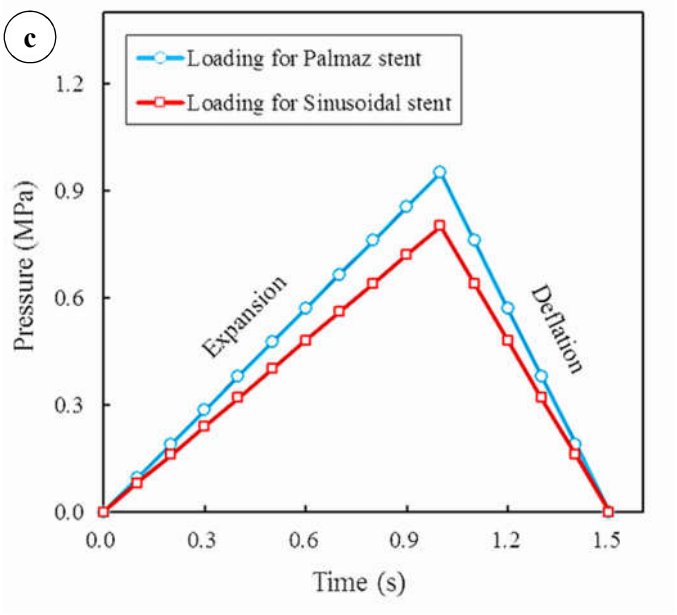

Figure 2-3: Boundary conditions and loading applied for both stent models: (a) Constraints and symmetry planes, (b) Off-side coupling connects both side of the model, (c) Time history of pressure loading.

The loading for both models is applied on the inner surface of the balloon in the outward direction as illustrated in Fig. 2-3b. Stent expands to the radial direction until the target diameter before the failure stress was reached. The ramped pressure is chosen as the loading as suggested by previous study [19]. Balloon inflates steadily until the 30–40 % expansion and deflates. The balloon was subjected to a uniform internal pressure from 0 to 0.95 MPa for the Palmaz model and from 0 to 0.80 MPa for the Sinusoidal model as shown in Fig. 2-3c. The magnitude of the pressure is not same for the models because of the difference in the surface area. The pressure is applied in 1.5 seconds; the expanding pressure is in 1 second and the remaining time is for balloon removal. The pressure rate is fixed automatically by ANSYS implicit solver.

2.3.3 Verification and Validation

There are two requirements for the use of computational tools in simulations: verification and validation. The verification can be defined as whether the simulations solve the equation or not, while the validation can be understood as whether the simulations used the right equations or not. Verification of simulation in a simple way can be conducted by comparing the results of simulation to other results, which has similar physical problem and system of FEMs. Validation is done by comparing with the experiments and by checking FEM model whether it represents the physics of the experiments or not.

In the case of the simulation of stent deployment, validation is the most difficult task because the displacement as the primer result of FEM cannot be validated through *in vitro* experiment. The micro

scale of stent struts is the main problem in the experiment. Therefore, some approaches are needed in order to look into what happening during stent deployment is. These approaches should be verified that the result represents a valid simulation result. The type of analysis, material model assigned for each component, type and size of elements, and contact model for element contact is verified by previous studies and ANSYS Element Reference, as following:

1. Type of analysis: Static and transient nonlinear analysis can be used in the simulation of stent deployment. However, transient analysis is more appropriate and represents the physics of stenting process [19][25][26].
2. Material model: Some researcher used bilinear isotropic material for the stent due to lack of experimental data [15][19][25]. Here the author used multilinear isotropic material that is derived from fitting curve of tensile test. In the transient analysis, multilinear isotropic material more represents material behavior. Material model for the balloon, plaque and vessel wall is hyperelastic material, which has been verified can be adopted in the simulation of stent deployment [15][19][25][26].
3. Element type and meshing size: Many researchers used 8-node hexahedra element in the FEM simulation to avoid hour glassing phenomenon on hyperelastic model. In this study, SOLID186 or 20-node hexahedra element is chosen to model the balloon, plaque and vessel wall. SOLID186 is well suited to model irregular meshes (such as produced by various CAD/CAM systems). To prevent volumetric mesh locking and hourglass mode propagation in nearly incompressible cases, ANSYS recommends to use uniform reduced integration method in SOLID186 option and to build at least two layers elements in each direction [20]. Meanwhile, the finer element size, the more accurate the simulation result and the longer the simulation time are. Besides, the size of element is also determined by the interaction among contact element.
4. Contact behavior: Contact problems fall into two general classes: rigid-to-flexible and flexible-to-flexible. In the case of stent simulation, the contact among components can be classified as a flexible-to-flexible contact. Even though the stiffness of stent is generally higher than that of balloon, plaque and blood vessel, but stent also undergoes large deformation as well as the balloon. Surface-to-surface contact model of solid model is used for the contact elements when contact regions are not known accurately and a significant amount of sliding is expected. Moreover, it covers interference fit assembly contact or entry contact. Therefore, the type of element used in this simulation is CONTA174 as the contact elements and TARGE170 as the target elements [21].

2.3.4 Measurement of surface roughness

The surface roughness changes of actual stent cannot be obtained due to limitation of microscopic

observation equipment. To derive the correlation between plastic strain and surface roughness changes, the large-scale experiment is performed. The large-scale experiment is the uniaxial tensile test using a standard specimen. Nowadays, advanced microscopic observation (like KEYENCE) is available and has capability to measure surface roughness of micro-scale specimen. However, the strain measurement using strain gauge becomes another problem. Therefore, large-scale experiment is preferable in this study.

The large-scale experiment is intermittent pure tensile test of the specimen made of SUS316NG, which correlates the plastic deformation and the changes in surface roughness. The data from intermittent tensile test is supposed to describe how the plastic deformation affects the changes in surface roughness, although the residual stress actually occurring due to the stent expansion is more complexity than that due to the tensile test. The geometry of the specimen is shown in Fig. 2-4*a*. The sheet geometry is chosen to obtain the close response to stent struts and the surface roughness. The material for the test is SUS316NG, whose chemical composition is shown in Table 2-2. The loading is not applied continuously until the specimen failure. This is because after each unloading, the surface roughness is measured as shown in Fig. 2-4*b*.

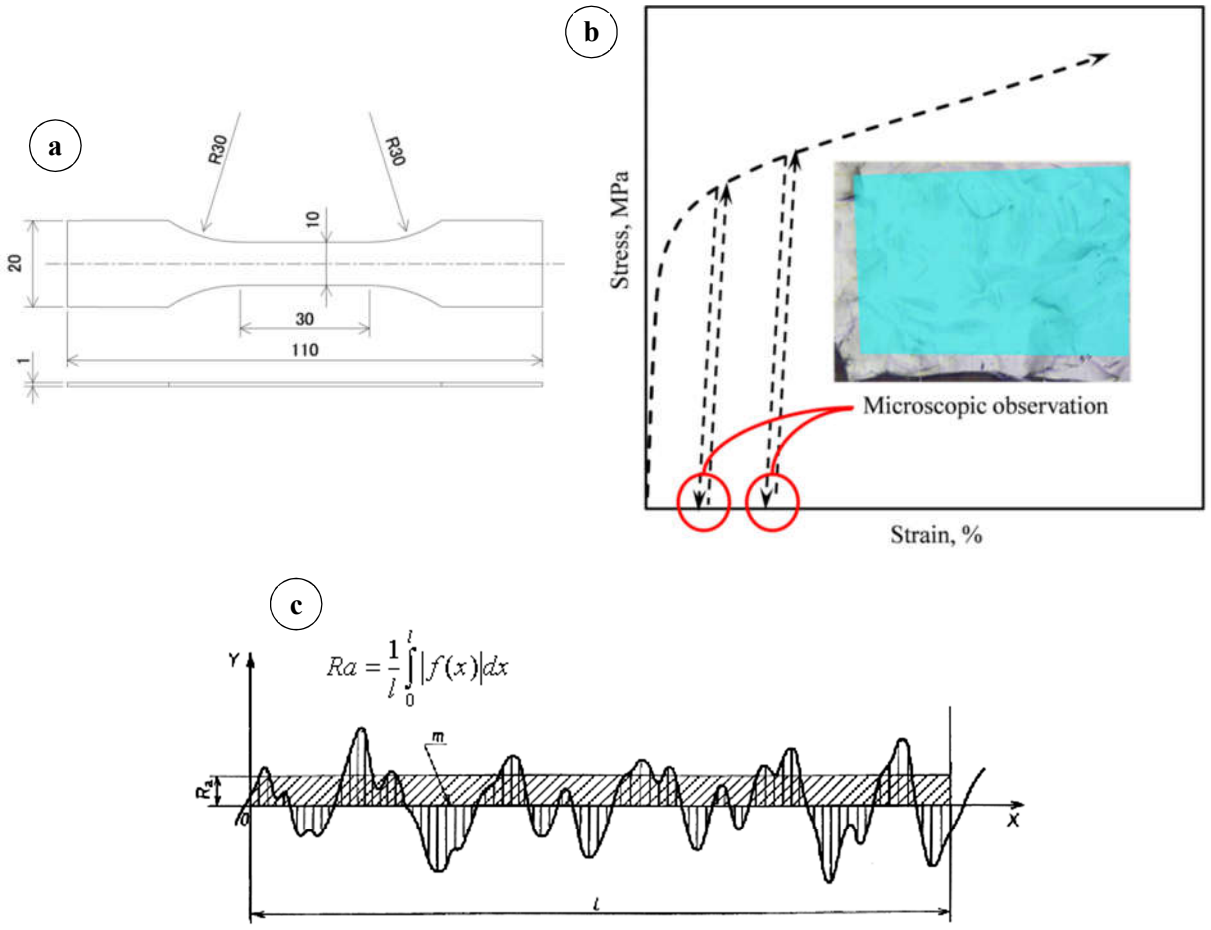

Figure 2-4: (a) Specimen of tensile test, (b) Illustration of intermittent tensile test, (c) Definition of R_a

The measurement of the surface roughness is performed on the same 2D area of the specimen (indicated by cyan color on the specimen surface) during intermittent tensile test using the color laser-scanning microscope. Namely, the obtained surface roughness is the 2D surface roughness. Two different strain intervals are chosen in the intermittent tensile test with the loading rate 0.005 mm/sec. The 0.5 % strain interval is for the smaller strain than the 5 % strain, and the 2.5 % strain interval for the remaining axial strain. The average roughness (R_a) is used as a parameter to evaluate the stent surface roughness. R_a is defined as the arithmetic average of the absolute values of the roughness profile ordinates (shown in Fig. 2-4*c*) and one of the most effective surface roughness measures commonly adopted in general engineering practice. It gives a good general description of the height variations in the surface.

Table 2-2: Chemical composition of SUS316NG

Steel type	Chemical composition (wt. %)								
	Cr	Ni	Mn	Mo	Si	C	S	P	Fe
SUS316NG	17.65	12.06	1.250	2.04	0.001	0.009	0.001	0.018	Bal

The results of the microscopic observation and measurement are shown in Fig. 2-5*a*. For the same magnification (400x), it is obvious that the plastic strain strongly affects the surface roughness of the specimen. Figure 2-5b shows the relationship between the 2D surface roughness and the plastic strain. From Fig. 2-5*b* the correlation between the plastic deformation and the 2D surface roughness can be expressed by

$$S.R. = 0.16\varepsilon^{p} + 0.19 \tag{2-1}$$

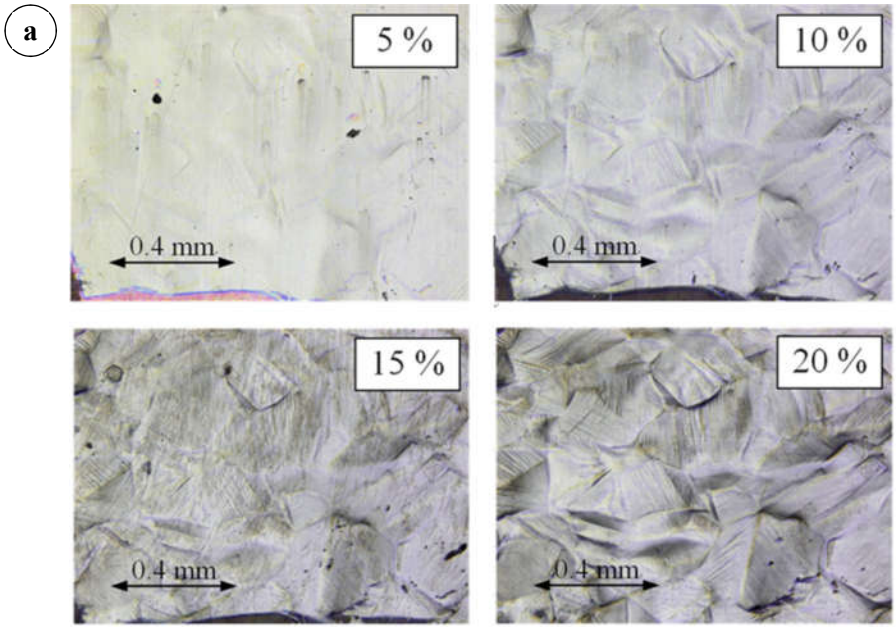

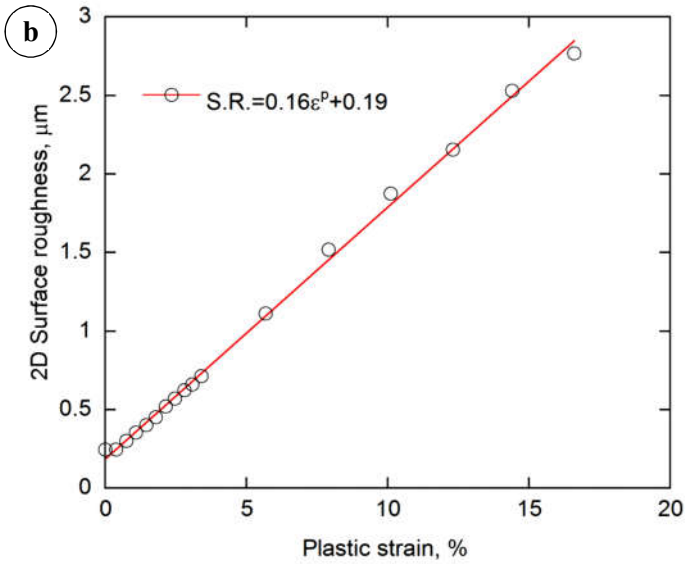

Figure 2-5: (a) The results of microscopic scanning photograph, (b) The linear correlation between plastic strains *vs.* 2D surface roughness of SUS316NG.

where *S.R.* is surface roughness in µm and ε^p the plastic strain in mm/mm. Equation 2-1 shows the lowest limit for SUS316NG from the experiencing surface roughness changes due to plastic deformation. We can derive from Eq. 2-1 that a strain endurance limit of SUS316NG that does not change the surface roughness is the strain of 0.012 mm/mm. By using this equation and the unloading plastic strain obtained by FEM simulation of the stent expansion, the surface roughness can be assessed and predicted immediately. Thus, the similar procedure can be applied to all node of the finite element model.

2.4 RESULTS AND DISCUSSION

The analysis of the plastic strain distribution of stent leads to consideration of the surface roughness changes. Then, the relationship between the plastic strain and the surface roughness was revealed in sub-section 2.3.3. The distribution of the surface roughness of both Palmaz and Sinusoidal models with a unified legend provided are shown in Figs. 2-6a and 2-7a, respectively. The *X*, *Y*, *Z* coordinates represent the global cylindrical system, where the *X*-axis is the radial direction, the *Y*-axis the circumferential direction, and the *Z*-axis the axial direction.

In Figs. 2-6*a* and 2-7*a*, the central zone of the stents is on the right side of figure, and the distal zone on the other side. The dark blue area of the stent shows the endurance area, which represents the part of the stent without any changes in the surface roughness. The strains of the endurance area is smaller than the 0.012 mm/mm strain, which is equivalent to 0.190 µm of surface roughness considering Eq. (2-1). The surface roughness changes are concentrated in the end of struts and bridges area. It is can be seen from

Figs. 2-6*a* and 2-7*a* that the length of plaque does not affect the critical changes in surface roughness. The critical changes in surface roughness for all type of plaque length are located on the distal area. The distal area of stent in the simulation shows the part of stent, which has the largest changing in the plastic strain because stent expands with the fewer obstacles from plaque.

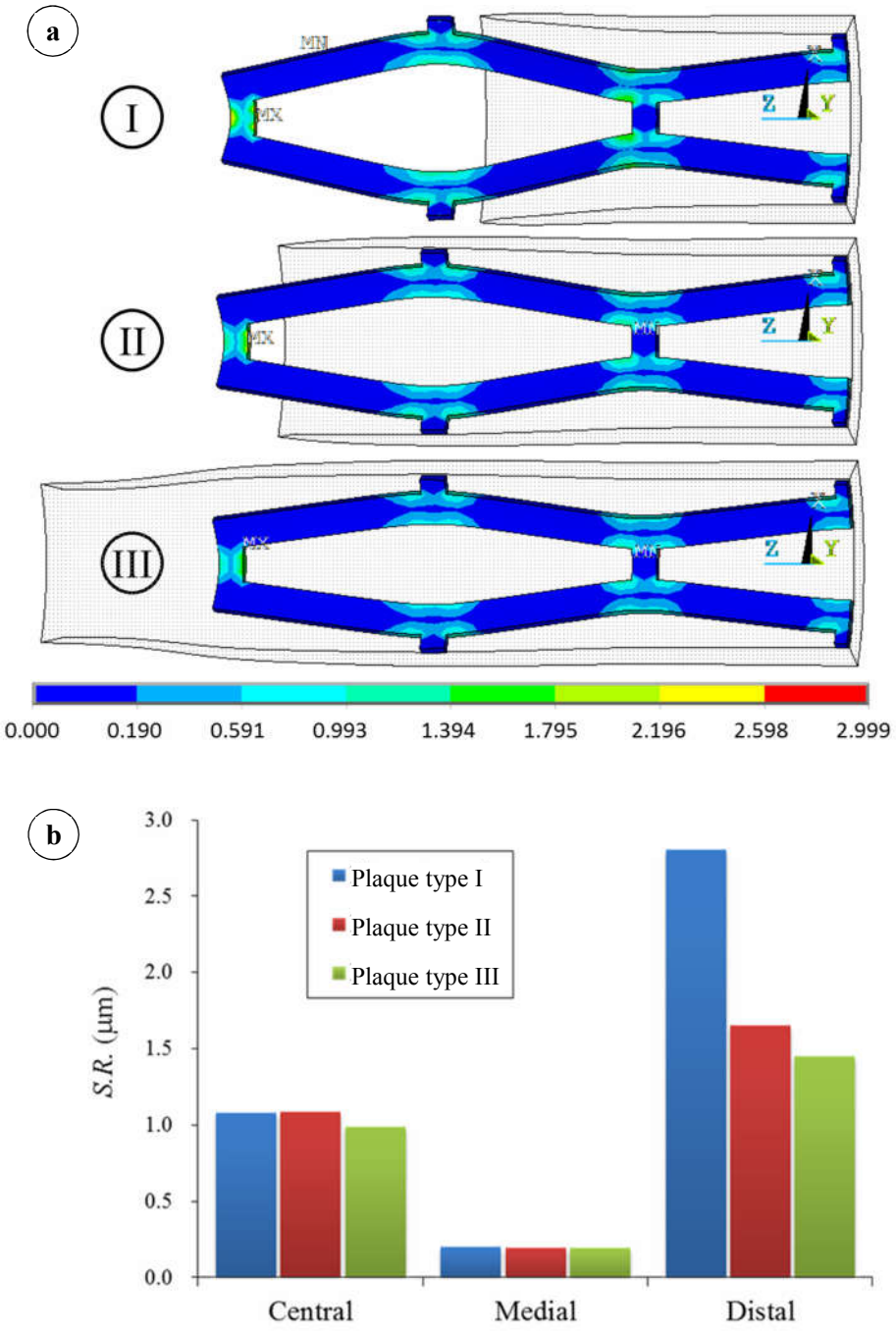

Figure 2-6: (a) Distribution of the changes in surface roughness for the Palmaz stent, (b) Corresponding changes in surface roughness.

The corresponding value of the changes in the surface roughness for each model for the longitudinal direction is shown in Figs. 2-6*b* and 2-7*b*. Both figures show the similar tendency of the changes in the

surface roughness that take place in central and distal area. For Palmaz model, the struts in medial area show the endurance from the changes in the surface roughness. Meantime, central and medial areas of Sinusoidal model show the endurance due to the flexibility of the Sinusoidal stent. The important finding from these figures is that the plaque length strongly affects the critical changes in the stent surface roughness. This is indicated by the value of SR in distal area, which type I has the largest changes.

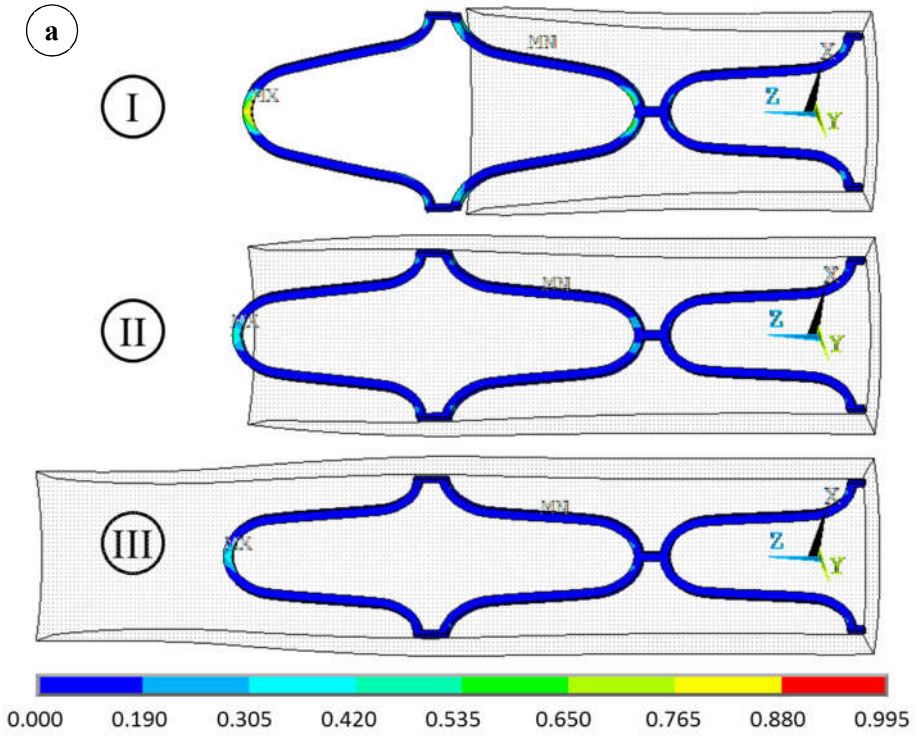

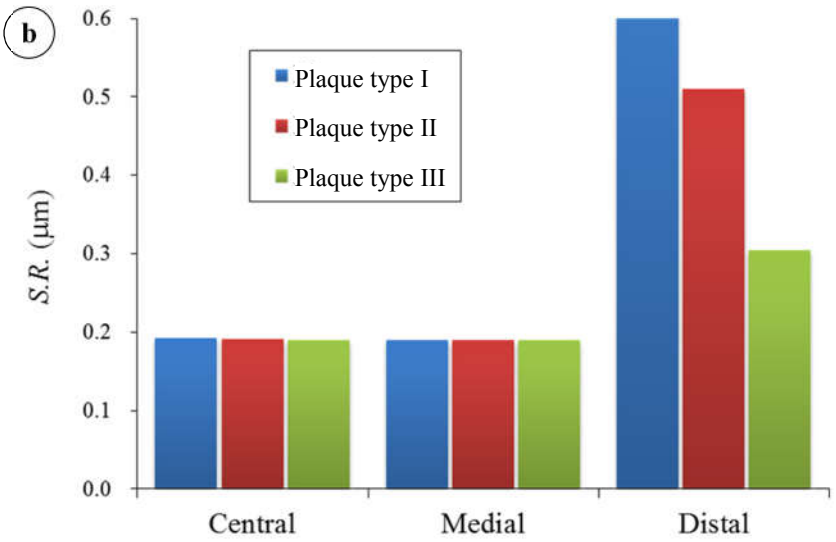

Figure 2-7: (a) Distribution of the changes in surface roughness for the Sinusoidal, (b) Corresponding changes in surface roughness.

The following important point is clarified from both models. Namely, the critical surface roughness changes in the model of type I is not covered by plaque. This is a main reason of severe damage of the vessel wall due to the largest surface roughness changes at the end of stent. Nevertheless, in the case of stent having longer length than plaque length, the area of the uncovered plaque remains as a stenotic blood vessel. On the other hand, the critical surface roughness changes in the simulation model of type II and III have no direct connection to the vessel wall. When the critical changes in the surface roughness take place in the direct contact area between the stent's distal zone and critical vessel wall, the vessel tissue may easily have damages. The damages lead to the open-lesion of the cell membrane structure. Moreover, the stent length is preferable to be as short as possible, because stent is the foreign material and, therefore, the smaller surface area of the foreign material is preferable based on the immunologic response standpoint. Considering those factors, the stent length equal to the plaque length may be the best choice.

The overall stress distribution within the vessel wall is shown in Fig. 2-8 with the unified legend provided below. The *X*, *Y*, *Z* coordinates represent the global cylindrical system, where the *X*-axis is the radial direction, the *Y*-axis the circumferential direction, and the *Z*-axis the axial direction. The stress distribution is focused on the vessel wall by neglecting that within the plaque, because the stresses induced within the vessel wall can be an undermined stimulus for the growth of restenotic tissue [22][23].

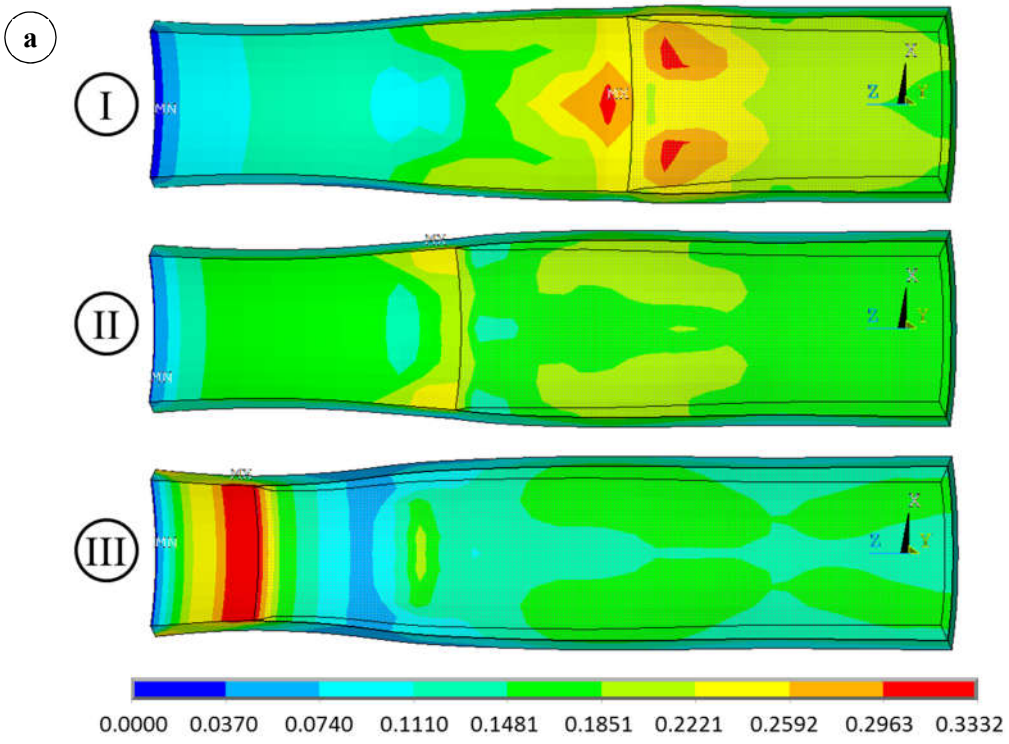

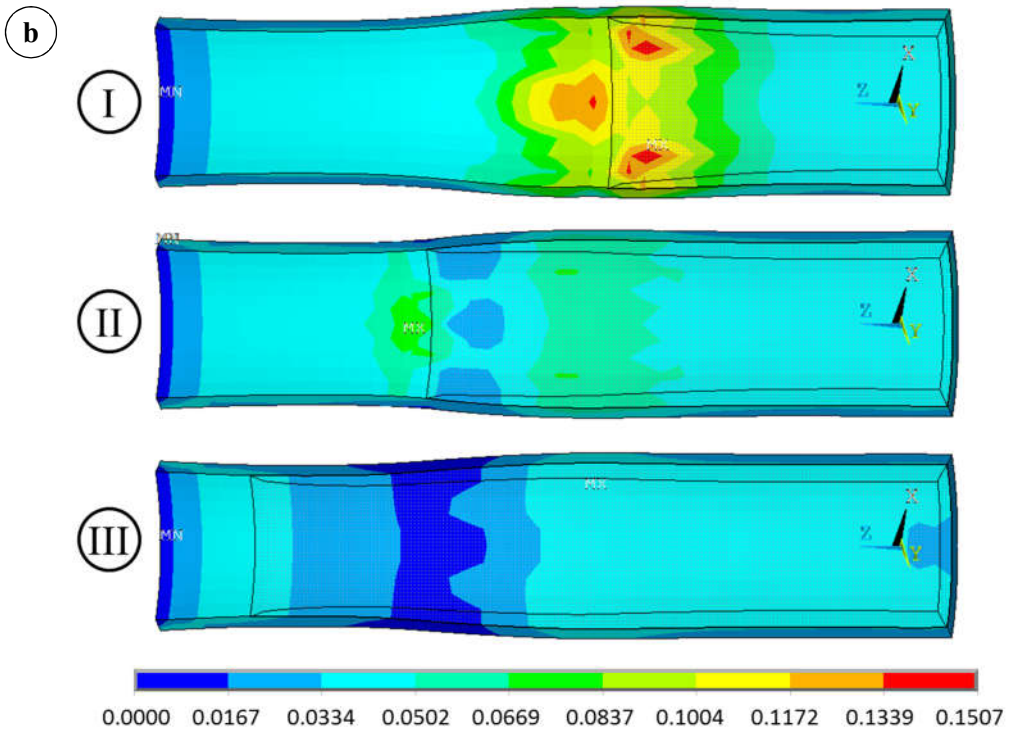

Figure 2-8: Stress concentration within the vessel wall after balloon removal. (a) Due to the Palmaz. (b) Due to Sinusoidal stent.

Figure 2-8*a* shows the residual von Mises stress distribution within the vessel wall after balloon removal induced by the Palmaz stent, and Fig. 2-8*b* shows that induced by the Sinusoidal stent combining with the appearance of the edge line of the plaque model. The plaque length of type I of both models causes direct contact between the stent and the vessel wall surface. As a result, the vessel walls of type I received larger pressure than that of type II and III. Meanwhile, stress within the vessel wall, which is induced by plaque type II and III, is shielded by the plaque. This phenomenon reduces the possibility of arterial lesion. Especially for type III plaque of Palmaz model, the critical stress emerges outside of stent surface area. Therefore, though there is the highest stress among the other types, it is safer for the vessel wall to use type III plaque of Palmaz stent.

For the better correlation between the effects the plaque length and the changes in the stent surface roughness, the changes in stent geometry due to plastic deformation should be characterized. There are five recommended parameters to be calculated in order to quantify the effects [24] as follows:

- Distal and central radial recoil, defined as

$$Distal\ radial\ recoil = \frac{R_{distal}^{load} - R_{distal}^{unload}}{R_{distal}^{load}} \tag{2-1}$$

$$Central\ radial\ recoil = \frac{R_{central}^{load} - R_{central}^{unload}}{R_{central}^{load}} \tag{2-2}$$

- The longitudinal recoil, defined as

$$Longitudinal\ recoil = \frac{L^{load} - L^{unload}}{L^{load}} \tag{2-3}$$

- The foreshortening, defined as

$$Foreshorte\ ning\ = \frac{L - L^{load}}{L} \tag{2-4}$$

- The Dogboning, defined as

$$Dogboning = \frac{R_{distal}^{load} - R_{central}^{load}}{R_{distal}^{load}} \tag{2-5}$$

All values of those parameters are summarized in Table 2-3.

Table 2-3: Calculation results

Stent	Type	Ratio plaque to stent	Distal radial recoil (%)	Central radial recoil (%)	Longitudinal recoil (%)	Foreshortening (%)	Dogboning (%)
Palmaz	I	0.67	6.20	8.12	-0.25	2.34	47.10
	II	1.00	8.35	9.62	-0.21	1.62	42.62
	III	1.33	15.72	10.27	-0.20	1.26	31.71
Sinusoidal	I	0.67	51.10	36.04	-6.44	10.63	55.27
	II	1.00	42.85	63.95	-3.04	6.06	-6.65
	III	1.33	66.71	65.48	-2.72	5.38	-6.28

It is seen that all parameters of expanded stent are sensitive to the variation of the plaque length. However, the sensitiveness becomes small with increase in the length of plaque. The longer plaque length leads to the larger elastic recoil of the stents. On the other hand, the plaque length succeeds decrease in the foreshortening and dogboning. Especially for Sinusoidal model, there is no dogboning when the plaque length is longer than the stent length. Namely, the elastic recoil followed by the increase in the foreshortening and the dogboning of stent tend to enlarge the possibility of the changes in the stent surface roughness.

2.5 CONCLUSIONS

The deformation analysis using the finite element simulation is particularly useful to identify the critical surface roughness of balloon-expanded stent based on its plastic strain distribution. The results of the present study demonstrated that the plaque size relative to the stent length significantly affects the critical surface roughness. It can be inferred for both type of stent that using shorter stent length than the plaque length leads to the decrease in the changes in surface roughness after balloon removal. This result demonstrated that the plaque length of type II, which had same length as the stent, is the most recommended model to be implemented in the actual stenting. This information may be valuable for practitioners and doctors to choose the stent length and to locate the appropriate stent in the implantation process. In addition, the simulation results can also be used as the basis to design the initial surface roughness for the improvements of the stent performance and to perform the stent coating at its critical surfaces.

2.6 STUDY LIMITATION AND FUTURE WORKS

This investigation presents the finite element analysis to predict the changes in surface roughness due to the different length of concentric plaque. In the actual conditions, the shape of the plaque is eccentric circumferentially and axially which become a cause of the plastic strain deformation in any part of the stent surface and eventually alter the surface roughness. In addition, the experimental data was not obtained from the actual Palmaz or Sinusoidal stent, but it came from a test piece of the tensile test specimen. There is only one directional stress acting in the tensile test specimen, i.e. the axial stress. However, in the expanding and deflating process of stent, the radial pressure loading gives three directional stresses acting in the stent, i.e. radial, axial, and circumferential stress [25]. The elevated stress level causes the different grain boundary elongation, which ultimately affects the magnitude of the plastic strain and the changes in surface roughness comprehensively. More sophisticated expansion models maybe required in future works. Addressing on the correlation between 2D surface roughness and plastic deformation of SUS316NG, safety factor may be applied and need to be investigated in future work, because the 2D surface roughness has obtained from average roughness (R_a), which is lower than actual peak of surface roughness profile.

References

[1] O'Brien, B. and Carroll, W., 2009. The evolution of cardiovascular stent materials and surfaces in response to clinical drivers: a review. Acta Biomaterialia 5, 945–958.

[2] DePalma, V.A et al., 1972. Investigation of three-surface properties of several metals and their relation to blood compatibility. Journal of Biomedical Materials Research 6, 37–75.

[3] Hecker, J.F. and Scandrett, L.A., 1985. Roughness and thrombogenicity of the outer surface of intravascular catheters. Journal of Biomedical Materials Research 19, 381–395.

[4] Denstedt, J.D. et al., 1998. Biomaterials used in urology: current issues of biocompatibility, infection, and encrustation. Journal of Endourology 12, 493–500.

[5] Palmaz, J.C. et al., 1999. Influence of surface topography on endothelialization of intravascular metallic material. Journal of Vascular and Interventional Radiology 10, 439–444.

[6] McLucas, E. et al., 2006. An investigation into the effect of surface roughness of stainless steel on human umbilical vein endothelial cell gene expression. Endothelium 13, 35–41.

[7] Tepe, G. et al., 2002. Thrombogenicity of various endovascular stent types: An in vitro evaluation. Journal of Vascular and Interventional Radiology 13, 1029–1035.

[8] Zhao, H. et al., 2002. Electrochemical polishing of 316L stainless steel stotted tube coronary stents. Journal of Materials Science: Materials in Medicine 13, 911–916.

[9] Hryniewicz, T. et al., 2008. Surface characterization of AISI 316L biomaterials obtained by electropolishing in a magnetic field. Surface and Coatings Technology 202, 1668–1673.

[10] Mizuno, T. and Mulki, H., 1996. Changes in surface texture of zinc-coated steel sheets under plastic deformation. Wear 198, 176–184.

[11] Wichern, C.M. et al., 2004. Surface roughness changes on a hot-dipped galvanized sheet steel during deformation at low strain levels. Acta Materialia 52, 1211–1222.

[12] Wichern, C.M. et al., 2005. Surface roughness of a hot-dipped galvanized sheet steel as a function of deformation mode. Journal of Materials Processing Technology 160, 278-288.

[13] Al-Qureshi, H.A. et al., 2005. Grain size and surface roughness effect on the instability strains in sheet metal stretching. Journal of Materials Processing Technology 170, 204–210.

[14] Wouters, O. et al., 2005. On the evolution of surface roughness during deformation of polycrystalline aluminum alloys. Acta Materialia 53, 4043–4050.

[15] Ju, F. et al., 2008. On the finite element modelling of balloon-expandable stents. Journal of The Mechanical Behavior of Biomedical Materials 1, 86–95.

[16] Jiménez, M.A. et al., 2007. The influence of contact pressure on the dynamic friction coefficient in cylindrical rubber-metal contact geometries. IUTAM Bookseries of Symposium on Computational Methods in Contact Mechanics 3, 257–275.

[17] Mummert, J. et al., 2012. Determination of radial force and coefficient of friction with a self-expanding transcatheter aortic valve stent. Bioengineering Conference (NEBEC) 38th Annual Northeast, 189–190.

[18] Dunn, A.C. et al., 2007. Macroscopic friction coefficient measurements on living endothelial cells. Tribology Letters 27, 233–238.

[19] Chua, S.N.D. et al., 2003. Finite element simulation of stent and balloon interaction. Journal of Material Processing Technology 143–144, 591–597.

[20] ANSYS Mechanical APDL Element Reference. ANSYS Inc., U.S.A., p. 1011.

[21] ANSYS Mechanical APDL Element Reference. ANSYS Inc., U.S.A., p. 673 and 739.

[22] Lally, C. et al., 2004. Elastic behavior of porcine coronary artery tissue under uniaxial and equibiaxial tension. Annals of Biomedical Engineering 32, 1355–1364.

[23] Lally, C et al., 2005. Cardiovascular stent design and vessel stresses: A finite element analysis. Journal of Biomechanics 38, 1574–1581.

[24] Migliavacca, F. et al., 2002. Mechanical behavior of coronary stents investigated through the finite element method. Journal of Biomechanics 35, 803–811.

[25] Chua, S.N.D. et al., 2004. Finite element simulation of slotted tube (stent) with the presence of plaque and artery by balloon expansion. Journal of Materials Processing Technology 155–156, 1772–1779.

[26] Pericevic, I. et al., 2009. The influence of plaque composition on underlying arterial wall stress during stent expansion: The case for lesion-specific stents. Medical Engineering & Physics 31, 428–433.

3 DEVELOPMENT OF ASYMMETRIC STENT FOR TREATING ECCENTRIC PLAQUE

3.1 INTRODUCTION

Development of stent as an effective treatment for peripheral artery diseases is growing rapidly with the finite element method (FEM). Types of stent structure and geometry vary over 100 different stent designs that are currently marketed and in evaluation [1]. Numerous studies have been performed associated with development and evaluation of the stent design using FEM, either by absence of plaque and arterial layer or with the interaction of both. Study considering the interaction of plaque and arterial layer was first promoted by Teo et al. in order to optimize the stent design by evaluating the displacement and stress distributions over the stent [2]. Accompanying this study, Auricchio et al. with absence of the expandable-balloon used a simple artery model and J&J Palmaz-Schatz like stent to investigate the actual cause for activation of the stent-related restenosis [3]. To characterize the stent deformation during the interaction with arterial layer, Chua et al. analyzed a slotted tube type of stent and obtained a conclusion that maximum surface contact stress becomes higher at the interaction point [4]. Following this work, Cui et al. examined a similar type of stent, which leads to a result that higher stress concentrations area in the vessel has a higher possibility of vascular injury [5].

In the meantime, Lally et al. compared two structural design of stents (S7 and NIR design) to examine the differences in the stress distribution within vessel wall. They found that there is strong proportional correlation between stress concentration within the vessel wall and restenosis rates [6]. Takashima et al. observed contact conditions between stent and the vessel wall. They found that the stent with higher number of cells and links distributed more contact area and might reduce the stimulus for induction of neointimal hyperplasia [7]. Expansion techniques for balloon expandable stent were studied by Gervaso et al. They concluded that the modelling technique of balloon seems essential to estimate a level of injury caused on arterial walls [8]. Meanwhile, more realistic simulation of stent deployment in human coronary artery was conducted by Gijsen et al. to avoid some limitations caused by the model simplication [9]. Continuing this work, Zahedmanesh et al. built almost similar simulation techniques but assigned the layer specific human coronary arterial wall properties to artery [10].

In the case of coronary bifurcations, Morlacchi et al. generated more realistic and comprehensive patient-specific simulation by comparing two clinical bifurcation cases [11]. More advanced study with various material properties was carried out by Pericevic et al. using three different plaque types; cellular, hypocellular, and calcified. They found that higher pressures can be applied to calcified plaques with a lower risk of arterial vascular injury and that the possibility of the plaques rupture was

still higher in spite of the lower fracture stresses [12]. Those studies employed unified layer assumption for both plaque and arterial layer because of the lack of experimental data for multilayer properties to save computational time. Some studies separately observed the characteristics of the arterial layer under certain pressure loading without stent intervention [13][14][15][16][17][18] [19].

3.2 BACKGROUND AND OBJECTIVE

Study on stent-plaque-vessel wall interaction using current multilayer properties materials for both plaque and vessel wall is quite limited. Both experimental study and numerical modeling are necessary to reveal the actual cause of the treatment failure using the stent. The first study on this area is conducted by Holzapfel et al. They used iliac artery with eccentric plaque shape. The study succeeded in generating scalar indicator for a better judgement of three different stent types for iliac artery treatment [20]. Another study used complex multilayer properties material to simulate a balloon type and system constraint using the artery constitutive model in FEM. Results indicated that a folded balloon is better than the rubber balloon for stent deployment. They also pointed out that the blood vessel should be modelled as a multilayer structure using a hyperelastic potential considering both the first and second stretch invariants as well as the anisotropy [21]. Nevertheless, none of the after-mentioned studies observed the effect of the plaque eccentricity on the design of stent geometry.

As shown above, almost all previous studies employed an assumption that both the symmetric stent geometry and the symmetric expansion are enough to treat all shape of stenosed artery. Applying the symmetric stent geometry to eccentric stenotic plaque shape generates non-uniform stress distribution within the vessel wall which lead to in-stent restenosis and also cause edge dissection [22][23][24][25]. Furthermore, deep injury induced by stent deployment is a more potent stimulus to neointima formation than stretch [26]. High-pressure deployment, wide strut openings, asymmetrical deployment, and increased balloon compliance may also contribute to vascular injury [27][28]. Therefore, the balance to be achieved is in attaining adequate final stent dimensions without an excess of vascular injury, because the vascular injury is intimately linked to in-stent neointima formation [29].

On the other hand, many experimental studies confirmed that the mechanical behavior of atherosclerotic plaque composition is dissimilar with healthy intimal layer, which also lead to the differences of its rupture criteria [30][31][32][33]. Therefore, redesigning stent using mechanical properties from current experimental data is needed. This chapter conducts the development of a new stent design to adapt the eccentric plaque obstruction using FEM.

3.3 METHODS

3.3.1 Finite Element Model

In order to develop new stent design, ANSYS R15.0 (ANSYS Inc., Pennsylvania, USA) was used as a simulation tool and CREO 2.0 (PTC Inc., Needham, USA) as a solid model builder. A stent model is made in CREO 2.0 because of its complexity, while models of balloon and stenosis carotid artery are directly built in ANSYS. Simulations contain three nonlinear dynamic transient analyses: i). Stent modification to build asymmetric-expanded stent, ii). Deformation characteristic changes during balloon dilatation, and iii). Induced stress distribution within arterial tissue and the surface roughness changes. The modification of stent can be conducted considering the simulation. There are four modifications to enable asymmetric dilatation: varying struts length, varying struts width, adding bridges, and varying curvature width of struts. Varying struts length is achieved by increasing incrementally the length of each strut 5% as long as the direction of stent expansion, while varying struts width is conducting the similar procedure for the width of each strut. Adding bridges is inserting connector links with different total length for each strut row. Varying curvature width of struts is conducted by widening curvature width of each strut 5% in the stages opposite to the direction of stent expansion.

Design consideration for modifying stent geometry is referred to Sullivan et al. [34] for retaining the profile of the stent surface and Chua et.al [35] for selecting the struts length and width variation. To examine each effect of the modification, FEM simulation of a symmetrical ring model from one unit strut cell is generated in ANSYS. The final design is compiled by combining positive results from the modification analysis. Following the final design, analyses on changes in deformation characteristic, induced stresses distribution and surface roughness changes are carried out. The effect of asymmetric geometry on the changes in deformation characteristic is observed by expanding the full stent model using the balloon. Meanwhile, stent should be inflated inside arterial tissue with atherosclerotic disease to observe the induced stress distribution and the changes in surface roughness.

There are two techniques to generate asymmetric expansion inside carotid artery narrowed by eccentric plaque: ordinary stent expanded by asymmetric type (offset) balloon and asymmetric stent type expanded by ordinary cylindrical balloon. Furthermore, to achieve better interpretation in comparative study, two others expansion techniques was also employed, i.e. ordinary stent expanded by ordinary cylindrical balloon and Asymmetric stent expanded by offset balloon. Combination of these expansion techniques in FEM simulation is expected to give better understanding of the deployment process of stent. The offset balloon is one of high-pressure balloons in medical device industry, which has expandable and non-expandable part [36], as displayed in Fig.3-1a. The ordinary cylindrical balloon used in this work (shown in Fig. 3-1b) is non-folded balloon type in order to simplify the finite element procedure and to obtain a more proportional comparison with the offset balloon.

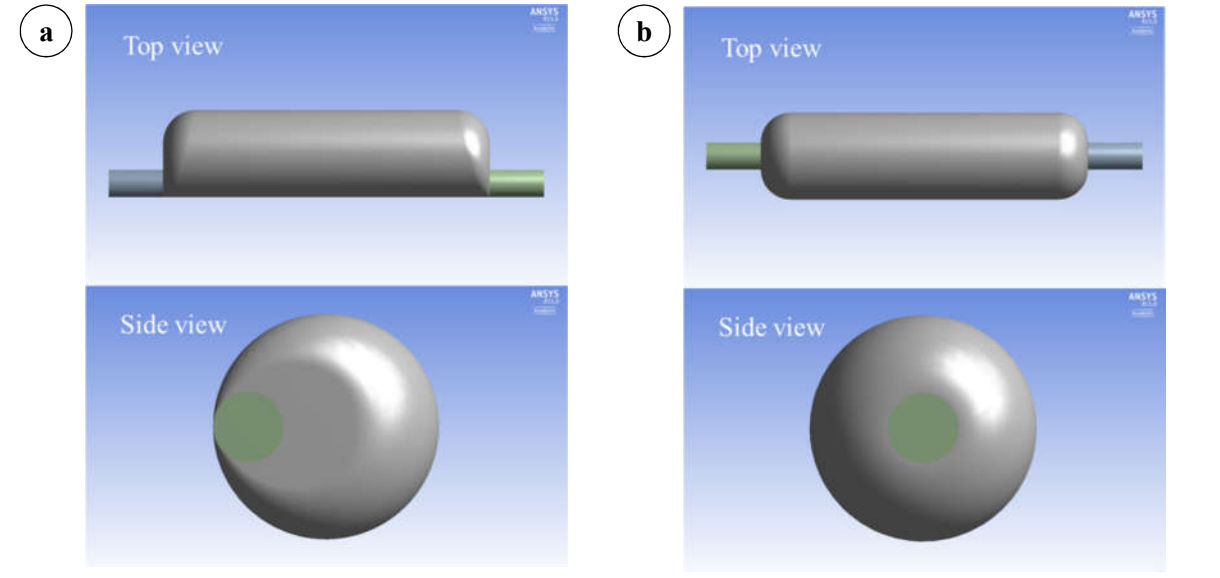
a
Top view
Side view
b
Top view
Side view

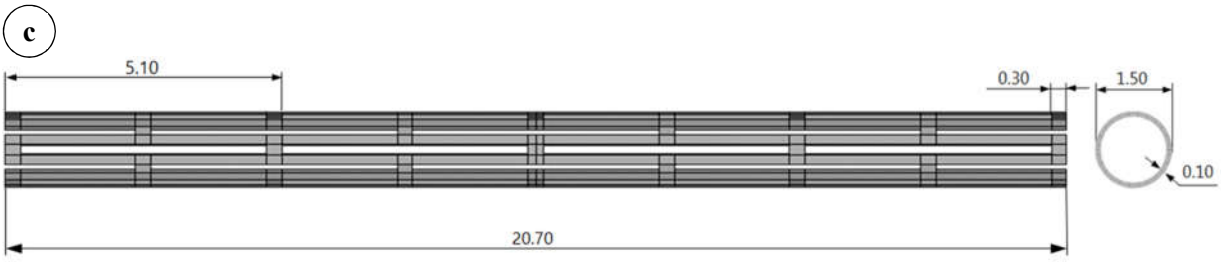
c
5.10
0.30
1.50
0.10
20.70

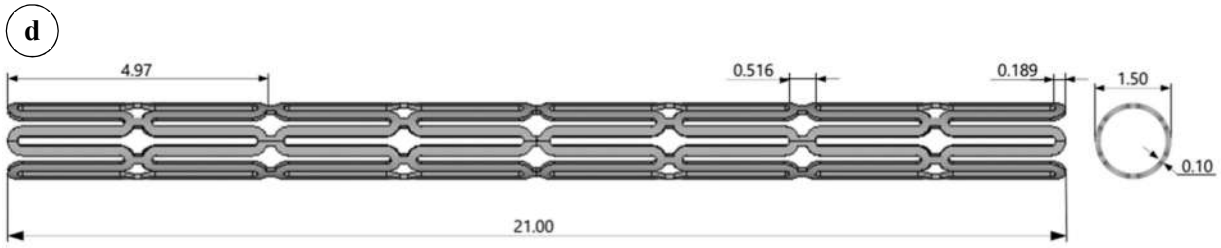
d
4.97
0.516
0.189
1.50
0.10
21.00

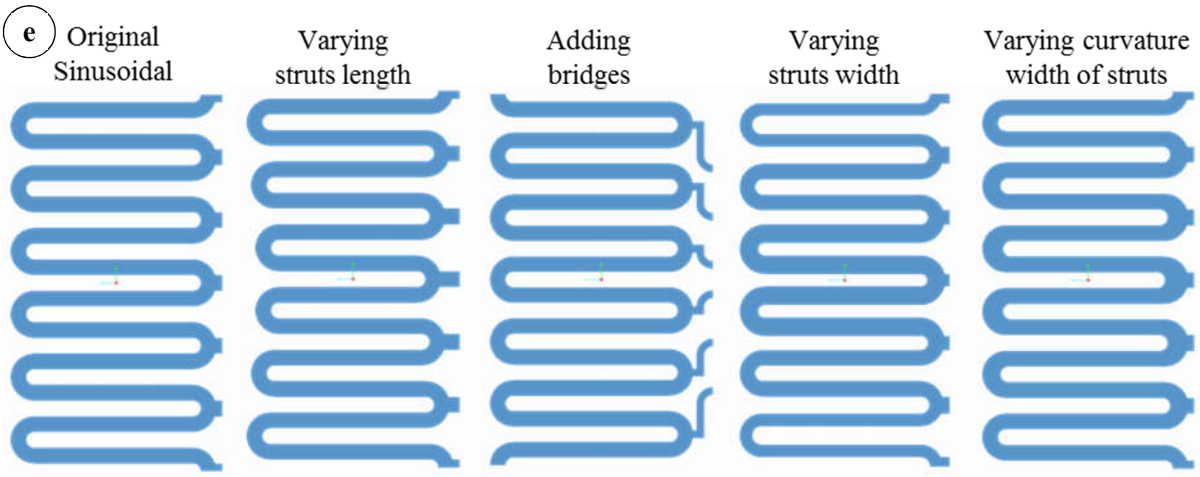
e
Original Sinusoidal
Varying struts length
Adding bridges
Varying struts width
Varying curvature width of struts

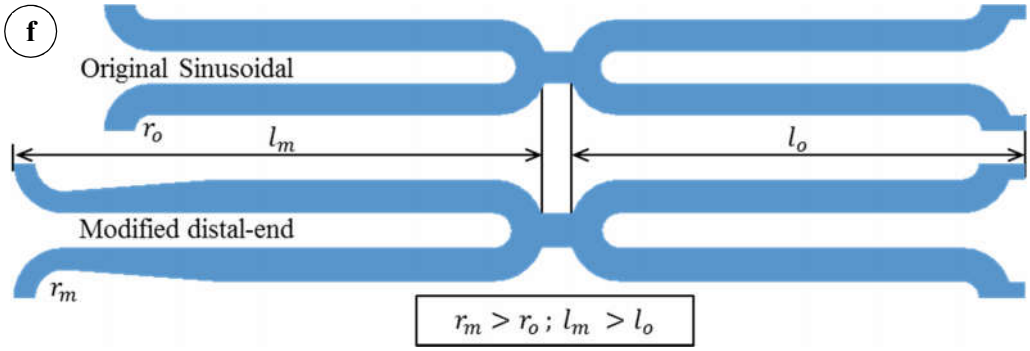

Figure 3-1: Balloons and stents type: (a) Offset, (b) Ordinary, (c) Front and side views of the Palmaz, (d) Front and side views of Sinusoidal stent. All units in mm. (e) Modification of Sinusoidal stent, (f) Modification to improve Ectropion angle.

Palmaz type is chosen for an ordinary stent model and the asymmetric-expanded stent is derived from Sinusoidal stent by modifying its struts length and width [37]. The geometry of Palmaz stent, Sinusoidal stent and modification techniques are shown in Fig. 3-1(c–e), respectively. One additional modification is needed to reduce Ectropion angle, which may be a cause of focal stresses on the vascular wall or plaque [5]. This modification is conducted on the end-struts of stent by lengthen the end-struts and straiten its curvature area as shown in Fig. 3-1f.

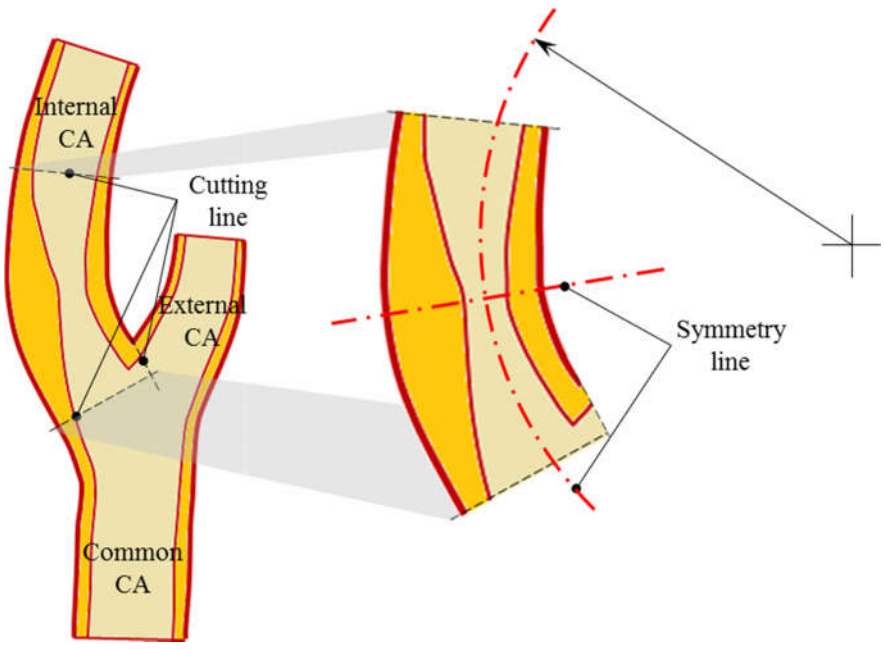

Figure 3-2: Axial section of the human carotid artery and cut ICA model.

For the analysis of the surface roughness changes and the stress distribution, carotid artery is chosen as a blood vessel type. The idealized model for carotid artery is derived from the human carotid artery

(CA), as performed by Iannaccone et al. [38] in their simulation. Internal carotid artery (ICA), where stent is located, has 5 mm diameter in the cross section and 3.5 mm diameter of it was the lumen. Considering ICA geometry approaches symmetric shape and for reducing computational time, the symmetrical geometric model with a little curvature is developed as shown in Fig. 3-3.

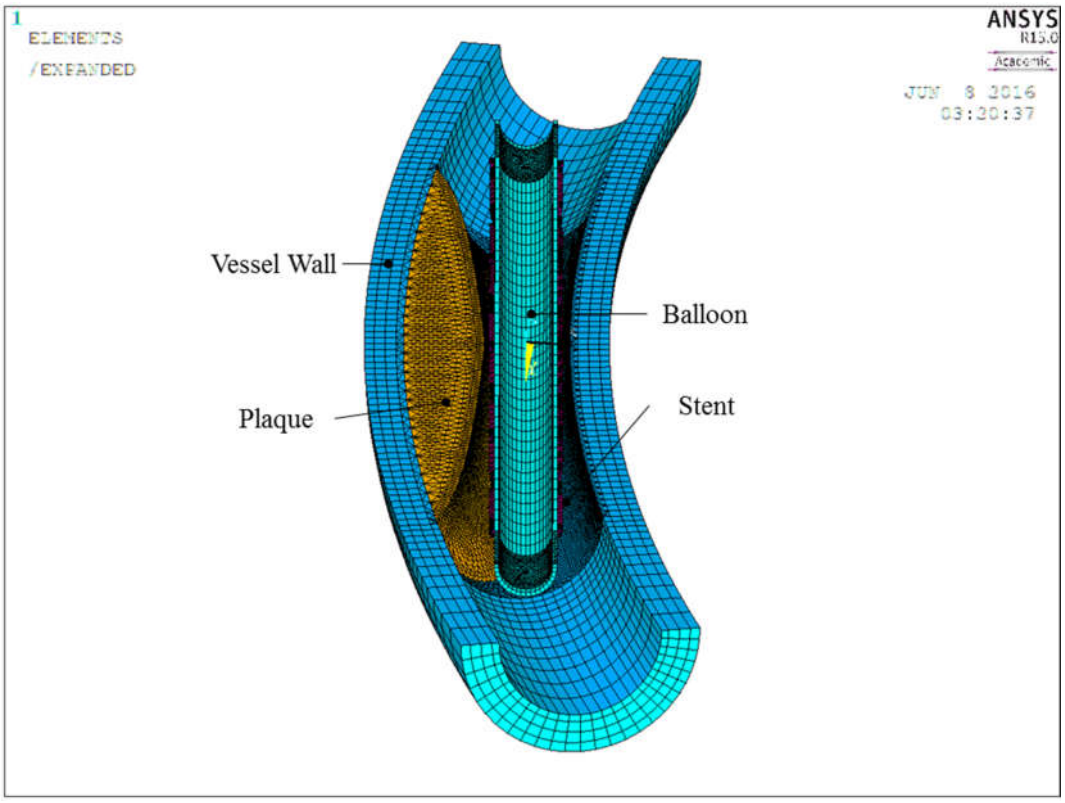

Figure 3-3: Finite element model used for stress distribution analysis.

One-fourth 3D simulation model for the analysis is shown in Fig. 3-3. The *X*, *Y*, *Z* coordinates represent the cylindrical coordinate system for both figures, where the X-axis is the radial direction, the *Y*-axis the circumferential direction, and the *Z*-axis the axial direction. The plane of symmetry that built the simulation model is the plane of *X*-*Y* and *X*-*Z*. The stent and plaque was designed to have the same length as suggested by the author [39] for minimizing the risk of edge dissection. To avoid difficulties in achieving convergence and to maintain reasonable element side size, the plaque edge could not follow a Gaussian shape.

The plaque is designed to have a little shorter than the stent, which covered in one side of vessel wall surface and another side is free-lesion area. It has a certain thickness so that would be a blockage for the blood vessel hole in with eccentricity index of 0.67. Eccentricity index is derived from the maximal and minimal thickness of the vessel [40][41], which is calculated by the formula as displayed in Fig. 3-4. The plaque was defined as concentric if this index was ≤ 0.5 and as eccentric if the eccentricity index was > 0.5.

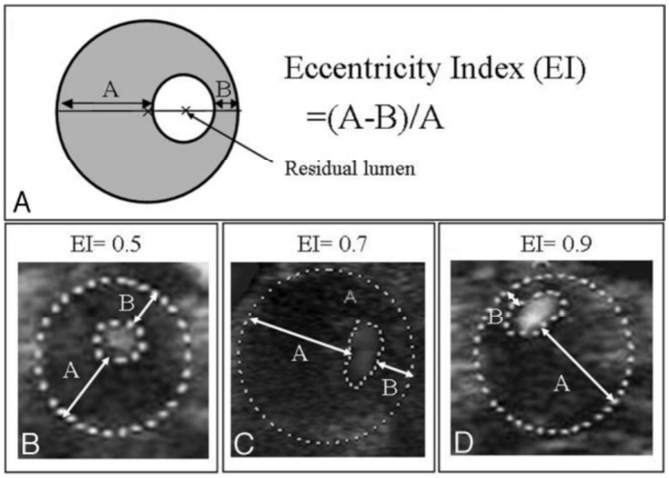

Figure 3-4: Measurement of eccentricity index.

3.3.2 Material Model and Behavior

All of simulation used material property of SUS316L for the stent and polyethylene terephthalate (PET) for the balloon. Multilinear isotropic properties for the stent are obtained by fitting curve from SUS316L tensile tests, whose chemical composition as shown in Table 3-1. Strain - stress curve from the tensile tests including the strain maintaining (tensile strain rate 0.1%/sec, 5% strain retained) and correlated multilinear isotropic properties is shown in Fig. 3-5.

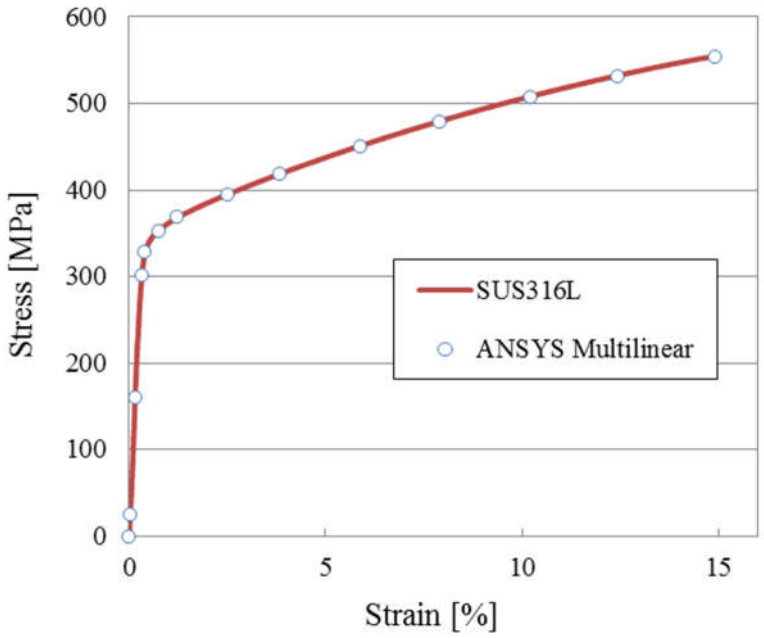

Figure 3-5: Stress-strain curve for SUS316L and corresponding 14 points multilinear properties

Particularly for analysis of surface roughness changes and induced stresses distribution, the human ICA and hypocellular plaque type are included in the simulation. The material models other than the stent were defined as isotropic hyperelastic (nearly incompressible) for the balloon, plaque, and arterial

tissue. The balloon used material properties defined by Chua et al. [4], both for the ordinary cylindrical balloon or the offset balloon. Material model for the plaque and vessel wall is compiled from Pericevic et al. [12]

Table 3-1: The chemical composition of SUS316L specimen

Steel type	Chemical composition (wt. %)								
	Cr	Ni	Mn	Mo	Si	C	S	P	Fe
SUS316L	18.0	15.0	2.0	3.0	≤1.00	≤0.03	≤0.03	0.045	Bal

Table 3-2: Material properties used in the analysis of surface roughness changes and stress distribution

Component	Material	Material behavior	Poisson's ratio	Density (tonne/mm^3)	Material constants
Balloon	Poly-urethane	Hyperelastic nearly incompressible	0.49	1.38E-9	Mooney-Rivlin 2 parameters: C_{10} = 1.0318 MPa; C_{01} = 3.6927 MPa d = 0.004261
Stent	SUS316L	Multilinear isotropic	0.33	7.99E-9	Fitting stress-strain curve resulted from pure tensile test
Hypocellular Plaque	Hypo cellular	Hyperelastic nearly incompressible	0.49	1.07E-9	Mooney-Rivlin 3 parameters: C_{10}= -0.8027 MPa; C_{01}= 0.8316 MPa C_{11}= 1.1576 MPa
Vessel Wall	Hypo cellular	Hyperelastic nearly incompressible	0.49	1.07E-9	Mooney-Rivlin 5 parameters: C_{10}= 0.0189 MPa; C_{01}= 0.00275 MPa C_{11}= 0.0857 MPa; C_{20}= 0.59043 MPa C_{30}= 0.00

3.3.3 Loading Conditions and Solution

Multiple load step of pressure loading of 1.6 MPa for the ordinary balloon and 1.75 MPa for the offset balloon was given to the inner surface of balloon in the outward direction for all simulation models during 1 second as shown in Fig. 3-6. After reaching 130% of the nominal diameter of the stent, it subsequently deflated for a half second to separate from the stent completely. For comparison analysis, starting time for balloon deflation is based on the similar nominal diameter of the stent rather than on the magnitude of the inflating pressure. This balloon deflation strategy is preferred for comparing stents with different total surface area, as conducted by Migliavacca et al. [43] and Zahedmanesh & Lally [44].

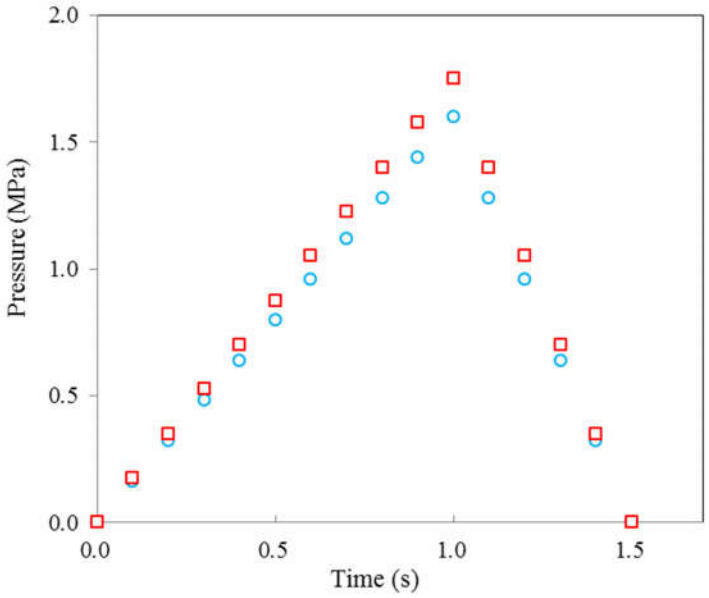

Figure 3-6: Time history of pressure loading

To maintain the dilatation shape of the offset balloon, coupling boundary conditions was used in the circumferential and radial direction as shown in Fig. 3-7. Global coordinate system used in Figs. 3-7*b* and *c* is the cylindrical coordinate system, which *X*, *Y* and *Z* axis are the radial, circumferential and longitudinal directions, respectively. The blue triangles show as the applied constraints and the *S* letters show as the symmetry boundary conditions. Coupling node, in order to generate the asymmetric expansion, is represented by green lines in the model. The red lines represent the pressure loading, which is in the outward direction, on the inner surface of balloon. In addition, the symmetry boundary conditions should be applied on the surface of the symmetry plane. Large deformation feature of ANSYS nonlinear transient analysis is activated in order to obtain Cauchy (true) stress and Hencky (logarithmic) strain as native FEM results.

The analysis of changes in the stent surface roughness can be conducted after balloon removal using the formulation obtained by the author [39]. It expressed the correlation between the 2D surface roughness and plastic deformation (*S.R.* – plastic strain) of SUS316NG, which has been previously stated in Eq. 2-1. In the FEM simulation, the plastic strains are derived from the equivalent plastic strains, while the induced stresses are taken from the von Mises equivalent stresses. Those values are recorded after nominal diameter of the dilated stent is achieved.

The relationship between strain and the surface roughness is obtained from the experiments using SUS316NG. The stress-strain relation of SUS316NG is a little bit different from that of SUS316L as shown Fig. 3-8. In this analysis, the relationship between strain and the surface roughness obtained from SUS316NG is used instead of that of SUS316L.

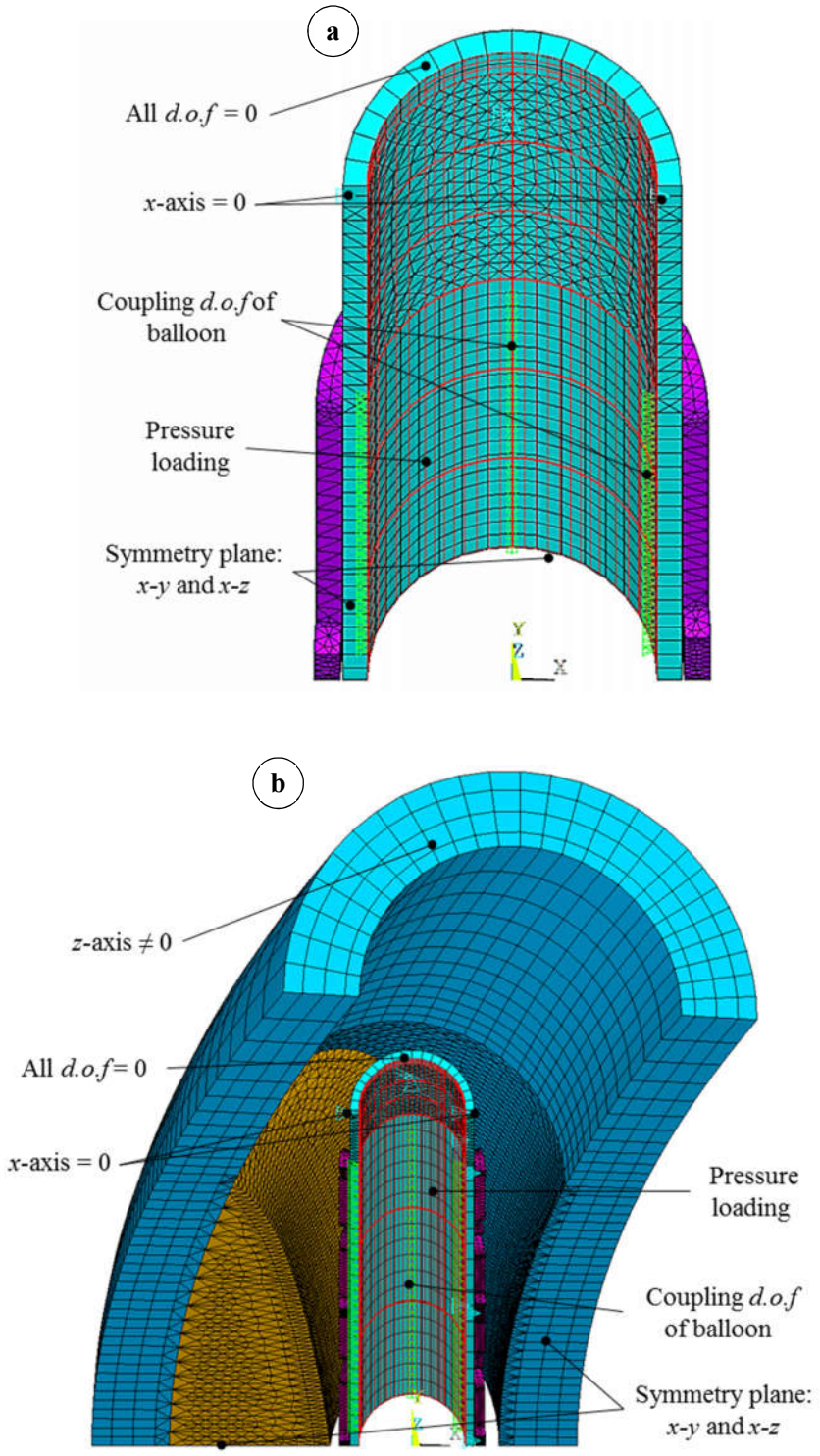

Figure 3-7: Boundary conditions applied for analyses of: (a) modification and deformation characteristics, (b) surface roughness changes and stress distribution.

There are mainly two reasons behind this. First reason is that the tendency of the relationship between strain and the surface roughness has not difference due to similar steel materials. The other is that the purpose of this analysis just is to show the method for estimating the surface roughness using the strain change due to the stent deformation, not to obtain the precise and specific surface roughness of the stent.

To discuss the precise surface roughness of the stent using the relationship between strain and the surface roughness, the scale effect should be considered. The scale effect may be huge effect on the surface roughness changes.

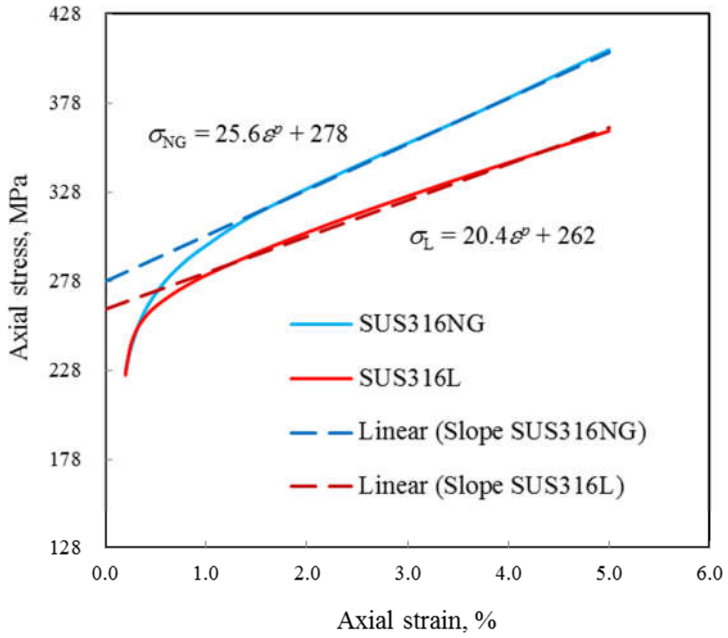

Figure 3-8: Comparison of the plastic deformation slope between SUS316NG and SUS316L

3.4 RESULTS AND DISCUSSION

3.4.1 Modification Analysis

Effect of modification on Sinusoidal stent is evaluated by measuring the distance between the struts, mapping the distribution of the equivalent plastic strain, and analyzing the geometrical shape after deformation. In this study, we introduce new definition to address a stent with non-symmetric dilatation, namely inflated- and fixed-side. The inflated-side is the distance between struts that face to the direction of expansion, while the fixed-side is vice versa. Figure 3-9 shows the modification effect of the struts on the maximum equivalent plastic strain. The distance between the stent struts affects the expansion of each strut in the circumferential direction. The corresponding equivalent plastic strain is needed to validate how large the dilatation between the struts affects the surface roughening after the plastic deformation.

It is indicated that all types of modification succeeded in inflating the stent asymmetrically. Varying struts width caused the largest asymmetric expansion by 1.83 mm of distance and had the minimal fixed-side by 0.41 mm of distance. While varying struts length had the minimal effect on the asymmetric expansion and its effect was almost equal to varying curvature width of struts. From the same bar chart in Fig. 3-9, it was also seen that the largest nominal diameter of stent is gained by adding

bridge because the distance summation of the inflated-side, middle-side and fixed-side are supposed as half of stent circumference. In the meantime, the maximum equivalent plastic strain after balloon removal was caused by varying struts width, which reached 0.2125 mm/mm. This tendency is more understandable by verifying the result with Fig. 3-10.

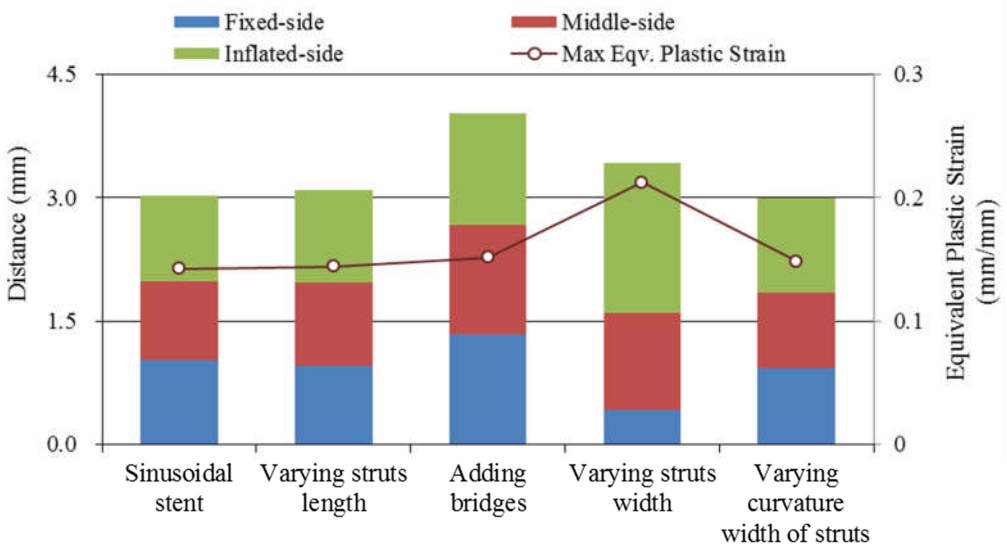

Figure 3-9: Composite bar chart displays effect of modifications on distance between the struts and corresponding equivalent plastic strain

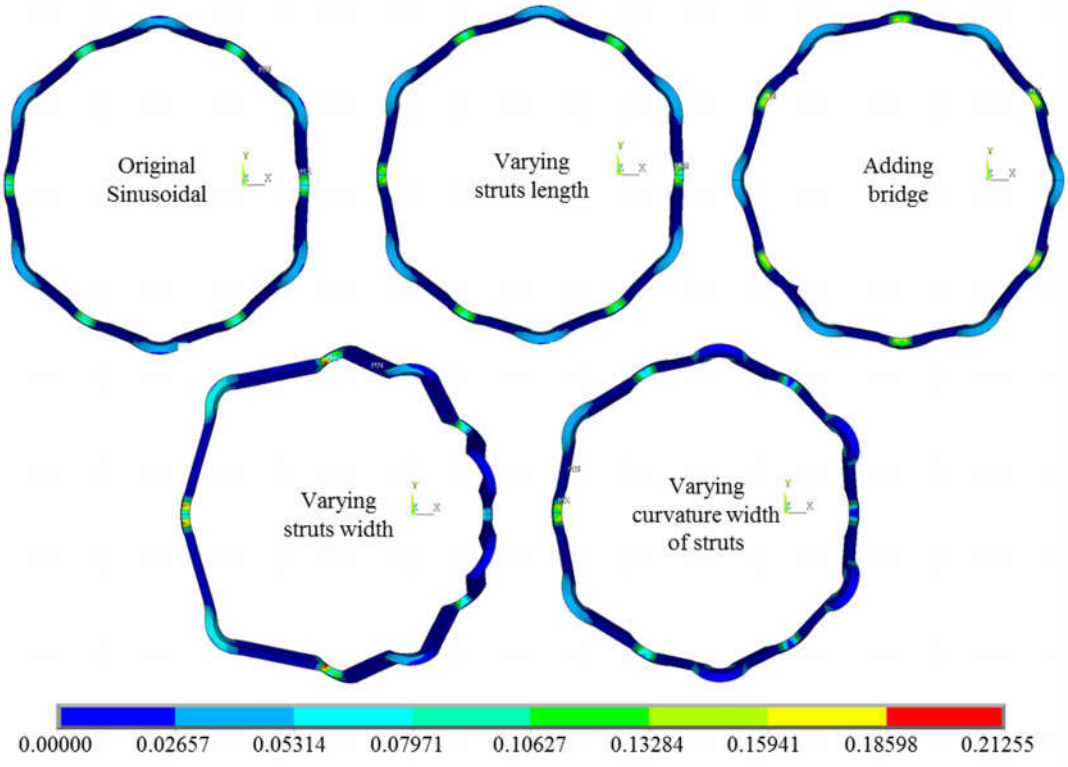

Figure 3-10: Side view of the models with unified legend below.

All type modification changed circumferential shape of stent, except for varying struts length. The most regular and better shape stent is achieved by adding bridges. Varying struts and curvature widths of struts should be carefully applied in design of the stent structure, because broadening a part of struts withstands stent expansion while another part without any modification is expanding freely. Another important finding is that adding the bridges/connector links in stent structure could decrease balloon pressure needed for the expansion. In order to generate moderate changes in the plastic strain and to have reasonable asymmetric expansion, combining positive modification results in structural stent geometry maybe a better solution to construct Asymmetric stent.

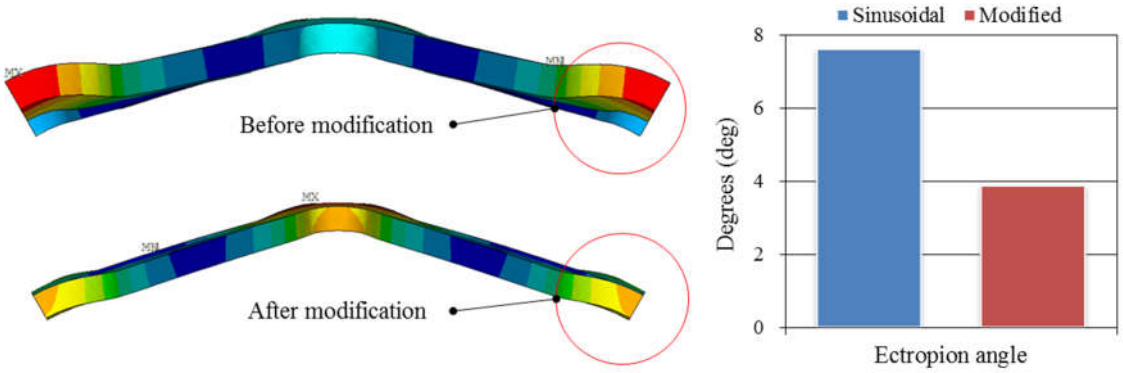

Figure 3-11: Modification effect on the end of stent struts.

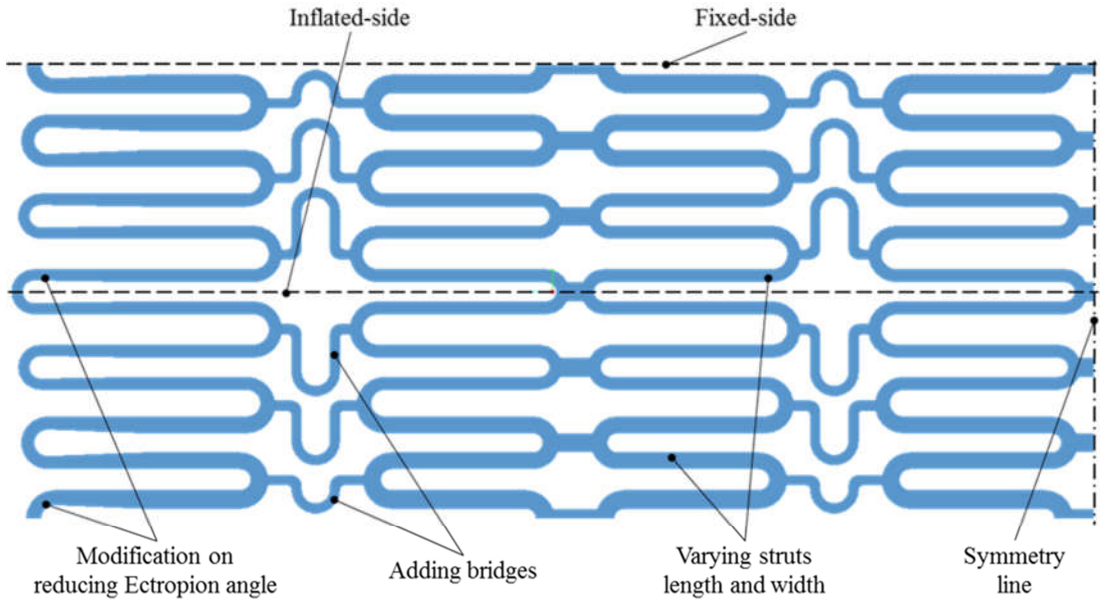

Figure 3-12: Flat view of final design of Asymmetric stent, shown from central part to distal one.

Figure 3-11 demonstrates how large reduction achieved by modifying the end of stent struts to reduce Ectropion angle. It can be seen by bar chart on the right side that lengthening the end-struts and straitening its curvature area decrease the degree of Ectropion angle significantly by 49% reduction.

This modification is expected to improve the stress distribution within the arterial layer surrounding the stent. Final design of Asymmetric stent is shown in Fig. 3-12. It is a flat view of the offset stent featuring with several types of modification. The length of struts is increasing 5% for each strut cell from the fixed-side to the inflated-side. On the contrary, the width of struts decreases 5% for each strut cell from the fixed-side to the inflated-side. An *U* bridge type is added, which has the shortest arm in the fixed-side and incrementally longer toward the inflated-side to support asymmetric expansion of struts. The design of the *U* bridge is chosen because it is short enough and enables the symmetrical modeling in the simulation. This model has similar nominal diameter and total effective length compared to Palmaz stent in the subsequent analyses.

3.4.2 Changes in Deformation Characteristic

Figure 3-13 depicts bar chart of the effect of stent geometry on the changes in deformation characteristic comparing between ordinary cylindrical balloon and offset balloon. It revealed that the offset balloon affects the changes of both dogboning and distal radii recoil. The most significant effect of the offset balloon is the dogboning. The dogboning is reduced 45.0% for Palmaz stent, 43.3% for Sinusoidal stent, and 41.8% for Asymmetric stent, respectively. As for the distal radii recoil, Asymmetric stent expanded by offset balloon had the largest reduction of 17.8%. While for the foreshortening, Asymmetric stent expanded by offset balloon has the opposite tendency compared to other stent type expanded by offset balloon. The other parameters such as the central radii and longitudinal recoils show small effect on the deformation characteristic changes.

It can be also noticed from Fig. 3-13 that longer slot of the struts of Asymmetric stent gives higher radial recoil compared to Palmaz with Sinusoidal stent. The result is in accordance with Migliavacca et al. [43] study. It is seen, however, that central radii recoil of Asymmetric stent decreased around 20% compared to Palmaz and Sinusoidal stent for both type balloon expansion. This opposite phenomenon between distal and central radii recoil is experienced by Asymmetric stent due to having longer struts. This result suggests that Asymmetric stent has more flexible geometry arrangement against Palmaz stent. Furthermore, the dogboning of Asymmetric stent is reduced more than 50% comparing with Sinusoidal stent. It also noted that the modification on the end stents is effective to recover Ectropion angle. This means that the focal stresses on arterial layer at the end of stent can be controlled by it [5][45].

It can be particularly seen from Fig. 3-13*c* that the dogboning phenomenon affects the foreshortening tendency in the case of Asymmetric stent, though improving the dogboning has a priority than reducing the foreshortening. The method to reduce the dogboning phenomenon has been conducted by Auricchio et al. and Wang et al. To keep uniformity of stent expansion, Auricchio et al. added small distal struts [3]. After stent deployed, the small distal struts deformed larger than other struts part so

that could aggravate surface roughening. Meanwhile, Wang et al. used a broadened strut of the end ring of stent [46].

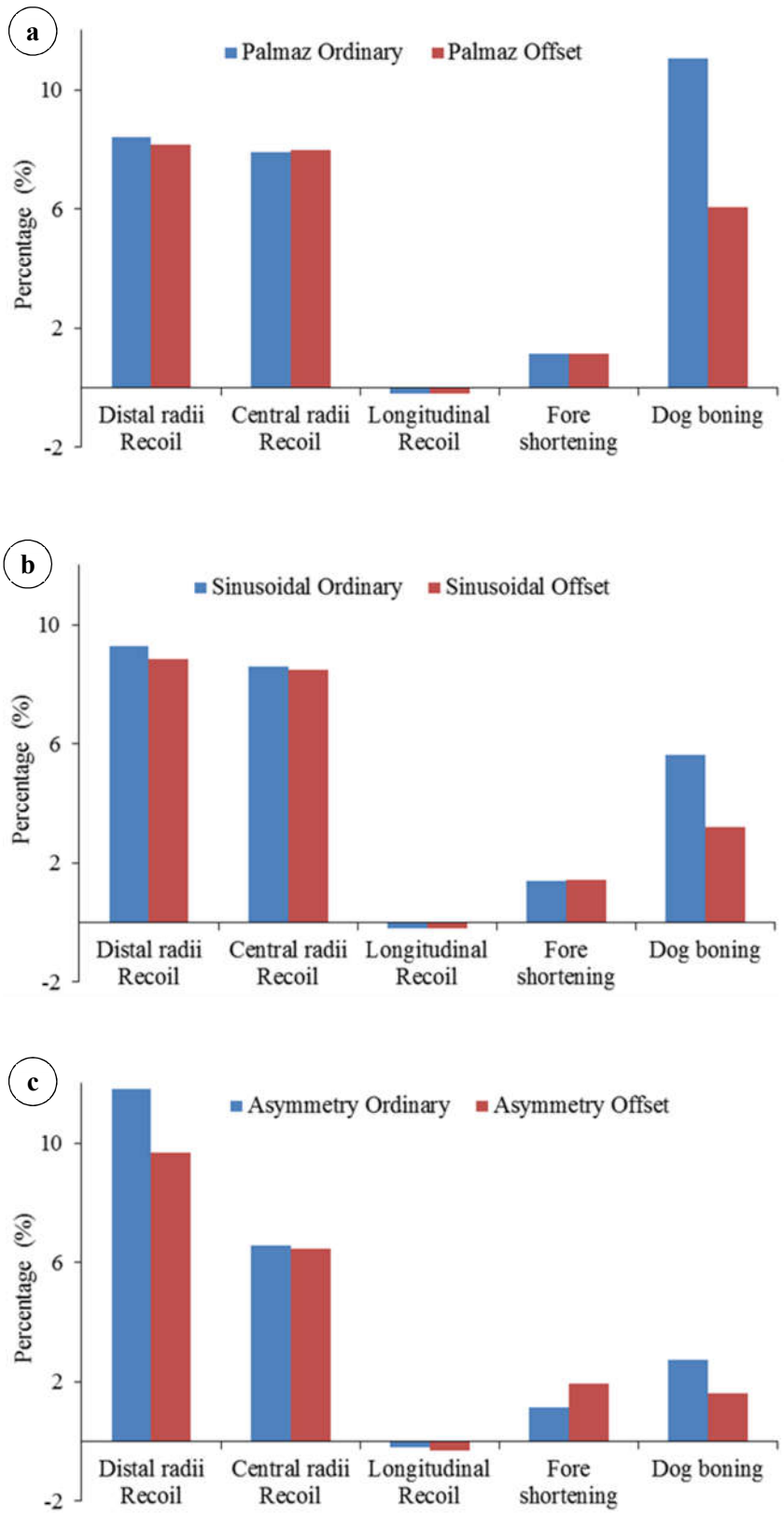

Figure 3-13: The changes of deformation characteristic after balloon removal: (a) The Palmaz, (b) Sinusoidal

stent, and (c) Asymmetric stent.

The aforementioned modification analysis demonstrated that the widening strut caused the difficulty to expand whereas other part still dilated normally. As also intended by Chua et al. [4], increasing the struts length may be better than increasing the struts width, because increasing the length of struts does not have a major impact on the stress distribution in the slotted tube stent. Therefore, lengthening the struts of the end ring of stent and narrowing curvature part of it is preferable in this study.

3.4.3 Changes in Surface Roughness

Figure 3-14 shows the surface roughening distribution on the stents surfaces for each expansion combination, with a unified legend provided below. Location of the fixed-side is on the top of stents and that of the inflated-side is vice versa. The red arrows show maximum changes in the stent surface roughness. The different distribution regions are clearly seen inside the red rectangle. It is described clearly that the geometry structure of the Asymmetric stent shifted the surface roughening distribution, particularly reduced the surface roughness changes on the fixed-side of Asymmetric stent using both the ordinary cylindrical and the offset balloon.

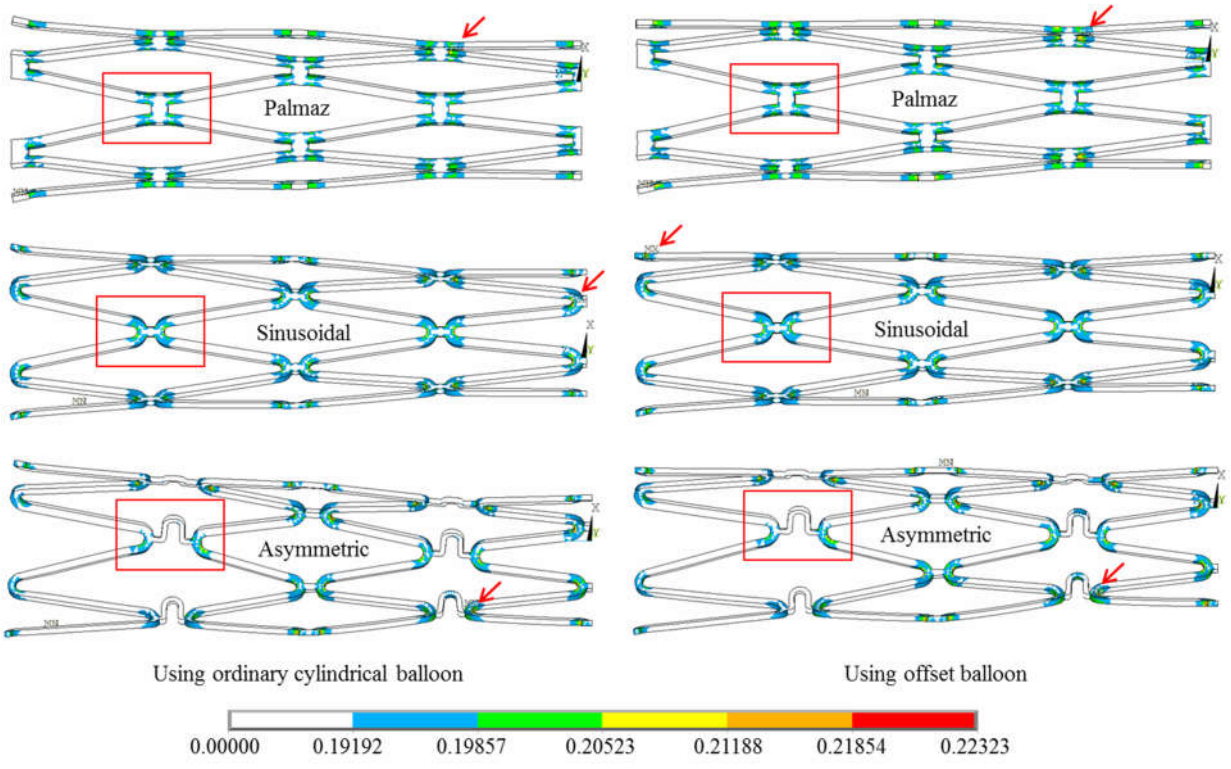

Figure 3-14: Distribution of surface roughening on the stent surfaces

Figure 3-15 shows the induced stresses within the vessel wall for each expansion combination, with a unified legend provided below. High concentration regions are bounded by the red rectangle. It can be seen that the offset balloon utilization tended to reduce the stress concentration area within the vessel

wall. It is also important to note that the highest stress regions are located at the vicinity of the shoulders of the plaque and do not affected by both type of balloons and stents. These results are consistent with the study of Li et al. [47] and Kiousis et al. [48]. The associated value of the surface roughness changes and the induced stresses are summarized in Table 3-2.

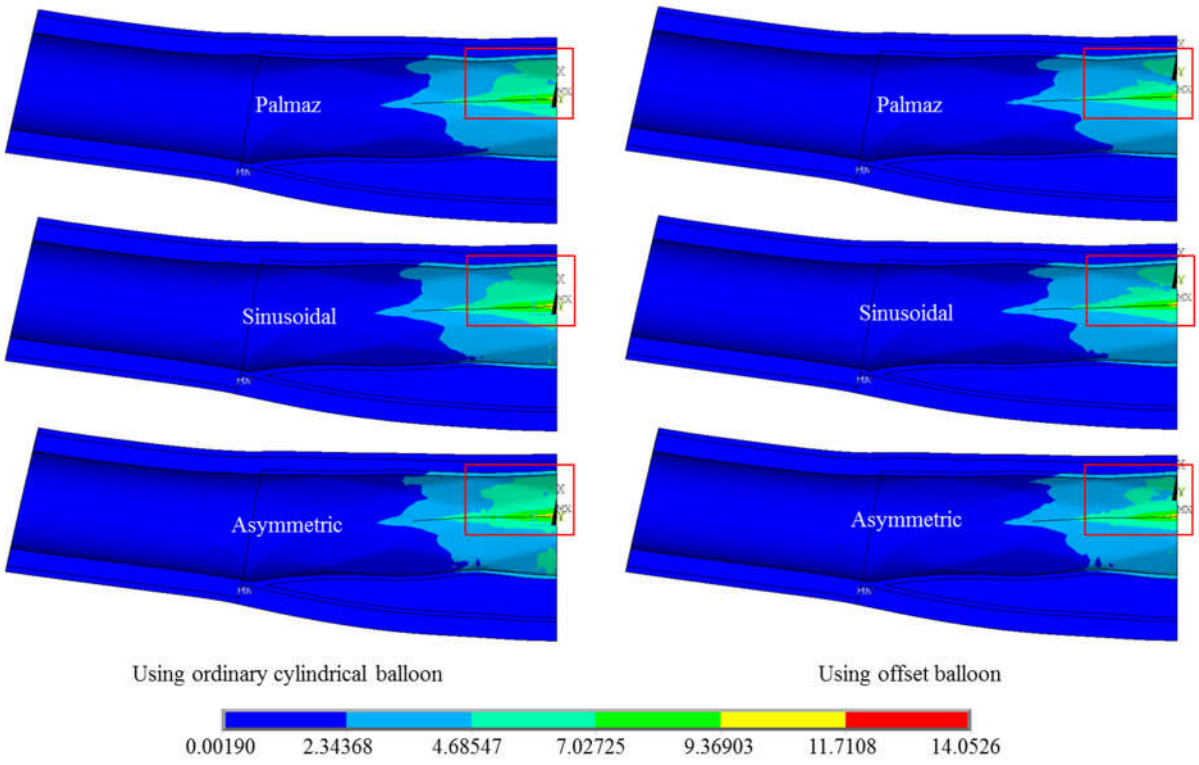

Figure 3-15: Distribution of induced von Mises stresses within intact arterial layer

Table 3-3: Magnitude of surface roughness changes and induced stresses

Combination of expansion	Surface roughness (μm)	Induced von Mises stress (MPa)
Palmaz - Ordinary	0.2111	13.62
Palmaz - Offset	0.2083	13.02
Sinusoidal - Ordinary	0.2110	14.02
Sinusoidal - Offset	0.2125	13.47
Asymmetric - Ordinary	0.2232	14.05
Asymmetric - Offset	0.2212	13.48

It is indicated that the various combination between stents and balloons type produce minor effect on all parameters observed. Asymmetric stent produced slightly larger surface roughening compared to

both Palmaz and Sinusoidal stents by 0.01 μm. Besides, it generated higher induced stresses than Palmaz and Sinusoidal stent by 0.4 MPa and 30 kPa, respectively. In combination with offset balloon, it could more drive the distribution of surface roughness changes. The offset balloon itself reduces the von Mises stresses in expansion all stents type by 4.13%. Important finding from the analyses is that the changes of surface roughness for all stent type was still below 0.671 μm, which is a threshold for stainless steel on the human vein endothelial cell to cause endothelial cell activation and inflammation [49]. Based on this threshold, Asymmetric stent type in this study was safely accommodated in the treatment as well as Palmaz or Sinusoidal stent.

3.5 CONCLUSIONS

This section conducted FEM simulation on the development of Asymmetric stent to treat eccentric plaque of carotid artery. Analyses to clarify the effect of modifications were conducted and comparison of changes in the deformation characteristics and the surface roughness were carried out. This study hypothesized that modified stent struts and bridges would affect its performance in the treatment of eccentric plaques. The results showed how geometry modifications affect the performance of stent expansion, as mentioned in following detail:

i. From the four implemented modification types, the struts length did not affect the change in the circumferential shape of stent. The additional bridges generated the better post-expansion circumferential shape of stent and decreased nominal pressure. The struts width and curvature width of struts should be carefully applied to avoid turning some struts part out.

ii. Lengthening the end ring of the stent struts and straitening its curvature area are effective to decrease in the degree of Ectropion angle. They also reduce the dogboning phenomenon.

iii. Asymmetric stent was succeeded to reduce the central radii recoiling and the dogboning phenomenon up to 20% and 50%, respectively. However, other parameters denoted a little influence on the changes in the deformation characteristic. The offset balloon demonstrated the significant effects on the dilatation of Asymmetric stent, especially in reduction of the distal radii recoiling. The offset balloon also increases the foreshortening a little.

iv. All type of the stent studied here was safely used in the treatment because the changes in the surface roughness remains small. Asymmetric stent has a comparable effect with Sinusoidal stent in terms of the changes in the surface roughness and the induced stresses. In combination with offset balloon, it could more drive the distribution of the surface roughness changes.

In the deployment of Asymmetric stent, positioning of its inflated-side inside a blocked artery to

oppose eccentric obstruction precisely without any malapposition becomes one of difficult task. Nowadays, the advanced technology has managed to find a better way in treatment of atherosclerotic diseases. Using Optical Coherence Tomography (OCT) in combination with steerable rotating catheter enables high-resolution intraluminal imaging of plaque shape and helps the doctors to locate Asymmetric stent properly. OCT is an emerging technology for performing high-resolution cross-sectional imaging. OCT is analogous to ultrasound imaging, except that it uses light instead of sound [50]. The steerable rotating catheter itself is a steerable catheter with rotating head, which is possible to be designed and developed further in order to locate Asymmetric stent properly. Besides, experience of a doctor or physician will greatly determine the outcomes of stenting process.

3.6 STUDY LIMITATION AND FUTURE WORKS

In the development of novel stent, analysis on the interaction between the stent and arterial tissue is necessity. As a first step of the new stent design, a series of analyses focused on the geometry characteristics and stress distribution was conducted. Further investigation should be considered the rupture analysis on arterial tissue using multilayer material properties and specific damage parameters for human carotid artery and human carotid plaque as recommended by Hozapfel et al. [51].

FE model simplification in this study and isotropic behavior used for the plaque or arterial tissue give room for the improvement. One may argue that considering internal CA from carotid bifurcation as a symmetry model is presumptuous step in FEM. Besides, using anisotropic behavior to analyze the stress distribution may be considered more appropriate. The study of the anisotropic model for stent-arterial layer interaction was conducted firstly by Holzapfel et al. [52]. Afterwards, the necessity of anisotropic model in the simulation of stent-arterial layer interaction is still a debate among researchers, because of its complexity in FEM application. On the other hand, even the anisotropic model of plaque or arterial layer is necessary, the results of simulation with the isotropic model remains able to be considered in accordance with the comparative study of Schmidt et al. [53]. Therefore, the authors believe that the method and result of the simulation could be useful as representatives of the development of new stent design. Nevertheless, considering asymmetric behavior in the analysis of plaque rupture or vessel wall inflammation may be a better method to observe Asymmetric stent in the future.

References

[1] Stoeckel, D. et al., 2002. A survey of stent designs. Minimally Invasive Therapy &Allied Technology 11, 137–147.

[2] Teo, E.C. et al., 2000. Design optimization of coronary stent using finite element analysis. Journal of American Society for Artificial Internal Organs 46 , 201.

[3] Auricchio, F. et al., 2000. Finite-element analysis of a stenotic artery revascularization through a stent insertion. Computer Methods in Biomechanics 4, 249–263.

[4] Chua, S.N.D. et al., 2004. Finite element simulation of slotted tube (stent) with the presence of plaque and artery by balloon expansion. Journal of Material Processing Technology 155–156, 1772–1779.

[5] Cui, F.S. et al., 2010. Effects of balloon length and compliance on vascular stent expanding. International Journal of Applied Mechanics 2, 681-697.

[6] Lally, C. et al., 2005. Cardiovascular stent design and vessel stresses: A finite element analysis. Journal of Biomechanics 38, 1574–1581.

[7] Takashima et.al, 2007. Simulation and experimental observation of contact conditions between stents and artery models. Medical Engineering and Physics 29, 326–335.

[8] Gervaso, F. et al., 2008. On the effects of different strategies in modelling balloon-expandable stenting by means of finite element method. Journal of Biomechanics 41, 1206–1212.

[9] Gijsen, F.J.H. et al., 2008. Simulation of stent deployment in a realistic human coronary artery. Biomedical Engineering Online 7, 23.

[10] Zahedmanesh, H. et al., 2010. Simulation of a balloon expandable stent in a realistic coronary artery: Determination of the optimum modelling strategy. Journal of Biomechanics 43, 2126–2132.

[11] Morlacchi, S. et al., 2013. Patient-specific simulations of stenting procedures in coronary bifurca-tions: Two clinical cases. Medical Engineering & Physics 35, 1272–1281.

[12] Pericevic, I. et.al, 2009. The influence of plaque composition on underlying arterial wall stress during stent expansion: The case for lesion-specific stents. Medical Engineerign & Physics 31, 428–433.

[13] Holzapfel, G.A. and Gasser, T. C., 2007. Computational stress-deformation analysis of arterial walls including high-pressure response, International Journal of Cardiology 116, 78–85.

[14] Akyildiz, A.C. et al., 2011. Effects of intima stiffness and plaque morphology on peak cap stress. Biomedical Engineering Online 10, 25.

[15] Cilla, M. et al., 2012. 3D computational parametric analysis of eccentric atheroma plaque: Influence of axial and circumferential residual stresses. Biomechanics & Modeling in Mechano-biology 11, 1001–1013.

[16] Khamdaengyodtai, P. et al., 2012. Effects of pressure on arterial failure. Journal of Biomechanics 45, 2577–2588.

[17] Wong et al., 2012. Effect of calcification on the mechanical stability of plaque based on a three-dimensional carotid bifurcation model. BMC Cardiovascular Disorders 12, 7.

[18] Badel, P. et al., 2014. Numerical simulation of arterial dissection during balloon angioplasty of atherosclerotic coronary arteries. Journal of Biomechanics 47, 878–889.

[19] Karimi, A. et al., 2014. Study of plaque vulnerability in coronary artery using Mooney–Rivlin model: A combination of finite element and experimental method. Biomedical Engineering: Applications, Basis and Communications 26, 1450013.

[20] Holzapfel, G.A. et al., 2005. Changes in the mechanical environment of stenotic arteries during interaction with stents: Computational assessment of parametric stent designs. Journal of Biomechanical Engineering 127, 166–180.

[21] Schiavone, A. and Zhao, L.G., 2015. A study of balloon type, system constraint and artery constitutive model used in finite element simulation of stent deployment. Mechanics of Advanced Materials and Modern Processes 1, 1–15.

[22] Schulz, C. et al., 2000. Coronary stent symmetry and vascular injury determine experimental restenosis. Heart 83, 462–467.

[23] Zahedmanesh, H. and Lally, C., 2009. Determination of the influence of stent strut thickness using the finite element method: Implications for vascular injury and in-stent restenosis. Medical & Biological Engineering & Computing 47, 385–393.

[24] Iannaccone, F. et al., 2014. The influence of vascular anatomy on carotid artery stenting: A parametric study for damage assessment. Journal of Biomechanics 47, 890–898.

[25] Schiavone, A. and Zhao, L.G., 2015. The importance of vessel factors for stent deployment in diseased arteries. Journal of Integrative Cardiology 1, 107–114.

[26] Gunn, J. et al., 2002. Coronary artery stretch versus deep injury in the development of in-stent neointima. Heart 88, 401–405.

[27] Rogers, C. et al., 1999. Balloon-artery interactions during stent placement: A finite element analysis approach to pressure, compliance, and stent design as contributors to vascular injury. Circulation Research 84, 378–383.

[28] Schulz, C. et al., 2000. Coronary stent symmetry and vascular injury determine experimental restenosis. Heart 83, 462–467.

[29] Schwartz, R.S. et al., 1992. Restenosis and proportional neointimal response to coronary artery injury: results in a porcine model. Journal of American College Cardiology19, 267–274.

[30] Maher, E. et al., 2009. Tensile and compressive properties of fresh human carotid atherosclerotic plaques. Journal of Biomechanics 42, 2760–2767.

[31] Teng, Z. et al., 2014. Material properties of components in human carotid atherosclerotic plaques: A uniaxial extension study. Acta Biomaterialia 10, 5055–5063.

[32] Akyildiz, A.C. et al., 2014. Mechanical properties of human atherosclerotic intima tissue. Journal of Biomechanics 47, 773–783.

[33] Chai, C.K. et al., 2014. Compressive mechanical properties of atherosclerotic plaques: Indentation test to characterize the local anisotropic behavior. Journal of Biomechanics 47, 784–792.

[34] Sullivan, T. et al., 2002. Effect of endovascular stent strut geometry on vascular injury, myointimal hyperplasia, and restenosis. Journal of Vascular Surgery 36, 143–149.

[35] Chua, S.N.D. et al., 2004. Effects of varying slotted tube (stent) geometry on its expansion behaviour using finite element method. Journal of Materials Processing Technology 155–156 , 1764–1771.

[36] Saab, M.A., 1999. Applications of high-pressure balloons. Advanced Polymers, Inc.

[37] Ju, F. et al., 2008. On the finite element modelling of balloon-expandable stents. Journal of Mechanical Behavior of Biomedical Materials 1, 86–95.

[38] Iannaccone, F. et al., 2014. The influence of vascular anatomy on carotid artery stenting: A parametric study for damage assessment. Journal of Biomechanics 47, 890–898.

[39] Syaifudin, A., 2013. Deformation analysis of balloon-expandable stents considering its surface roughness and viscoplasticity. Master Thesis of Graduate School of Engineering, Hokkaido University.

[40] Yamagishi, M. et al., 2000. Morphology of vulnerable coronary plaque: Insights from follow-up of patients examined by intravascular ultrasound before an acute coronary syndrome. Journal of American College of Cardiology 35, 106–11.

[41] Ohara, T. et al., 2008. Eccentric stenosis of the carotid artery associated with ipsilateral cerebrovascular events. American Journal of Neuroradiology 29, 1200–1203.

[42] Sommer, G. et al., 2010. Biaxial mechanical properties of intact and layer-dissected human carotid arteries at physiological and supraphysiological loadings. American Journal of Physiology: Heart and Circulatory Physiology 298, 898–912.

[43] Migliavacca, F. et al., 2002. Mechanical behavior of coronary stents investigated through the finite element method. Journal of Biomechanics 35, 803–811.

[44] Zahedmanesh, H., Lally, C., 2009. Determination of the influence of stent strut thickness using the finite element method: Implications for vascular injury and in-stent restenosis. Medical and Biological Engineering and Computing 47, 385–393.

[45] Migliavacca, F. et al., 2005. A predictive study of the mechanical behaviour of coronary stents by computer modelling. Medical Engineering & Physics 27, 13–18.

[46] Wang, W.Q. et al., 2006. Analysis of the transient expansion behavior and design optimization of coronary stents by finite element method. Journal of Biomechanics 39, 21–32.

[47] Li, Z.Y. et al., 2006. Stress analysis of carotid plaque rupture based on in vivo high resolution MRI, Journal of Biomechanics 39, 2611–2622.

[48] Kiousis, D.E. et al., 2009. A methodology to analyze changes in lipid core and calcification onto fibrous cap vulnerability: The human atherosclerotic carotid bifurcation as an illustratory example, Journal of Biomechanical Engineering 131, 121002.

[49] McLucas, E. et al., 2006. An investigation into the effect of surface roughness of stainless steel on human umbilical vein endothelial cell gene expression. Endothelium 13, 35–41.

[50] Fujimoto, J.G. et al., 2000. Optical coherence tomography: An emerging technology for biomedical imaging and optical biopsy 1. Neoplasia 2, 9–25.

[51] Holzapfel, G.A. et al., 2014. Computational approaches for analyzing the mechanics of atherosclerotic plaques: A review. Journal of Biomechanics 47, 859–869.

[52] Holzapfel, G.A. et al., 2005. Changes in the mechanical environment of stenotic arteries during interaction with stents: Computational assessment of parametric stent designs. Journal of Biomechanical Engineering 127, 166−180.

[53] Schmidt, T. et al., 2015. Influence of isotropic and anisotropic material models on the mechanical response in arterial walls as a result of supra-physiological loadings. Mechanics Research Communications 64, 29–37.

4 GEOMETRY ASSESSMENT OF ASYMMETRIC STENT

4.1 INTRODUCTION

Assessment on the geometry of new stent design is important. A stent is inserted through tortoise artery, which is often aggravated by the plaque obstruction; produce the track to be passed becomes more complex. Stent with good performance in geometric assessment should pass the flexibility, trackability, and conformability tests. The flexibility itself is an essential property in the stent delivery and long term results of stenting. Colombo et al. reported the hinge effect of the NIR stent on a tortuous vessel [1]. They also reported the longitudinal straightening effect of stents contributed on the occurrence major adverse cardiac events and angiographic restenosis [2]. Furthermore, flexible stents are easily inflated and show great adaptability to vasculature compared with a rigid stent. However, the flexible ones have smaller crush resistance. On the other hand, the flexibility is the one of the most important parameters allowing the restenosis to be prevented. The stent collapse incidence can achieve 5% of the implantation due to very flexible configuration [3].

A comparative analysis on coronary stent has been started by Rieu et al. [4], by conducting *in vitro* evaluation on the trackability, flexibility, and conformability of coronary stents. They tested 16 different types of coronary stents and determined a measurement for each parameter. The trackability of a stent was assessed by pulling each stent across both of tortuosities (90^o and 135^o angle with a radius curvature of 5 mm), while the flexibility was assessed by using the three-point flexion test. The conformability was also assessed by inflating the stent inside a rigid cylindrical tube with a 90° angle with a radius of curvature of 10 mm, as displayed in Fig. 4-1. It was indicated that their developed tools could be used by clinicians to evaluate mechanical characteristics of various coronary stents available on the market.

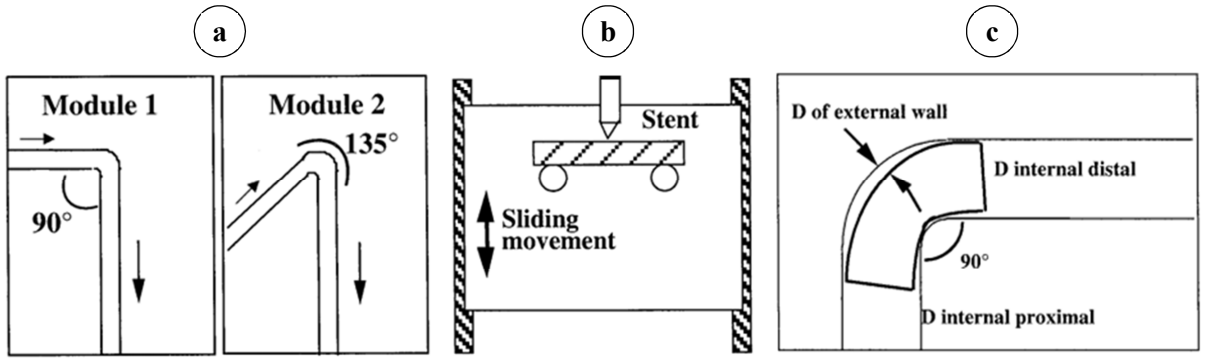

Figure 4-1: Assessments by Rieu et al.: (a) Trackability, (b) Flexibility, and (c) Conformability.

Different method of flexibility assessment was conducted by Mori and Saito [3]. The bending stiffness of a stent can be used as a proxy for stent flexibility. Two criteria are required for the precise assessment of the bending stiffness. First, the radial stent deformation must be restrained during testing to separate deformation by the bending moment and the radial load. Second, the bending test must be performed under the uniform moment conditions. Previous studies have proposed measurement of the stent bending stiffness using the cantilever beam method and the three-points bending test method. However, these methods do not satisfy the two requirements described above. Thus, Mori and Saito suggested that the four-point bending test has a benefit to measure the stent flexibility.

Following the study of Mori and Saito, Szabadits et al. [5] built an *in vitro* coronary vessel model with several tortoises of different angle for the trackability assessment, while one-point and four-point bending tests were chosen for the flexibility assessment, as shown in Fig. 4-2. The four-point bending test allowed a uniform bending moment without the radial deformation to the specimen, while the one-point bending test caused the maximum moment acts on the fixed end.

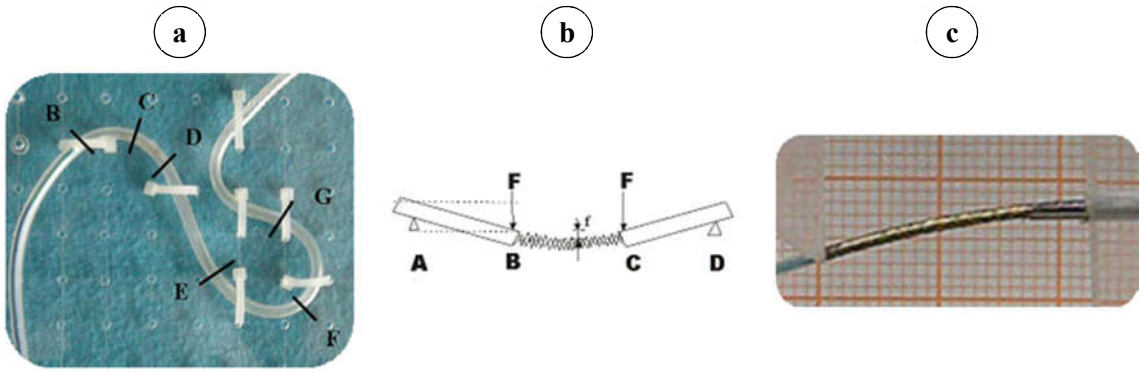

Figure 4-2: Assessments by Szabadits et al.: (a) Trackability, (b) 4-point bending flexibility, and (c) 1-point bending flexibility

They found that the flexibility of stents depends on the stent design more than raw materials. In general, a more flexible stent needs lower tracking force during the implantation. The L-605 raw material stents need lower track force to pass through in the vessel model than the 316L raw material stents. The sort and long stents passed through the curved vessel model in the different ways. The long stents nestled to the vessel wall at the outer arc and bent, while the short stents did not bend in the curve, only the delivery systems bent. Using the one-point bending, the author studied on five balloon-expandable coronary stent whose bending stiffness was lower comparing with the closed-cell stent [6].

First flexibility assessment (three-point bending test) using FEM was carried out by Petrini et al. [7] on Cordis BX-Velocity and Carbostent Sirius coronary stent. Two sets of simulations were performed: i.e. bending test in the unexpanded configuration and bending test in the expanded configuration.

Simulations were carried out with an increase of rotation up to 20° in the case of unexpanded stents and 10° in the case of expanded stents. The expanded configurations were obtained imposing a displacement to the external nodes on the unexpanded models up to an outer stent diameter equal to 2.5mm. Results expressed that the Cordis model showed a higher flexibility. Lower flexibility in the expanded configurations for both models was detected. However, this flexibility depends on the contact condition between the different parts of the struts.

In contrast to Petrini et al., Mori and Saito [3] built FEM simulation methods corresponded with their in vitro experiment. The in vitro experiment was the four-point bending test. Instead of using simulation of a complex 3D model with a large number of nodes and elements, they generated a simplified 2D model with two cells and one link for the investigation of the deformation mode and resistance under the longitudinal compressive load, as displayed in Fig. 4-3. In their study, the deformation mode simulated under compressive load was compared with the deformation mode observed in the bending test. The results indicated that the simplified FEM model, consisting of two cells and one link, was suitable to for the characterization of various stent structures.

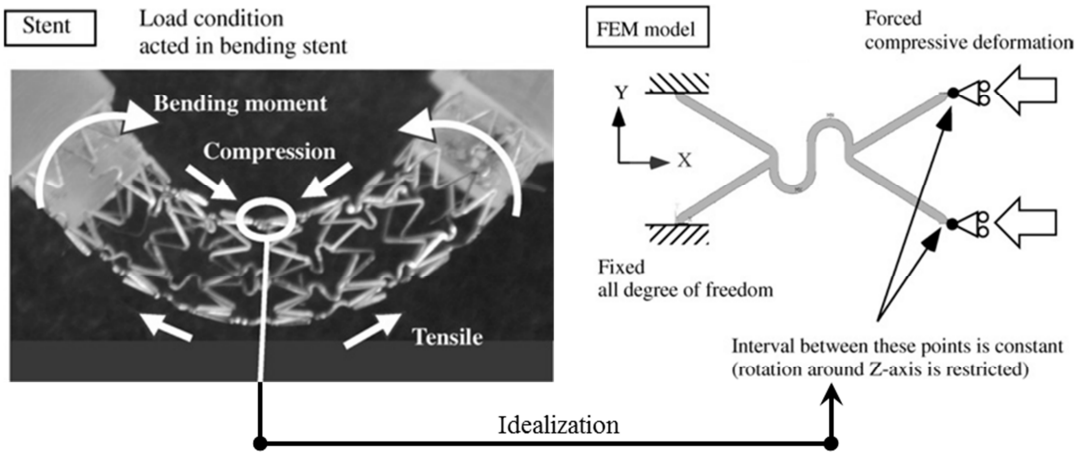

Figure 4-3: A simplified 2D model from four-point bending test

Wu et al. [8] introduced the multipoint constraint elements (MPC) to apply uniform bending moment on a unit model of an expanded coronary tubular stent, as depicted in Fig. 4-4*a*. Two types moment bending such as four-point and multiple bending were subjected to the models. It was concluded that this method can be used to compare the flexibility of different stents and provides a convenient tool for designers to pretest and improve bending characteristics of new stents. In other hand, a less complicated FEM study on unexpanded stent flexibility was performed by Kim et al. [9]. It was the three-point bending test, where three solid half-ring was used as the bending load and bending support, as shown in Fig. 4-4*b*.

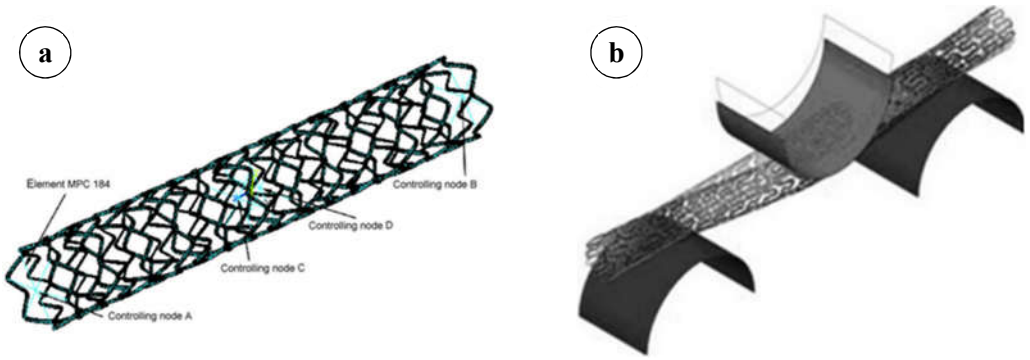

Figure 4-4: FEM of flexibility assessment: (a) MPC, (b) Three solid half-ring as load and supports.

4.2 BACKGROUND AND OBJECTIVE

The importance of mechanical characteristics assessment is revealed in aforementioned section. It is required for each new stent design before the clinical trial. This following sub chapter attempts to examine flexibility of Asymmetric stent, either in unexpanded or in expanded configuration, under single- and multi- point loading through FEM. Deriving an FEM assessment method from an actual test is often not an easy way, because of calculation time and number of *d.o.f* (degree of freedom) limitation. A simplification based on appropriate assumption should be taken into account carefully to avoid oversimplifying the problem, which could lead to the inaccurate solution.

4.3 METHODS

ANSYS R 15.0 is used to analyze structural displacement in all section of the assessment process. Nonlinear static analysis with the large deformation capability is chosen for analysis type. Sinusoidal stent is used as comparison in the assessment of Asymmetric stent.

4.3.1 Finite Element Method

There are two kind of assessment for stent flexibility, i.e. unexpanded and expanded stages. The flexibility in unexpanded configuration is needed to assess stent performance while delivered through tortuous vessel with catheter system. The flexibility in expanded configuration, indeed, is important information for a doctor / practitioner in choosing more appropriate stent type to be deployed in the treatment. The flexibility of stents in this study, either unexpanded or expanded one, is assessed utilizing Multi Point Constraint (MPC814) elements in ANSYS R15.0. Wu et al. [8] firstly introduced MPC184 to assess the expanded coronary stent, commercial Nirflex stent (Medinol Ltd., Tel Aviv, Israel), by comparing a unit cell of stent and whole stent model.

MPC184 comprises a general class of multipoint constraint elements that apply kinematic constraints between nodes. The elements are loosely classified here as *constraint elements* (rigid link, rigid beam, etc.) and *joint elements* (revolute, universal, etc.). All of these elements are used in situations that require some constraints to meet certain requirements. Since these elements are implemented using Lagrange multipliers, the constraint forces and moments are available for output purposes [10]. The constraint may be as simple as that of identical displacements between nodes. The constraints are also more complicated, such as those modeling rigid parts, or those transmitting motion between flexible bodies in a particular way. For example, a structure may consist of rigid parts and moving parts connected together with the rotational or sliding connections. The rigid part of the structure may be modeled with the MPC184 link/beam elements, while the moving parts may be connected with any of the MPC184 joint elements. The kinematic constraints are imposed using one of the following two methods:

- The direct elimination method, wherein the kinematic constraints are imposed by internally generated constraint equations. The degrees of freedom of a dependent node in the equations are eliminated in favor of an independent node.

    - The dependent degrees of freedom are eliminated. Therefore, the constraint forces and moments are not available from the element output table for output purposes. However, the global constraint reaction forces are available at independent nodes in the results file.
    - The direct elimination method should be used whenever it is available since the degrees of freedom at the dependent nodes are eliminated. Then, the problem size and solution time can be reduced.

- The Lagrange multiplier method, wherein the kinematic constraints are imposed using Lagrange multipliers. In this case, all the participating degrees of freedom are retained.

    - The Lagrange multiplier method should be used when the direct elimination method is not available or not suitable for the analysis purposes. In this method, the constraint forces and moments are available from the element output table.
    - The disadvantage of the Lagrange multiplier method is that the Lagrange multipliers are additional solution variables and, hence, the problem size and solution time become larger comparing with the direct elimination method.

Currently, the MPC184 rigid link/beam elements can use the direct elimination method or the Lagrange multiplier method. All other MPC184 element options use the Lagrange multiplier method only [11].

For expanded stent simulation, particularly, using feature UPGEOM (update geometry) in ANSYS is

necessity. This is useful to subject moment loading after balloon removal and stent deformed. MPC elements could also be built after executing UPGEOM. This command updates the geometry of the finite element model according to the displacement results of the previous analysis and creates a revised geometry at the deformed configuration. This command works on all nodes (default) or on a selected set of nodes. If this command is issued repeatedly, it creates a revised geometry of the finite element model in a cumulative fashion, i.e., it adds displacement results on the previously generated deformed geometry. The solid model geometry is not updated by this command [12].

Asymmetric stent from SUS316L, either unexpanded or expanded condition, is assessed its flexibility using the three-point bending, because this method is more simple and saving calculation time. Hyperelastic PET balloon is chosen to apply uniform pressure onto stent surface, while inflating the stent to achieve the expanded configuration. To restrain angular deformation and more save the computation process, a symmetry model (due to longitudinal and angular plane) of each stent type is constructed. Boundary conditions used in the flexibility assessment under the single-point loading is shown in Figs. 4-5 and 4-6 for the unexpanded and expanded configuration, respectively. Meanwhile, boundary conditions used in the flexibility assessment under the multi-point loading are shown in Fig. 4.7 for the unexpanded configuration.

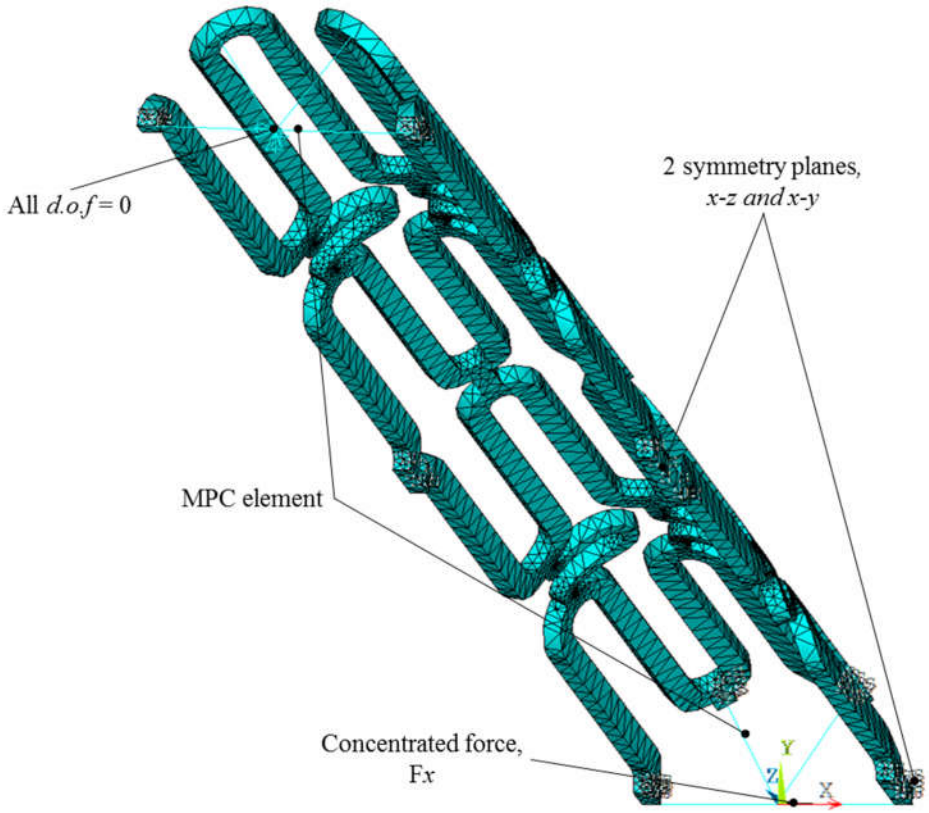

Figure 4-5: BC`s in single-point loading of unexpanded stent

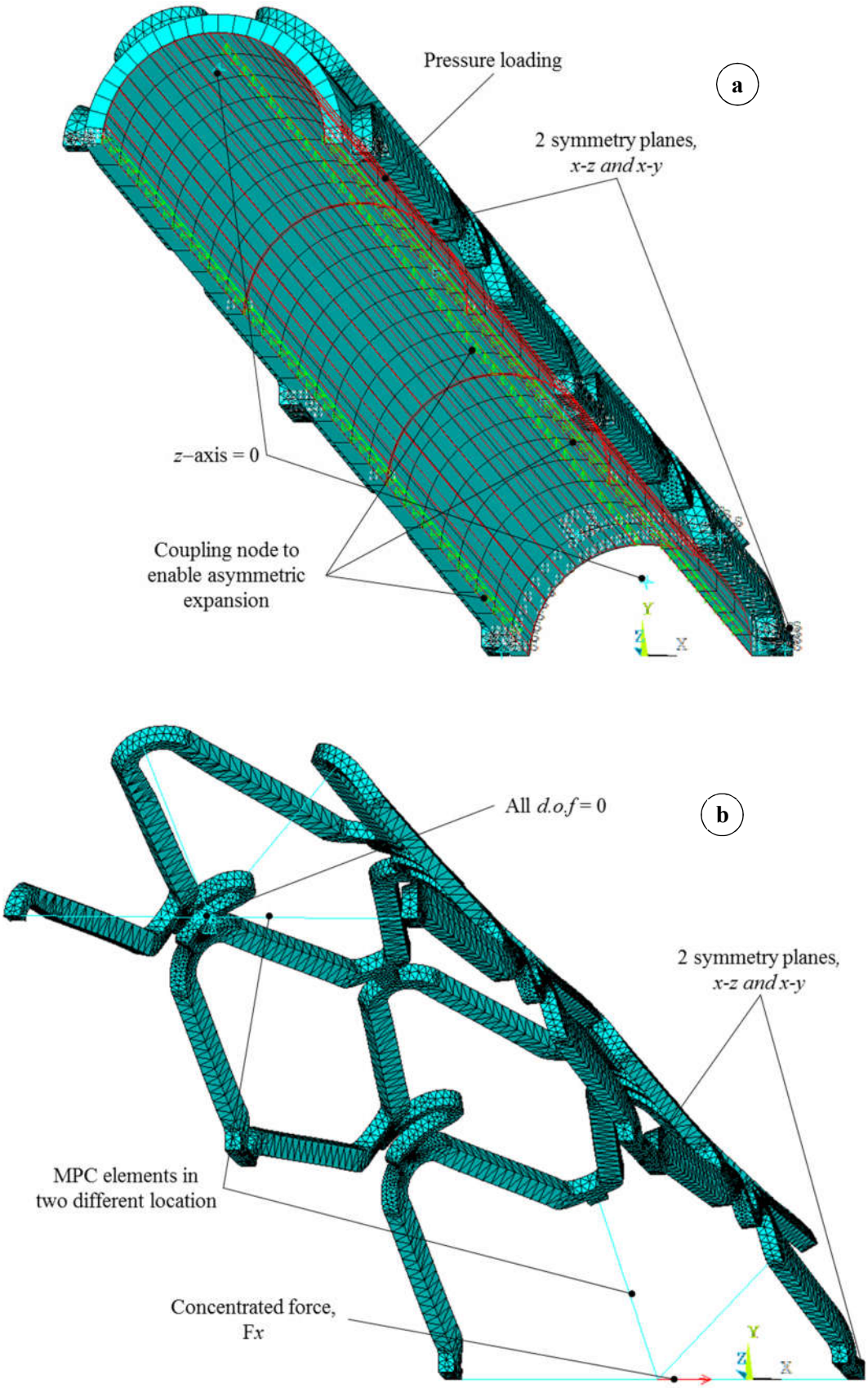

Figure 4-6: BC`s in single-point loading of expanded stent: (a) Before expansion, (b) After expansion and applying UPGEOM for stent component and EKILL for balloon component.

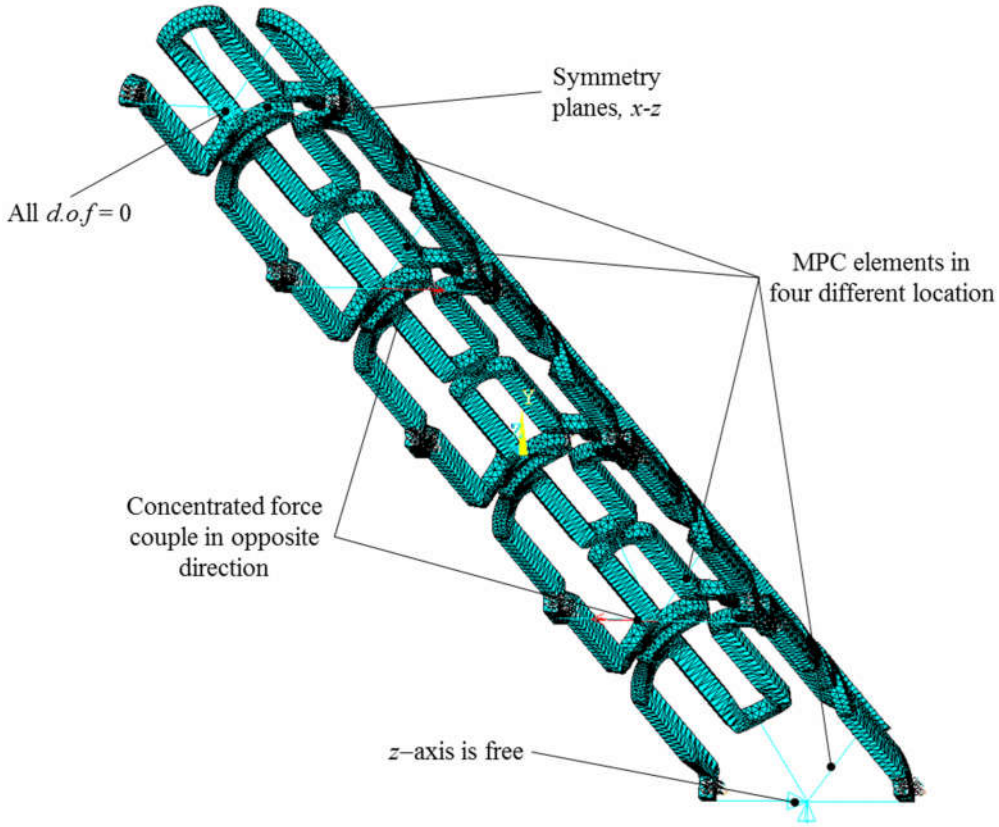

Figure 4-7: BC`s in multi-point loading of unexpanded stent

In the case of single-point loading, a concentrated force is imposed on the middle of stent in order to generate the moment loading as depicted in Figs. 4-5 and 4-6b. In term of multi-point loading, a couple of loading is imposed upon two points with the opposite direction as depicted in Fig. 4-7. All stent types, either unexpanded or expanded stents, are bent to a certain deflection magnitude by radial direction (x-axis). Determination of the stent flexibility, either single-point or multi point loading, is performed by correlating moment loading, bending stiffness, and flexibility versus deflection along x-axis direction.

4.3.2 Flexibility Measurements

According to the simply supported beam theory (as denoted in Fig. 4-8), the deflection caused by imposing concentrated force P (for single-point loading) on a stent can be obtained by Eq. 4-1:

$$def = \frac{PL^3}{48\,E \cdot I} \qquad (mm) \tag{4-1}$$

In this case, the deflection is the maximum displacement of the stent along x-axis direction and is easy to be obtained from FEM simulation. As a result, the bending stiffness $E{\cdot}I$ of the stent under the

single-point loading can be determined by Eq. 4-2. That shows the relationship between the moment of inertia *I*, the Young modulus *E*, free bending length *L*, and the bending deflection *def* and the concentrated force *P*.

$$E \cdot I = \frac{PL^3}{48\,def} \qquad \left(N \cdot mm^2\right) \tag{4-2}$$

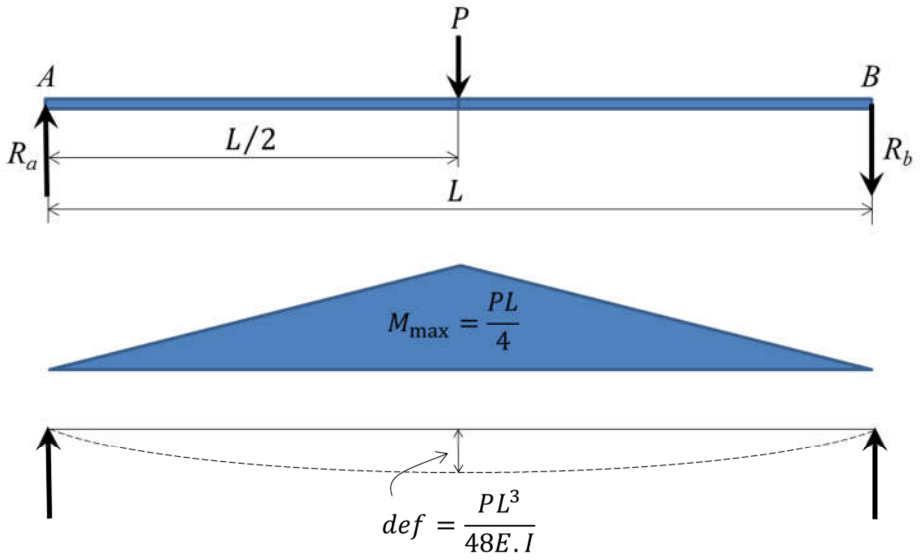

Figure 4-8: Flexibility for one-point bending test

The flexibility of a stent *F* can be easily expressed as follows [3][7],

$$F = \frac{1}{E \cdot I} = \frac{48\,def}{PL^3} \qquad \left(N^{-1} \cdot mm^{-2}\right) \tag{4-3}$$

In term of the multi-point loading, because of similar value of the point forces couple *P*, the generated reaction moment couple will also be similar each other. However, the deflections caused by the point forces couple is deferent each other. For the symmetric stent geometry, the deflection $(def)_1$ and $(def)_2$ is equal. Therefore, the bending stiffness, which is caused by a couple point forces *P* acted on the different surface of the stent with opposite directions in Fig. 4-9, can be determined in following Eq. 4-4, which is affected by deflection.

$$\left(E \cdot I\right)_1 = \frac{PL^3}{48\left(def\right)_1} \qquad \left(N \cdot mm^2\right)$$

$$\left(E \cdot I\right)_2 = \frac{PL^3}{48\left(def\right)_2} \qquad \left(N \cdot mm^2\right) \tag{4-4}$$

While the flexibility form can be expressed as follows:

$$F_1 = \frac{1}{(E \cdot I)_1} = \frac{48(def)_1}{PL^3} \quad \left(N^{-1} \cdot mm^{-2}\right)$$

$$F_2 = \frac{1}{(E \cdot I)_2} = \frac{48(def)_2}{PL^3} \quad \left(N^{-1} \cdot mm^{-2}\right) \tag{4-5}$$

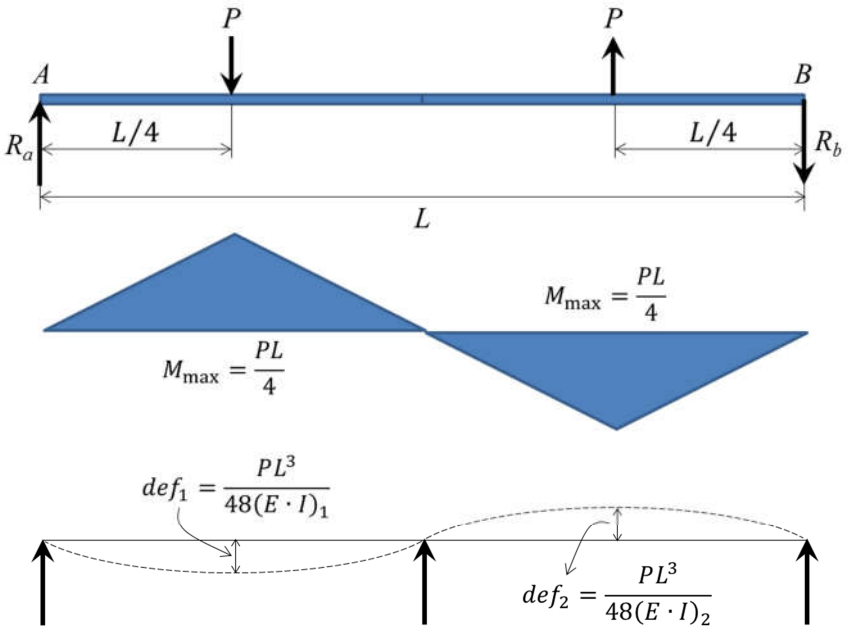

Figure 4-9: Flexibility for multi-point bending test

The flexibility F_1 and F_2 will be similar for the stents with symmetric geometry.

4.4 RESULTS AND DISCUSSION

Figure 4-10 shows the reaction moment versus the deflection for the unexpanded configuration under the single-point loading and its corresponding bending stiffness. It is denotes that for the similar point force, Sinusoidal stent yielded larger reaction moment than Asymmetric stent, with a mean slope difference of 2.91±0.67. In term of Asymmetric stent, its inflated-side produced lower reaction moment than the fixed-side, by a slope margin of 1.36. The correlation of bending stiffness and deflection in Fig. 4-10*b* describes a similar phenomenon with that of reaction moment and deflection. Namely, Sinusoidal stent has higher bending stiffness than Asymmetric stent with a mean difference of 345.14±14.68 N.mm^2. In term of Asymmetric stent, its inflated-side generated lower bending stiffness than the fixed-side by a margin of 29.35 N.mm^2.

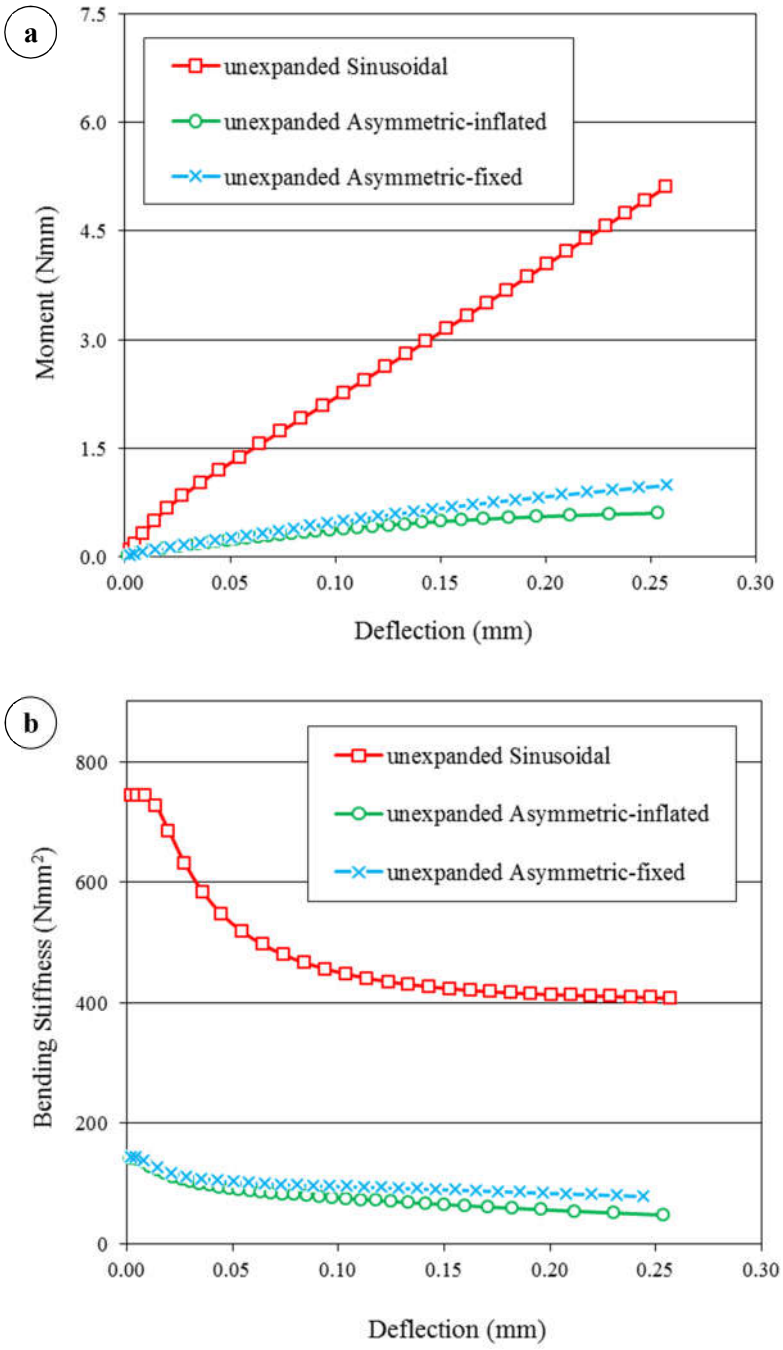

Figure 4-10: Unexpanded configuration under single-load: (a) Reaction moment, (b) Bending stiffness.

Figure 4-11 represents the reaction moment versus the deflection for the unexpanded configuration under the multi-point loading denoted by the bending moment number (1) and (2). From Figs. 4-11*a* and *b*, it is obviously seen that a couple of the opposite bending moment produced the similar reaction moment on the stent with symmetric geometry. For Asymmetric stent, the reaction moment of the inflated-side is equal to that of the fixed-side though those have different deflection values. Because of the different deflection value, the bending stiffness of both side of Asymmetric stent is not similar each other. This result suggests that the flexibility assessment using the multi-point loading is useful to identify the difference in the stent deflection with non-symmetric geometry.

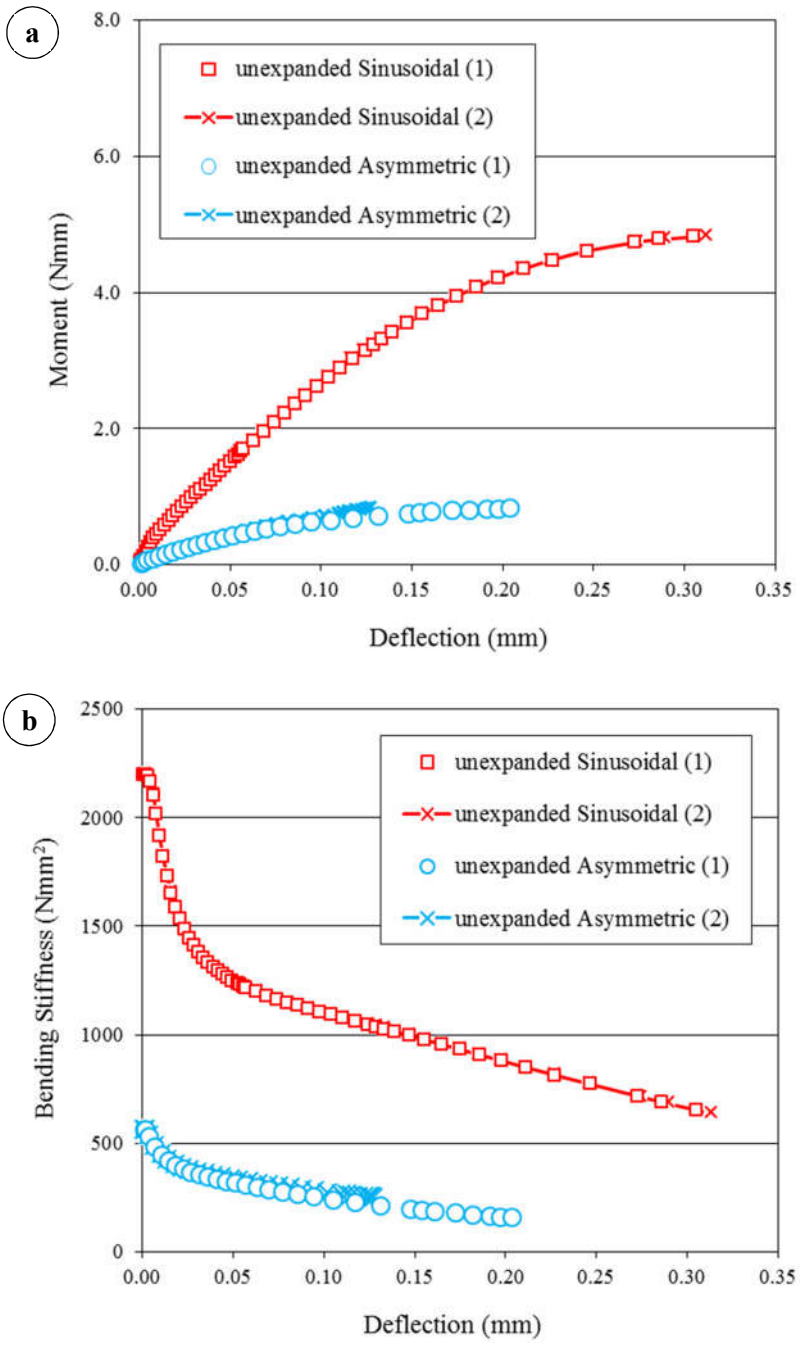

Figure 4-11: Unexpanded configuration under multi-load: (a) Reaction moment, (b) Bending stiffness.

Figure 4-12 shows reaction moment versus deflection for expanded configuration under single-point loading and its corresponding bending stiffness. It is denotes that for the similar deflection value, Sinusoidal stent yielded larger reaction moment than Asymmetric stent. Besides, the maximum deflection of Sinusoidal stent (0.548 N.mm) is quite small comparing with that of Asymmetric stent (1.309 N.mm). Meanwhile, the correlation of bending stiffness and deflection in Fig. 4-12*b* describes that Sinusoidal stent has only a few remaining bending stiffness to resist bending deformation. In the contrary, Asymmetric stent still could withstand more bending deformation, with a difference deflection of 0.1916 mm. These results lead to an important note that flexibility assessment of

expanded stent is very useful to reveal potential-configuration of stent.

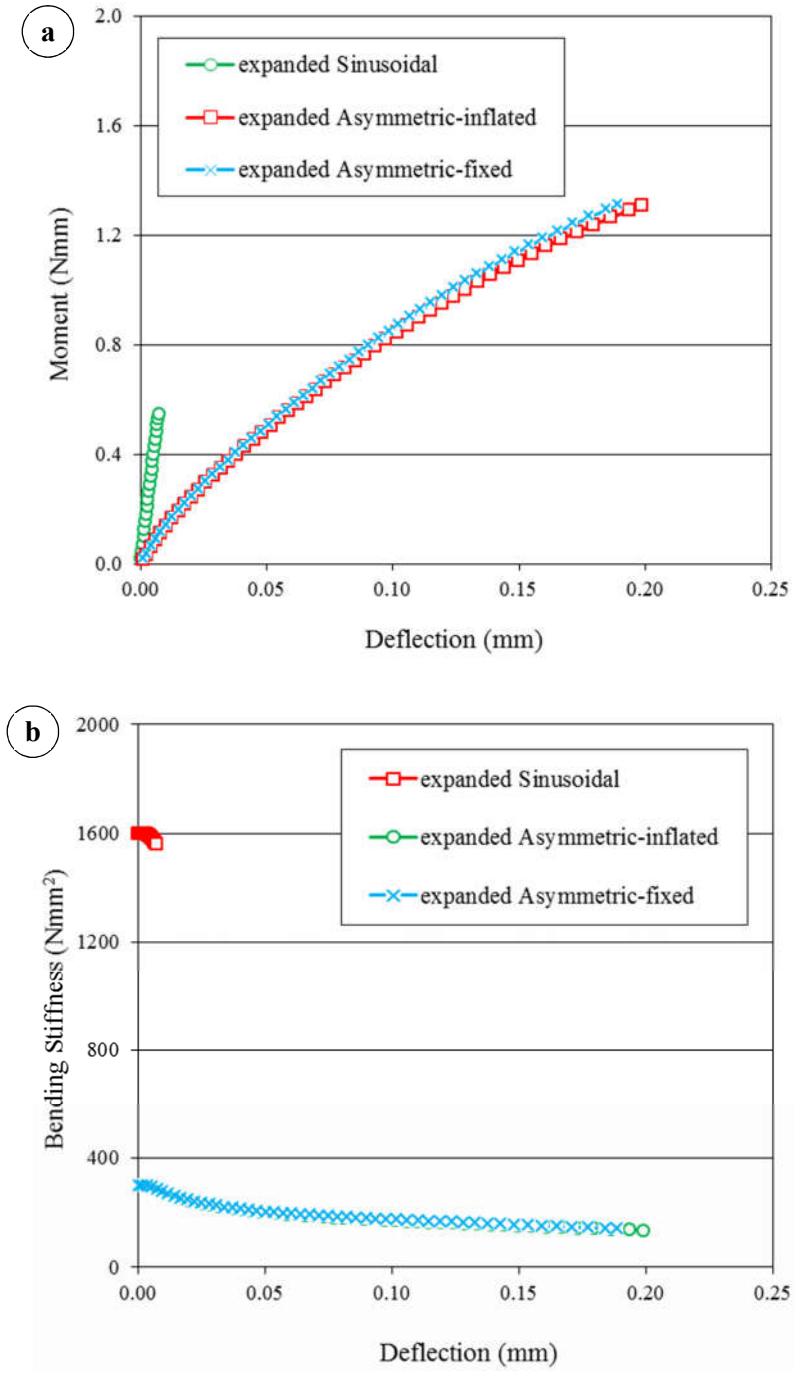

Figure 4-12: Expanded configuration under single-load: (a) Reaction moment, (b) Bending stiffness.

According to aforementioned sub Section 3.4.1, adding the bridges seems to affect the potential-configuration of Asymmetric stent. The bridges or connecting links make a stent more flexible in the radial and axial direction [3][6][13]. In the modern design of stents, the bridges are almost provided in the geometry design of stents in order to increase the stent flexibility. However, it should be constructed carefully to avoid the less axial rigidity. For the treatment of the carotid artery, the less axial rigidity could cause the *concertina effect* (Fig. 4-13), which is defined as the longitudinal

deformation of the proximal segments of a deployed stent [14].

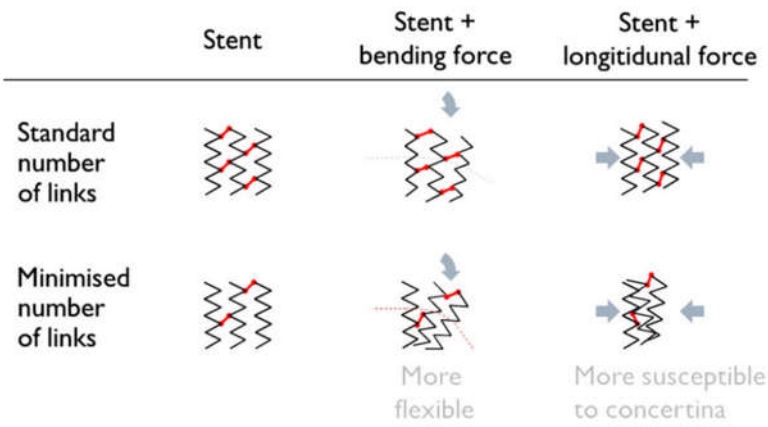

Figure 4-13: Concertina effect due to fewer bridges

The flexibility of both stents for the unexpanded configuration, which can be calculated using Eq. 4-3 for single-point loading and using Eq. 4-5 for multi-point loading, is listed in Table 4-1. These results demonstrate that the geometry modification could change the stent flexibility significantly. The flexibility of Asymmetric stent is higher than Sinusoidal stent for both loading types, i.e. the single-load and multi-load. It also can be noted that the stent is more flexible in the case of the single-point loading test. Since all stents tested in this study have similar length, the effect of the stent length on the flexibility cannot be observed.

Table 4-1: Flexibility of Sinusoidal and Asymmetric stents

Configuration		Sinusoidal stent ($N^{-1} \cdot mm^{-2}$)	Asymmetric stent ($N^{-1} \cdot mm^{-2}$)	
			Inflated-side	Fixed-side
Single-load	Unexpanded	0.0025	0.0209	0.0129
	Expanded	0.00064	0.0075	0.0071
Multi-load	Unexpanded	0.0016	0.0060	0.0040

4.5 CONCLUSIONS

This chapter demonstrated the geometry assessment on Asymmetric stent through FEM. The assessment on Sinusoidal stent for the comparative analysis is figured out as well. This study indicated that the geometry modifications such as varying the struts length and width, adding the bridges, and varying the curvature width of struts affect the stent flexibility. Particularly, adding the bridges/connector between stent segments yields the largest effect on the stent flexibility and affects the potential-configuration after expansion. The FEM protocol used in this assessment is also useful to

identify the geometry characteristics of stent. Then, the FEM protocol might be adopted for stent assessment widely.

4.6 STUDY LIMITATION AND FUTURE WORKS

The geometry assessment conducted in this chapter considers only the radial deflection under the unexpanded configuration. The flexibility in the expanded configuration, indeed, is the important information for a doctor / practitioner in choosing an appropriate stent type to be deployed in the treatment. Besides, as for stent with the bridges such as Asymmetric stent type, it is necessary to be assessed its axial rigidity. Adding the bridges increases the stent flexibility. The flexibility of a stent may be also achieved by reducing the number of bridges and using a helical arrangement of the connecting links. Then, each stent segment has high abilities to change its length longitudinally when the stent is bended in the curved segment. As a side effect, a more flexible stent may also have a greater susceptibility to deformations when force is applied in its longitudinal axis [14]. Therefore, future studies should develop the axial rigidity assessment to identify the minimum number of bridges/connecting links.

References

[1] Colombo, A. et al., 2002. Selection of coronary stents. Journal of the American College of Cardiology. 40 (6), 1021–1033.

[2] Gyongyosi, M. et al., 2000. Longitudinal straightening effect of stents is an additional predictor for major adverse cardiac events. Journal of the American College of Cardiology. 35 (6), 1580–1589.

[3] Mori, K. and Saito, T., 2005. Effects of stent structure on stent flexibility measurements. Annals of Biomedical Engineering. 33 (6), 733–742.

[4] Rieu, Regis et al., 2003. Assessment of the trackability, flexibility, and conformability of coronary stents: A comparative analysis. Catheterization and Cardiovascular Interventions. 59, 496–503.

[5] Szabadits, P. et al., 2009. Flexibility and trackability of laser cut coronary stent systems. Acta of Bioengineering and Biomechanics. 11 (3), 11–18.

[6] Szabadits, P. et al., 2008. Comparison the flexibility of balloon-expandable coronary stents. 3rd Hungarian Conference on Biomechanics. 315–319.

[7] Petrini, L. et al., 2004. Numerical investigation of the intravascular coronary stent flexibility. Journal of Biomechanics. 37, 495–501.

[8] Wu, W. et al., 2007. An FEA method to study flexibility of expanded coronary stents. Journal of Materials Processing Technology. 184, 447–450.

[9] Kim, D.B. et al., 2013. A comparative reliability and performance study of different stent designs in terms of mechanical properties: foreshortening, recoil, radial force, and flexibility. Artificial Organs. 37 (4), 368–379.

[10] ANSYS Mechanical APDL Theory Reference. ANSYS Inc., U.S.A., p. 590.

[11] ANSYS Mechanical APDL Element Reference. ANSYS Inc., U.S.A., p. 873.

[12] ANSYS Helps 15.0. Coupling and constraint equations. ANSYS Inc., U.S.A.

[13] Kim, D.B. et al., 2013. A Comparative reliability and performance study of different stent designs in terms of mechanical properties: Foreshortening, recoil, radial force, and flexibility. Artificial Organs 37, 368–379.

[14] Foin, N. et al., 2013. Stent flexibility versus concertina effect: Mechanism of an unpleasant trade-off in stent design and its implications for stent selection in the cath-lab. International Journal of Cardiology 164, 259–261.

5 FEM ANALYSIS ON RUPTURE OF ARTERIAL TISSUE AFTER ASYMETRIC STENTING

5.1 INTRODUCTION

The existence of plaque narrowing blood vessel mainly forms the eccentric protrusion. *In vivo* studies found that eccentric lesions were significantly more frequent than concentric ones [1][2][3][4], in which its tendency increases for the case of unstable angina [1]. The treatment of the eccentric plaque using ordinary cylindrical balloon will lead to non-uniform stress distribution within the vessel wall [5]. The non-uniform stress distribution, which takes place at a plaque with thin fibrous cap, could be beginning of the inflammatory cells activation. The inflammatory cells activation may contribute to rupture of the atherosclerotic plaque [6][7], and may cause more severe problem such as carotid artery dissection [2]. Therefore, it is necessary for the redesigning mesh structure of stent to reduce non-uniform stress distribution due to eccentric geometry of plaque. Moreover, recently *in vitro* experimental studies show that either plaque or underlying layer surrounding the stent has different material properties. All soft atherosclerotic tissues are having non-linear material properties, and both media and fibrous cap are stiffer than either lipid core or thrombus [8]. Comparing with the healthy intima tissue, the diseased intima tissue can be expected to be stiffer as well as the underlying media tissue [9][10]. The development of a new stent should consider these differences.

Before FE studies concerning with the rupture analysis of arterial tissue due to the stent deployment, numerous FE studies for atherosclerotic disease was conducted separately. There are two basic FE assessment methods to ascertain the rupture tendency in the stenting process such as the patient-specific computational studies, and the residual stress/strain [11]. Several correlated studies on carotid artery using patient-specific computational analysis are conducted. Li et al. performed two investigations on carotid plaque through computational analysis based on the method. In the first investigation, they combined the finite element analysis (FEA) and MRI as shown in Fig. 5-1. By using the isotropic hyperelastic model, the high stress concentrations were predicted at the shoulders and the thinnest fibrous cap regions. Thus, they concluded that the high stress concentrations in vulnerable plaque might cause the plaque rupture [12]. Secondly, they examined the effects of the varying fibrous cap thickness, lipid core size, and lumen curvature on the plaque stress distributions using the similar method as mentioned above. The results pointed out that the large lumen curvature and the thin fibrous cap is closely related to plaque vulnerability [13].

Considering anisotropic arterial tissue, Kiousis et al. investigated fibrous cap vulnerability on the human atherosclerotic carotid bifurcation. They reported that their results agree with the results of Li et

al. Namely, the highest stress regions are located at the vicinity of the plaque shoulders and in the stiff calcified tissue. They also identified a positive correlation between the increase in lipid core portion and the mechanical stress in the fibrous cap (the risk for cap rupture) [14]. This work also confirmed that there is no fundamental difference in the arterial tissue component whether the isotropic or anisotropic material model is used. Sadat et al. extended the work of Li et al. by carrying out the FE analysis of the vulnerable carotid artery disease using the high-resolution MRI data. They reported that the maximum plaque stresses were significantly higher in the patients with the acute symptoms than those in recently symptomatic patients [15].

The latest patient-specific images to the FE analysis was conducted by Auricchio et al. on self-expanding stent designs in a carotid artery using the computed angiography tomography (CTA) method. This methodology may become a quantitative assessment of the relation between the complex mechanical features and the patient-specific anatomy [16]. These aforementioned studies suggest that the 3D models in the analysis of atherosclerotic diseases needed based on the patient-specific computational studies.

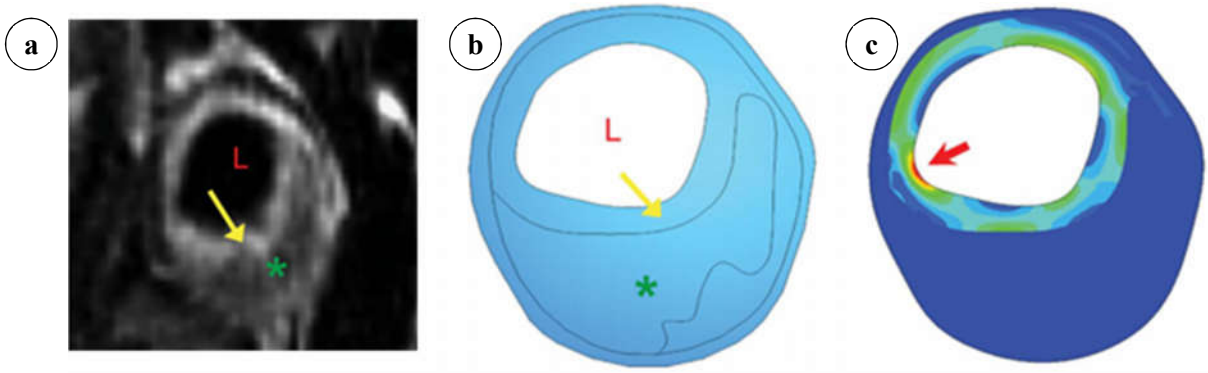

Figure 5-1: Combining MRI and advanced FEA. (a) Identification of plaque components (L: lumen; yellow arrow: fibrous cap; green star: lipid pool). (b) Geometry of plaque model. (c) Von Mises stress contour that indicated the peak stress concentration on the shoulder of the plaque (red thick arrow).

The second method in the FE studies of atherosclerotic diseases is using the idealized model and considering the residual stresses/strains inclusion. A number of idealized FE studies to investigate the residual stresses/strains are performed. In investigation of the residual stresses inclusion, Gasser and Holzapfel simulated the balloon angioplasty on the elastic tissue that adapted the anisotropic model. They found that the compressive normal stresses occur in the media after dilation [17]. Using the opening angle technique in *in vitro* experiment, Ohayon et al. investigated the influence of the residual stress/strain on the biomechanical stability of the vulnerable coronary plaques. It was found that the residual stresses/strains cannot be negligible and dramatically affects the physiological peak stress amplitude in the thin fibrous cap [18]. Latest FE study of Cilla et al. showed that the plaque rupture should be observed not only as a consequence of the cap thickness but also as a combination of the

stenosis ratio, the fibrous cap thickness, and the lipid core dimensions [19].

A review study by Holzapfel et al. is quite helpful to collect the information deal with the computational approaches of both the patient-specific and the idealized model for analyzing the mechanics of atherosclerotic plaques. They pointed out a necessity to develop a more location and tissue-specific threshold value, and a more appropriate failure criterion. They also pointed out that the future FE studies should consider the strain-energy functions to obtain more precise simulation results [11].

5.2 BACKGROUND AND OBJECTIVE

In the reviewing literatures related to rupture analysis of the arterial tissue due to balloon expandable stent deployment, the author found a limited number of supporting studies. To the best knowledge of the author, there are two detail studies in this field. Karimi et al. executed the finite element study of balloon expandable stent for the plaque and arterial tissue vulnerability assessment. They studied effect of the plaque composition (calcified, cellular, and hypocellular) on the stresses induced in the arterial layers (intima, media, and adventitia), which was modeled using the isotropic hyperelastic behavior of Ogden parameters. It was reported that the stress on the stiffest calcified plaque wall was in the fracture level (2.38 MPa), whereas the cellular and hypocellular plaques remain stable due to the less stress on the walls. They also pointed out that the highest von Mises stresses were observed on the stiffest intima layer, while the lowest stresses were seen to be located in the less stiff media layer [20]. To find out the role of calcification in the plaque vulnerability and the wall rupture, Riyahi-Alam et al. evaluated preoperatively in silico analysis of atherosclerotic calcification vulnerability in carotid artery stenting. The in silico results showed that the average ultimate stresses of 55.7±41.2 kPa and 171±41.2 kPa as well as the average plaque wall stresses of 19.03 ±16.05 kPa and 64.3±63.3 kPa were obtained on calcifications [21].

The FE study for the non-symmetric expansion considering the rupture of arterial tissue has not been investigated yet. Therefore, the study of rupture analysis on arterial tissue considering Asymmetric stent deployment would enrich the literatures in the field study of both the plaque vulnerability and the arterial tissue rupture. On the other hand, as a series of a new stent development, the rupture analysis after the stent deployment is essential problem. Using the finite element method in the analysis is quite helpful, because FEM has transformed into a useful tool to observe the rupture tendency, which is difficult to accomplish through *in vivo* and *in vitro* experimental studies. In Chapter 3, the final design of Asymmetric stent is already determined as shown in Fig. 3-7. In this chapter, the rupture analysis is performed considering the interaction between Asymmetric stent and intact arterial layer (vessel wall), the dissection of plaque shoulder, and the inflammation tendency of the healthy intimal layer.

5.3 METHODS

5.3.1 Finite Element Model

The transient nonlinear structural analyses are built using ANSYS R15.0 (ANSYS Inc., Pennsylvania, USA) to identify the deformation. Two types of balloons and stents are utilized in the simulation. Totally, four finite element models are developed for the comparison analysis, i.e. (a) sinusoidal stent expanded by the offset balloon [22], (b) Sinusoidal stent [23] expanded by the ordinary cylindrical balloon, (c) Asymmetric stent expanded by the offset balloon, and (d) Asymmetric stent expanded by the ordinary cylindrical balloon. The geometries of offset and ordinary cylindrical balloon are displayed in Fig. 3-1. CREO 2.0 (PTC Inc., Needham, USA) is used as a solid model builder. The stent models are made in CREO 2.0 because of its complexity, while models of the balloon and the stenosis carotid artery are directly built in ANSYS R15.0. Asymmetric stent is derived from Sinusoidal stent by modifying its struts length and width as previously explained in Chapter. 3. The geometry of Sinusoidal and Asymmetric stent is displayed in Fig. 5-2.

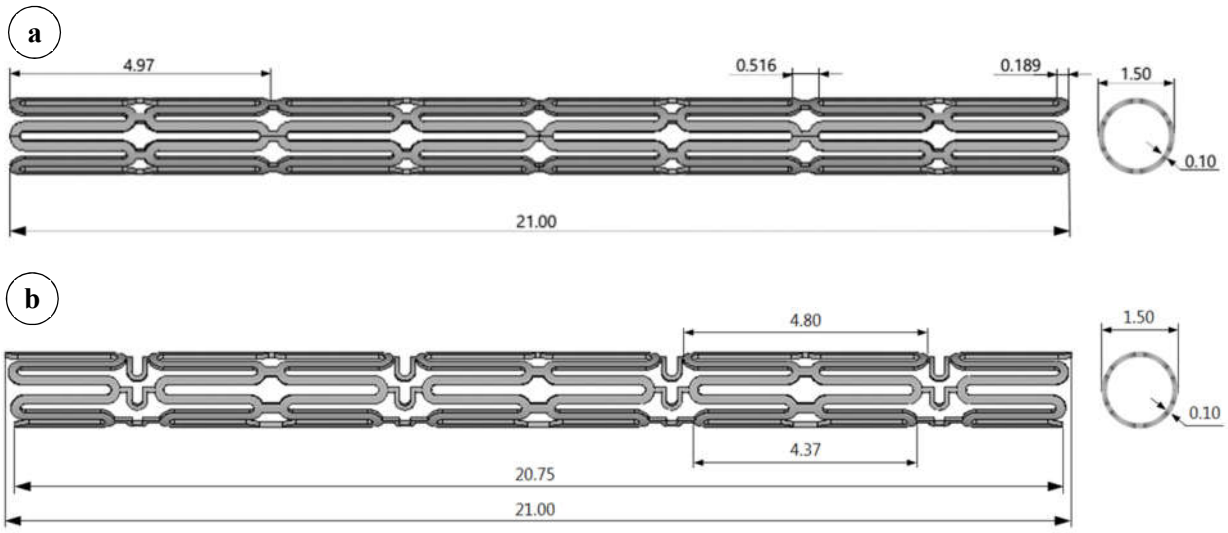

Figure 5-2: Geometry of FE model. (a) Sinusoidal stent. (b) Asymmetric stent.

In this study, an idealized model of the internal carotid artery (ICA) is adopted and the residual stresses inclusion is considered for the finite element simulation. The idealized ICA model used is taken from Chapter 3 with multilayer properties material added in the model as shown in Fig. 5-3. The plaque is designed has a little shorter than the stent which covered in one side of the vessel wall surface and another side is free-lesion area. Plaque type is fibro atheroma, which is characterized with the large lipid pool and the thin fibrous cap. According to the American Heart Association (AHA), the fibro atheroma is classified as type V of atherosclerotic plaque [27]. The thin fibrous cap also indicates the vulnerability of the plaque (unstable plaque) and the tendency to rupture [24][25][27][28]. In this case, the arterial layer under and surrounding the plaque is treated as the diseased intima and media. The

length of healthy carotid artery is built to be equal with that of the diseased carotid artery so that the effect of zero degree of the freedom at the end of carotid artery is neglected.

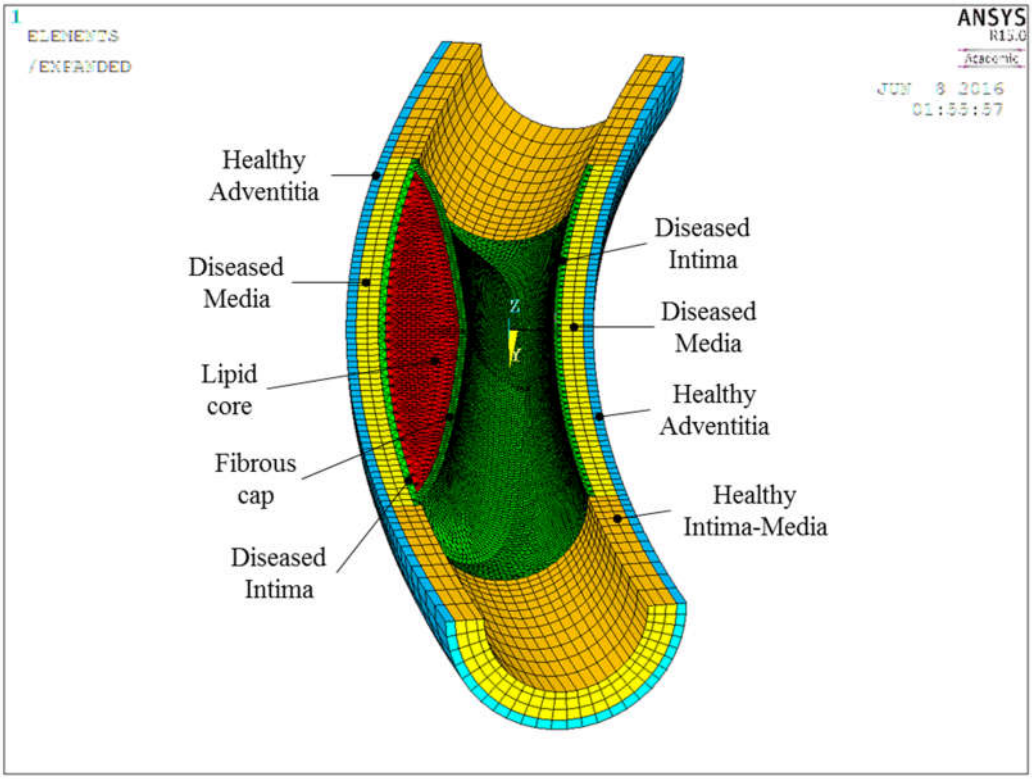

Figure 5-3: FE model for rupture analysis

A number of idealized FE studies have reported that the inclusion of the residual stresses/strains in the arterial models is important for more accurate evaluations of the stress distribution within the atherosclerotic plaque [29][30][18][17][19]. Those studies also pointed out that the models without the residual strains overestimate the stresses in the atherosclerotic plaque. Besides, the inclusion of the residual stresses has a significant effect on the resultant stress values. These are important information for the future studies considering the residual stresses in the computational analyses. The reason is the difficulty in quantifying the residual strain state *in vivo* is through measurements of the opening angle after longitudinal incision *in vitro*, whereas with the opening angle method the 3D residual strain state still cannot be identified [31].

5.3.2 Material Model and Behavior

Material properties used in the simulation are SUS316L for the stent; polyethylene terephthalate (PET) for the balloon; fibro atheroma for the plaque; and carotid artery for the vessel wall (including intima, media and adventitia layer). The material models are defined as isotropic multilinear for the stent and isotropic hyperelastic (nearly incompressible) for the balloon, plaque, and arterial tissue. To conform material properties referred from the previous literatures, two layers of the healthy carotid artery is

defined as the healthy media-intima and the healthy adventitia. As for stenotic artery, the layers consist of fibrous cap, lipid core, diseased intima, and diseased media. The fibrous cap and the diseased intima in this case were assumed to have the same material properties. The multilinear properties for the stent are obtained by the fitting curve from SUS316L tensile test as shown in Fig. 3-5.

Mooney-Rivlin 2 parameters are set for the hyperelastic behavior of the balloon. The hyperelastic behavior for the human carotid plaque is extracted from the uniaxial tension test data of the human carotid stenotic artery by Teng et al. [8]. They determined the material constants of each tissue type from their uniaxial tension test as following: media, c_1 = 0.138 kPa, D_1 = 3.833 kPa and D_2 = 18.803; fibrous cap, c_1 = 0.186 kPa, D_1 = 5.769 kPa and D_2 = 18.219; lipid, c_1 = 0.046 kPa, D_1 = 4.885 kPa and D_2 = 5.426; and thrombus, c_1 = 0.212 kPa, D_1 = 4.260 kPa and D_2 = 5.312. All these parameters are obtained from the Cauchy stress – stretch ration as shown in Fig. 5-4. It is concluded that all soft atherosclerotic tissues are non-linear, and both media and fibrous cap are stiffer than both lipid and thrombus. Meanwhile, the biaxial tension tests data provided by Sommer et.al [32] is chosen to derive the hyperelastic behavior for the healthy arterial tissue. They found that the adventitia is compliant at low pressures, but change into the stiff tubes at high pressures. The burst pressure of the adventitia is beyond 250 kPa. Relatively low burst pressure of ~60 kPa is found in the media-intima tubes, in which the pressure/circumferential stretch relationships are not dependent on the axial stretches.

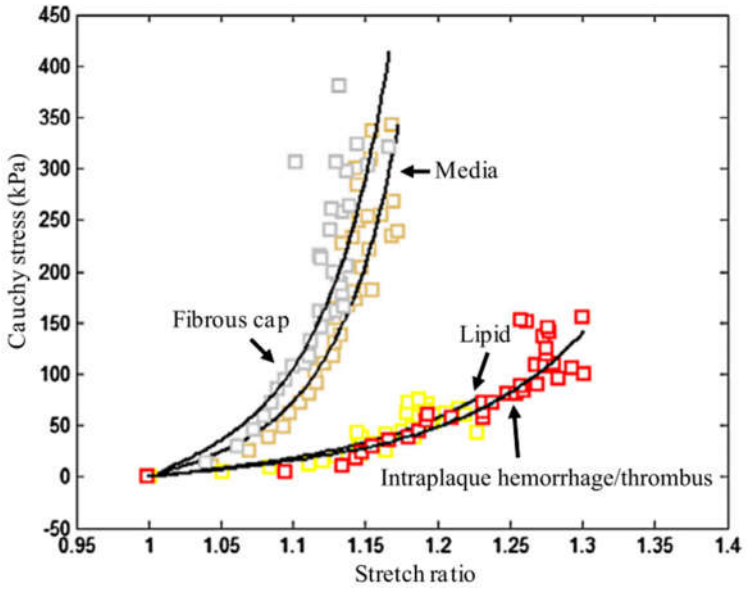

Figure 5-4: Comparison of averaged data points and fitted curve from each tissue type.

Figure 5-5 shows the experiment results of Sommer et al. study representing the mechanical response of the adventitia and media-intima composite of the healthy internal carotid artery (ICA) in the circumferential direction for both the physiological and the supra-physiological loading. The study assumed that the physiological loading is range from 1.0 to 33.3 kPa (250 mmHg). These values were

obtained from the mechanical response of healthy ICA. Based on the testing protocol of both the tension tests, the author concluded that the mechanical response in the circumferential direction is closed to the uniaxial test data of Teng et al. study. Sommer et al. also provided the slopes list of the Cauchy stress-transmural pressure relations (Table 5-1). Hence, the mechanical response – stretches curve can be converted into Cauchy stress – stretch ratio relationship.

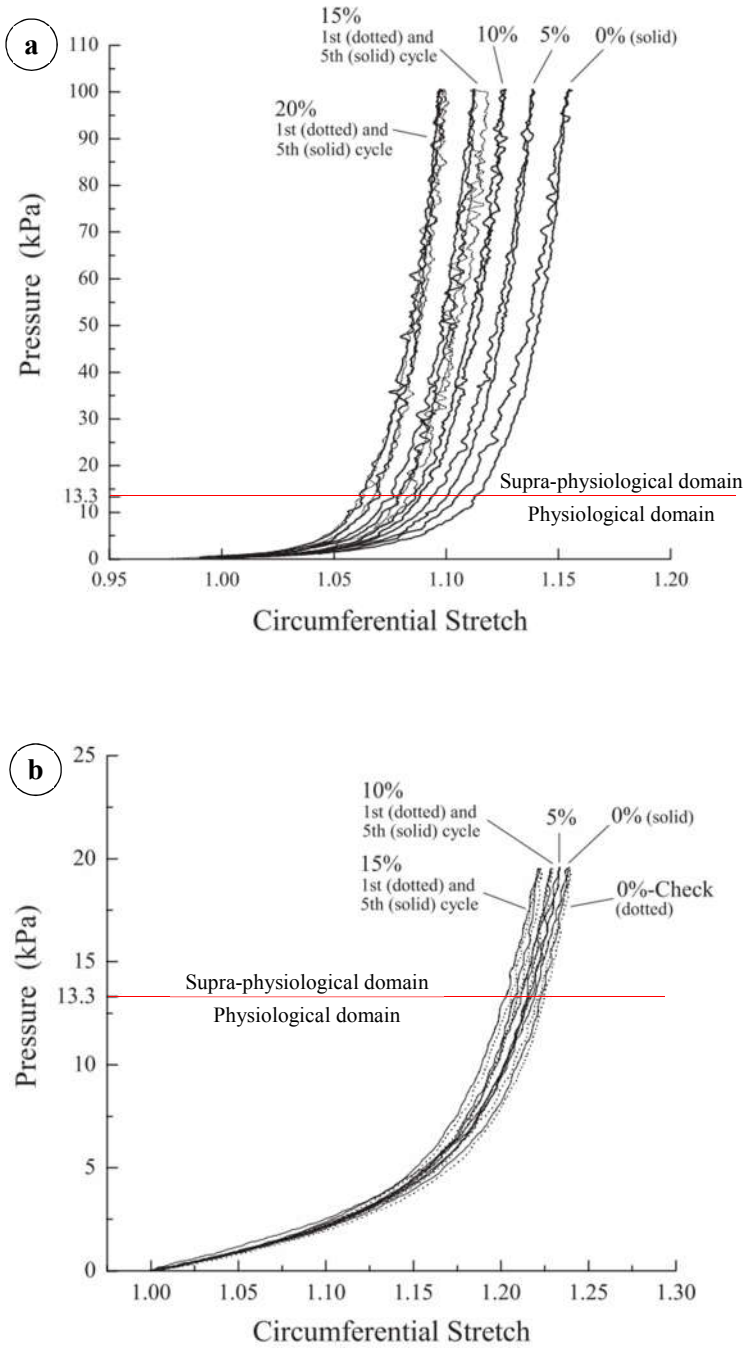

Figure 5-5: Mechanical responses of the media-intima composite of the ICA, in circumferential direction: (a) the adventitia, (b) the media-intima composite.

Table 5-1: Slopes of the Cauchy stress-transmural pressure relations at different axial stretches

Layer	Stress-Pressure Slopes				
	$\lambda z = 1.0$	$\lambda z = 1.05$	$\lambda z = 1.1$	$\lambda z = 1.15$	$\lambda_z = 1.2$
Adventitia	6.06 (0.96)	6.62 (1.26)	6.85 (1.28)	7.77 (1.40)	8.49 (1.29)
Media-Intima	10.63 (0.72)	10.86 (0.73)	10.98 (0.74)		

To extract the parameters from the experimental data for the material properties of the arterial tissue, HyperElastic Curve Fitting feature in ANSYS is utilized. The hyperelastic constants in the strain-energy density function of a material determine the mechanical response. Therefore, in order to obtain successful results during a hyperelastic analysis, it is necessary to accurately assess the material constants. The material constants are generally derived for the experimental stress-strain data. It is recommended that this test data should be taken from several modes of deformation over a wide range of strain values. In fact, it has been noted that the material constants should be fit using the test data obtained from the deformation states experienced in the analysis. For the hyperelastic materials, the simple deformation tests (consisting of six deformation modes) can be used to accurately characterize the material constants [33].

Hyperelastic curve fitting is a tool to estimate the material constants using the experimental data and to compare with the hyperelastic material models. The stress-strain curves can be converted to the supported hyperelastic models including Mooney-Rivlin, Ogden (hyper-foam), Neo-Hookean, Polynomial, Arruda-Boyce, Gent, Blatz-Ko, and Yeoh. The hyperelastic models define three types of behavior: the purely incompressible, the nearly incompressible, and the compressible [34]. The procedure to perform the curve fitting in ANSYS R.15 is as follows:

- Input experimental data
- Select a model from one of the provided hyperelastic models
- Perform a regression analysis
- Graphically view the curve-fitting results
- Compare the fits to the experimental data
- Write the fitted coefficients to the database as nonlinear data table commands for the subsequent finite element analyses.

From the hyperelastic curve fitting, 3-parameters Mooney-Rivlin is chosen to fit the uniaxial tension data by Teng et al. [8], which is adopted for the fibrous cap/diseased intimal layer, lipid core, and diseased medial layer. Meanwhile, 1-parameter Ogden is used to model the hyperelastic behavior of the healthy arterial tissue surrounding the stent, which is fit the biaxial tension data (the circumferential

direction only) provided by Sommer et al. [32]. All parameters derived by the curve-fitting calculation method have stable behavior for nonlinear simulation. After trial and error, Ogden 1 parameter for the healthy CA is used in the simulation. In this case, for the same value of high strain generated, lower stress value would be identified within the healthy CA. It is assumed that there is no influence to the stress distribution because the stent expansion is not directly upon the healthy CA layer. The relationship between the Cauchy stresses – stretches for material properties of the plaque and arterial tissue surrounding is shown in Fig. 5-6. The parameters for all material properties are summarized in Table 5-2.

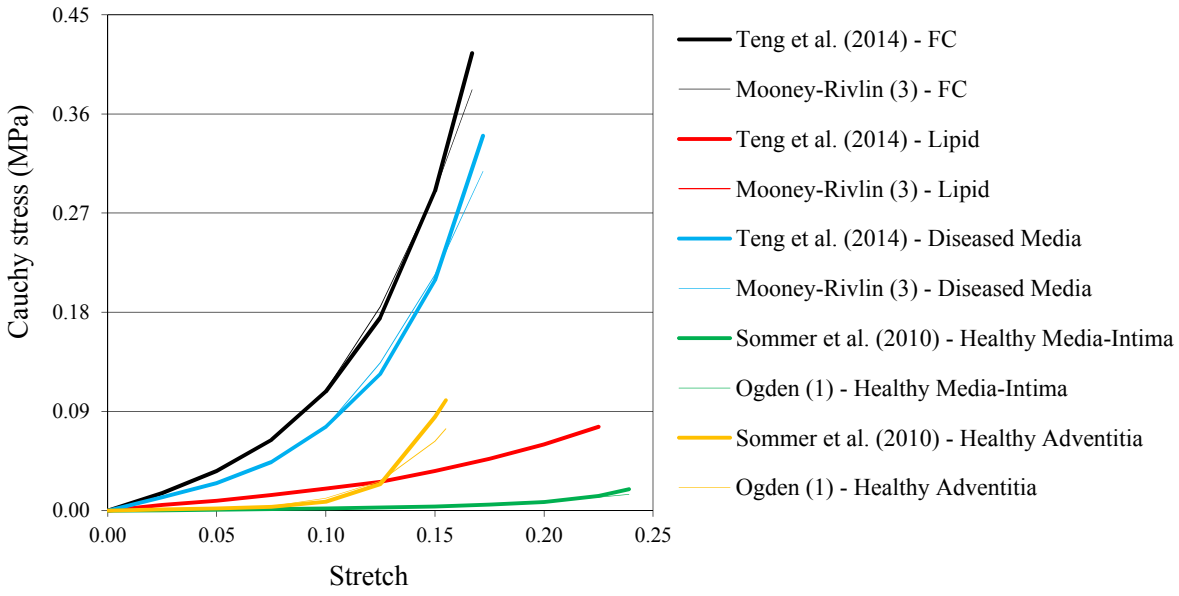

Figure 5-6: Curve fitting result for FC, lipid core, diseased media, healthy intima-media and healthy adventitia.

Table 5-2: Material properties used in the rupture analysis

Component	Material	Material behavior	Poisson's ratio	Density (tonne/mm^3)	Material constants
Balloon	Poly-urethane	Hyperelastic nearly incompressible	0.49	1.38E-9	Mooney-Rivlin 2 parameters: C_{10} = 1.0318 MPa; C_{01} = 3.6927 MPa d = 0.004261
Stent	SUS316	Multilinear isotropic	0.33	7.99E-9	Fitting stress-strain curve resulted from pure tensile test
FC/Diseased Intima	Hypo cellular	Hyperelastic nearly incompressible	0.49	1.07E-9	Mooney-Rivlin 3 parameters C_{10} = -1.3192 MPa; C_{01} = 1.4533 MPa C_{11} = 3.8801 MPa; d = 0.1501
Lipid	Hypo cellular	Hyperelastic nearly incompressible	0.49	1.07E-9	Mooney-Rivlin 3 parameters C_{10} = -0.1362 MPa; C_{01} = 0.1729 MPa C_{11} = 0.2816 MPa; d = 0.5477

Diseased Media	Carotid artery	Hyperelastic nearly incompressible	0.49	1.07E-9	Mooney-Rivlin 3 parameters C_{10} = -1.4174 MPa; C_{01} = 1.5274 MPa C_{11} = 3.2808 MPa; d = 0.1830
Healthy Intima-Media	Carotid artery	Hyperelastic nearly incompressible	0.49	1.07E-9	Ogden 1 parameter μ_1 = 0.00042369 MPa; α_1 = 17.539 MPa d_1 = 10.8382
Healthy - Diseased Adventitia	Carotid artery	Hyperelastic nearly incompressible	0.49	1.07E-9	Ogden 1 parameter μ_1 = 0.00024647 MPa; α_1 = 40.561 MPa d_1 = 8.0563

It should be noted that the material model has an essential role to achieve convergent results in the transient nonlinear simulation. As it is known, the arterial tissue has hyperelastic behavior expressed by an exponential equation. The characteristic appears mainly for the healthy arterial tissue and does not for the calcified plaque. The exponential equation often produces the singularity in the computational analysis. Therefore, to avoid unconvergent solution during the supra-physiological loading domain, FEM simulation in this study chooses the curve-fitting results that have less agreement with the provided experimental data.

5.3.3 Loading Conditions and Solution

Boundary conditions applied in the model are displayed in Fig. 5-7*a*. Global coordinate system used is the cylindrical coordinate system, which X, Y and Z axis are the radial, circumferential and longitudinal directions, respectively. The blue triangles show as the applied constraints. To maintain the dilatation shape of offset balloon, the node coupling and constraint equations were subjected in the circumferential and radial direction. The coupling will cause only the prime degree of freedom (DOF) to be retained in analysis' matrix equations, and will cause all the other DOFs in a coupled set to be eliminated. The value calculated for the prime DOF will then be assigned to all the other DOFs in a coupled set [35]. This method is useful to maintain the inflated side of the offset balloon. The large deformation feature of ANSYS nonlinear transient analysis should be activated in order to obtain Cauchy (true) stress and Hencky (logarithmic) strain as native FEM results.

In the computational analyses of stent deployment, which are considering the residual stresses inclusion, the stresses generated after balloon removal are taken into account. Therefore, multiple load step of pressure loading consists of the inflation, deflation and steady phases are considered in this simulation. The pressures of 1.6 MPa for the ordinary balloon and 1.75 MPa for the offset balloon were subjected to the inner surface of balloon during 1 second. After reaching 130% of its nominal diameter, the balloon subsequently deflated for half second to secede from the stent completely. The steady phase is subsequently applied in order to neglect the impact effect after balloon removal as shown in Fig.

5-7*b*.

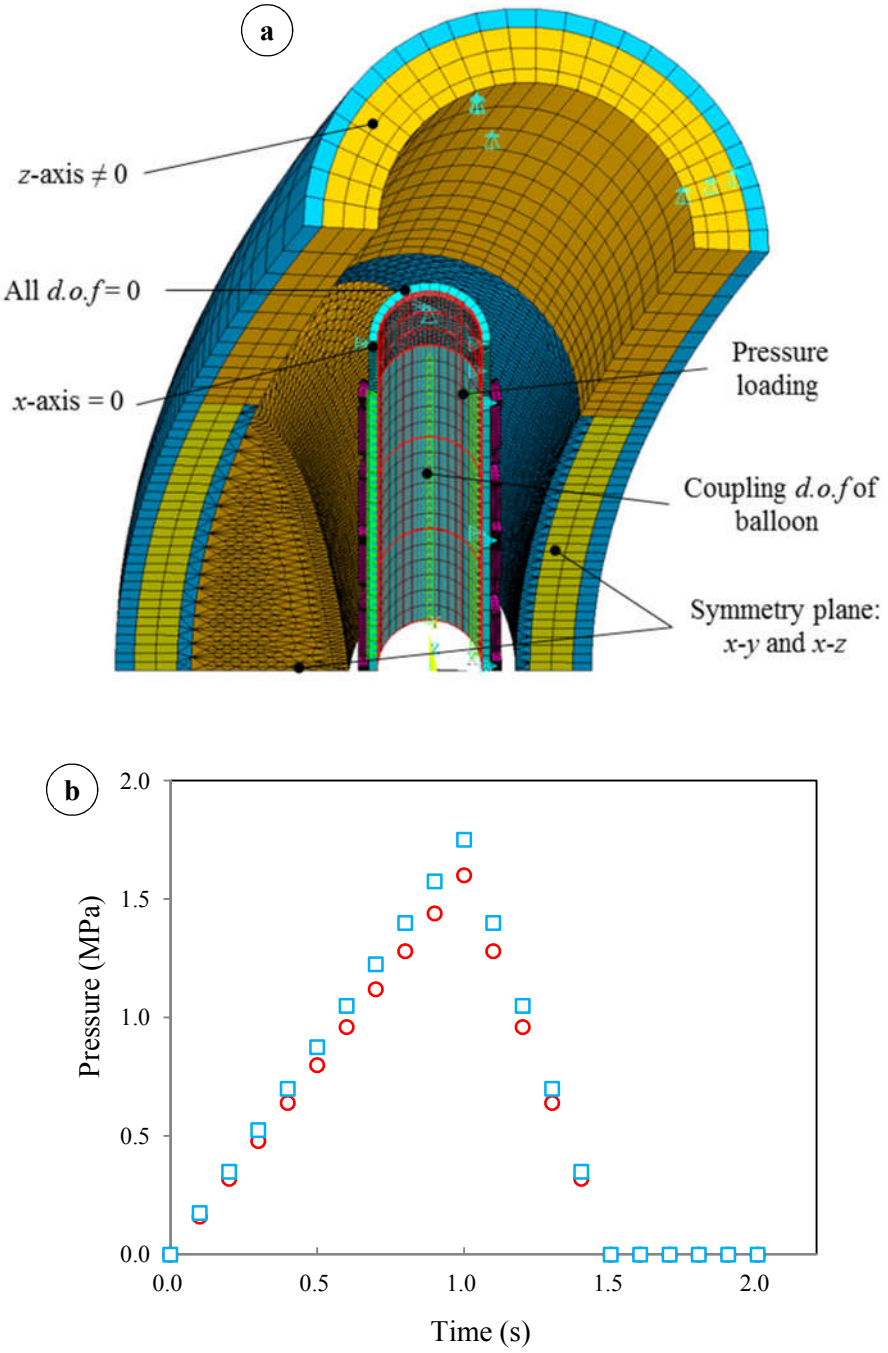

Figure 5-7: (a) Boundary conditions, (b) Time history of pressure loading

5.3.4 Stress Measure

The stress levels at post-processing stage are calculated using the maximum principal stresses in a number of FE studies [36][37][38][39][40][14]. While many researchers have used (and continue to use) the von Mises stress to assess the maximum stress in an atherosclerotic plaque [41][12][13][18][15][16]. As pointed out by Humphrey and Holzapfel (2012) the von Mises stress is a

useful measure in the classical engineering analyses of yielding due to excessive shear stresses, however, data on the aortic tissue suggest that the maximum normal stress governs the failure [42]. In addition, as mentioned by Kock et al. (2008), the tensile and compressive stresses are not distinguishable by the von Mises stresses [43]. Holzapfel et al. (2014) also addressed the rupture-potential of atherosclerotic plaques without the von Mises stress. The normal and shear stress measures, compiled with experimental data could identify new failure criteria, preferably in terms of failure properties of the plaque components. The failure criteria developed for the atherosclerotic plaques is used in FE studies to serve the basis for a better comparison of all future atherosclerotic plaque models. Without the appropriate failure criteria, the plaque models remain incapable of addressing the issue of rupture-potential [11].

In this study, the author agrees with Kock et al. (2008) and Holzapfel et al. (2014) in utilizing the tensile stresses to address plaque vulnerability, because these measures are easy to compare with the uniaxial/biaxial tension test data. From the experimental data, the circumferential and axial true stresses are obtained, as well as the circumferential and axial stretches. These data can be compared with the Cauchy stresses and Hencky strains, which are as native FEM results from the post-processing stage of computational analyses.

5.3.5 Rupture Criterion

The plaque rupture represents the failure due to the morphological/material and geometrical changes within the plaque at which higher stress levels occur. This is an important aspect of understanding and characterizing the plaque vulnerability [11]. Currently, the most used threshold value within FE studies is 300 kPa (0.3 MPa) which goes back to a comparative FE stress analysis of the specific coronary artery lesions that causes the lethal myocardial infarction (at a pressure of 110 mmHg) and controls the stable lesions [44]. However, it should not be assumed that all plaques rupture at this stress level. Hence, a more location-specific threshold value is required rather than a one-for-all value. In addition, the morphological and the mechanical features of the different vasculatures are not the same. Therefore, individual material and structural properties are needed [46][47][55].

The location-specific threshold value for the diseased carotid artery is presented by Teng et al. [8]. They determined that the rupture (engineering) stresses of the human carotid artery sections containing type II and III lesions (AHA classifications). A mean of 1996±867 and 1802±703 kPa for the adventitia in the axial and circumferential directions and corresponding mean values of 519±270 and 1230±533 kPa for the media were used for the analysis. The rupture stretches in both the axial and circumferential directions were 1.50±0.22 [48] as shown in Fig. 5-8. The mean ultimate strength of adventitia was about 280% and 50% higher than that of media in the axial and circumferential directions, respectively. The mean ultimate strength of media in the axial direction (520kPa) was considered as a reference

threshold value for the assessment schemes of the plaque vulnerability. According to Schmermund and Erbel [49], type II and III lesions according to AHA classification are not potential to rupture. Therefore, this study used the result of Teng et al. to represent the arterial layer (media and adventitia) of the diseased carotid artery or the arterial tissue surrounding the plaque.

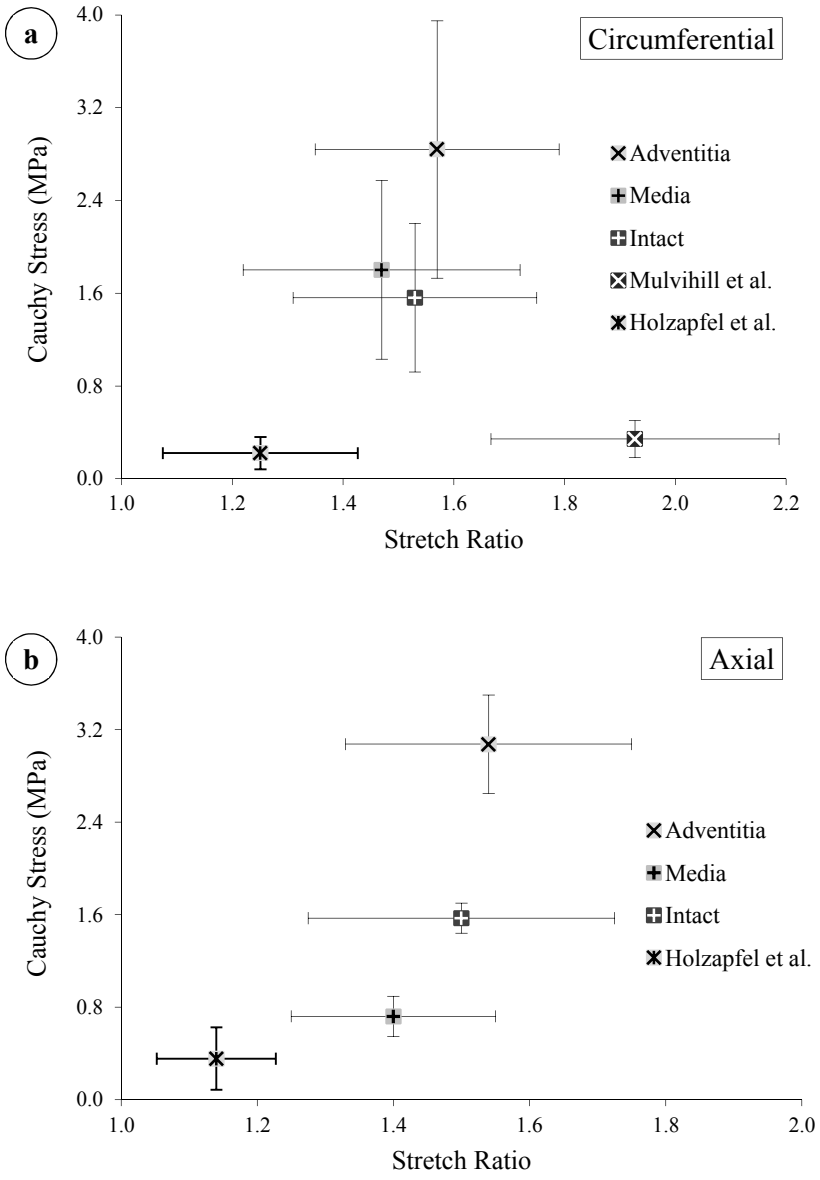

Figure 5-8: Rupture criterion for diseased carotid artery and for human carotid plaque.

Further study by Mulvihill et al. [50] provided the rupture criterion for the human carotid plaque in the circumferential direction only as shown in Fig. 5-8a. They found that the average rupture stress and average rupture stretch values for the lipid-dominant plaques is 0.342 ± 0.16 MPa and 1.927 ± 0.26 stretches, respectively. To the best knowledge of the author, there is no rupture stresses and stretches criteria for the human carotid plaque in the axial direction. Therefore, the study of Holzapfel et al. [51] regarding with anisotropic mechanical properties of the human atherosclerotic plaque in the stenotic

iliac arteries will be adopted in this work. They investigated the mechanical response of the fibrous plaque caps. They found that the average rupture stress and average rupture stretch values for fibrous plaque caps in the circumferential direction is 0.221 ± 0.14 MPa and 1.251 ± 0.176 stretches, respectively, and that in the axial direction is 0.354 ± 0.27 MPa and 1.14 ± 0.0875 stretches, respectively. The rupture criteria for the human atherosclerotic plaque provided by Mulvihill et al. and Holzapfel et al., which is included in Fig. 5-8, will be adopted in this study.

Addressing on the different rupture stretch criteria between Mulvihill et al. and Holzapfel et al., the rupture stretch criterion provided by Holzapfel et al. has much lower stretch at rupture (1.251 ± 0.176 stretch) comparing with that by Mulvihill et al. (1.927 ± 0.26 stretch). This is caused by the difference of the atherosclerotic plaque type, in which Holzapfel et al. used calcified-dominant plaque [50].

In order to analyze the plaque and the intimal layer rupture tendency, the normal stress in the circumferential and axial direction from each simulation is compared. The simulation results used in the analysis are the normal Cauchy (true) stresses and Hencky (logarithmic) strains in both circumferential and axial direction after balloon removal, namely residual Cauchy stresses and stretches. The author used the residual stresses rather than the maximum/peak stresses within arterial layer (induced stresses after balloon removal rather than that before balloon removal). There are three underlying reasons behind this choice. First reason is that the residual stresses represent resultant stress values of not only the external pressure but combinations of external loading, geometrical configuration, and intra-plaque residual stresses. This approach has been confirmed by Cilla et al. through a 3D parametric study [19]. A number of studies still used the maximum principal stresses in order to analyze plaque rupture though it overestimates the stresses in the atherosclerotic plaque [11]. Second reason is that the pressure loading used to dilate the stents occurs in a short time (a second or less) and is only once inflation process. Last reason is that vessel wall tissue consists of many smooth muscle cells (SMCs) in its medial layer, which is capable to stretch under supra physiological loading. The trauma of endothelial cells (ECs) is mainly caused by the surface profile of stent rather than the peak of pressure loading.

5.4 RESULTS AND DISCUSSION

Figure 5-9 shows comparative chart between the simulation results and the rupture stress/stretch data, provided by Teng et al., Mulvihill et al. and Holzapfel et al., in the circumferential direction. Figure 5-10 shows those comparisons in the axial direction with the rupture stress/stretch data provided by Teng et al. and Holzapfel et al. The adventitia and media in Figs. 5-9 and 5-10 refer to the diseased adventitia and diseased media surrounding the plaque, while the intact refers to the free-lesion area of the arterial tissue that opposite the plaque.

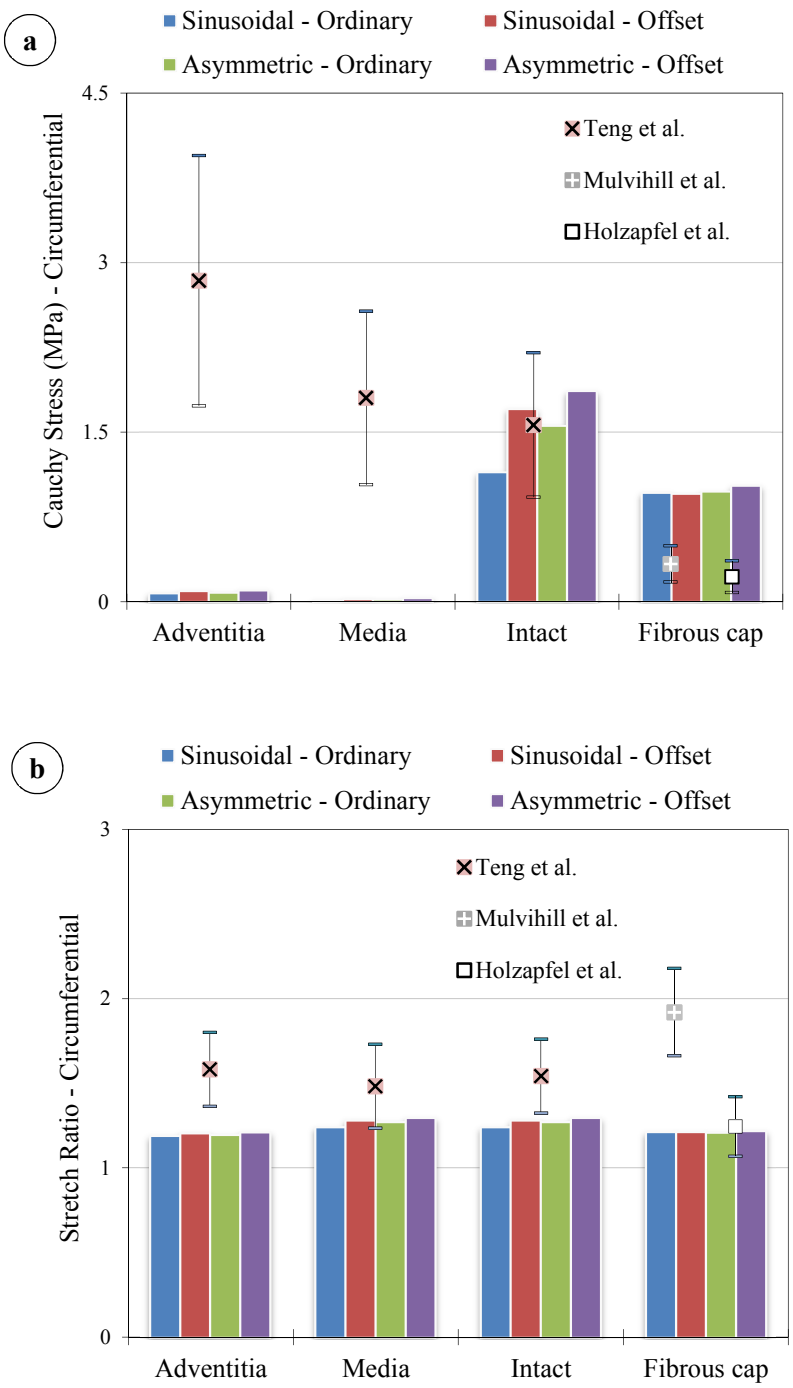

Figure 5-9: Comparative chart in circumferential direction: (a) Cauchy stresses, (b) Stretches ratio.

It can be seen form Fig. 5-9*a* that there is no significant effect of the combination of expansion, except for the residual Cauchy stress generated by the stents within the intact layer. It is indicated that Asymmetric stent – the offset balloon combination produced the highest residual Cauchy stress within the free-lesion area in front of the plaque. While Sinusoidal stent – the ordinary cylindrical balloon combination produced the smallest one. Furthermore, the residual Cauchy stress within the diseased adventitia and media was quite small to cause the edge dissection/fissure of arterial layer. This result affirmed the FE studies of Li et al. [12][13] that the higher stress concentration area was taken place in

the vicinity of the plaque shoulder.

In the contrary, the carotid plaque and arterial tissue around the free-lesion area stored a large amount of the residual stress. The high residual stress stored in the arterial tissue of the free-lesion area was still around the critical limit of rupture. However, this phenomenon is an initial symptom that causes the inflammation of the free-lesion area of vessel wall. Moreover, the residual stress within the carotid plaque should get more attention because of both rupture criterions; even the carotid plaque quantitatively stored lower amount of the residual Cauchy stress.

Comparative chart for the stretches ratio in the circumferential direction is shown in Fig. 5-9*b*. It is clearly indicated that the stretch ratio in the circumferential direction tents to be similar for each expansion combination and its values remain under all rupture criteria, except for minimum limit of the rupture stretches data of Holzapfel et al. It means all combination model of expansion used in the simulation can be applied in the treatment. It is noted that the stretches ratio of the plaque was slightly lower than that of the other arterial tissue. It is interesting phenomenon due to the direction of the balloon inflation is directly onto the plaque surface. However, because its stiffness is higher than the arterial tissue of the free-lesion area, lower stretch value becomes a result.

Figure 5-10 shows the relationship between the residual Cauchy stresses and stretches ratio in the axial direction for each expansion combination. In the case of the Cauchy stresses, the tendency is equal to the simulation results in the circumferential direction, though the intact has lower residual stress than the carotid plaque. Nevertheless, the Cauchy stress stored within the carotid plaque both in the circumferential and axial direction has comparable values. It is caused by the thickness of fibrous plaque cap that is thinner than that of the intact. In the case of the stretch ratio, the simulation result in both directions represented similar tendency for each layer though the stretch ratio in the axial direction was slight lower than that in the circumferential direction.

It is important to note that both the diseased adventitia and the diseased media store high residual stress within both in the circumferential and axial direction, which leads to a rupture. The rupture occurs in the fibrous plaque cap rather in the intact. The author supposed that the large size of the lipid core and the quite thin fibrous cap are the major causes of the high residual stress stored in the plaque. Considering the thickness of the fibrous cap used in the simulation model, it is classified as *in vivo* critical fibrous cap thickness as shown by Yonetsu et al. [28]. The thinner fibrous cap thickness leads to the higher residual stress store in it. Further simulation model with the thicker fibrous cap may be useful to identify the real effect of the asymmetric expansion. All simulation models generated almost similar amount of residual stress within it except for the high residual stress stored in fibrous cap, which is equal to 200% of plaque rupture threshold (0.342 ± 0.16 MPa). This condition may more severe comparing with the *in vivo* rupture stress values predicted by Maldonado et al. [52], which suggests that

non-calcified tissue ruptures at 0.107 MPa. Moreover, the studies of Cheng et al. [53] and Huang et al. [54] confirmed that the lipid component of the plaque specimens is a main contributor to the rupture of plaque and a key factor in plaque vulnerability.

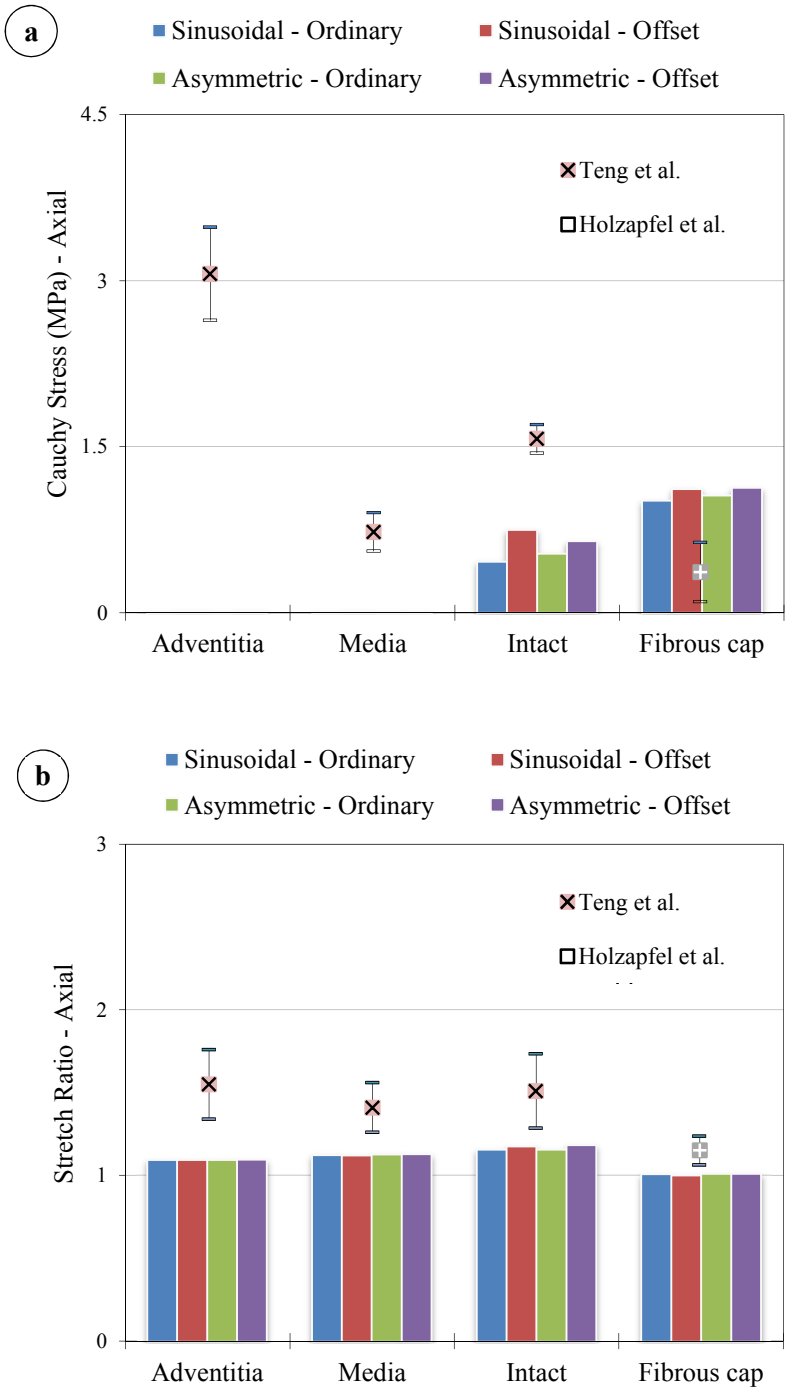

Figure 5-10: Comparative chart in axial direction: (a). Cauchy stresses, (b) Stretches ratio.

5.5 CONCLUSIONS

The finite element analysis on the development of the asymmetric stent to treat the eccentric plaque of

the human carotid artery considering the plaque vulnerability and the arterial wall rupture was carried out in this chapter. Four combination of expansion consist of Asymmetric stent, Sinusoidal stent, offset balloon, and ordinary cylindrical balloon were analyzed. The following conclusions were obtained:

i. Four types expansion combination did not cause the major influence to produce the residual Cauchy stress and stretch within the diseased adventitia, the diseased media, and the fibrous plaque cap. A little influence of the residual Cauchy stress was observed on the intact of the arterial wall opposite the plaque in both directions. In this case, the combination of Asymmetric stent – offset balloon generates the highest residual Cauchy stress in the circumferential direction, while the combination of in the Sinusoidal stent – cylindrical balloon generates the highest one in the axial direction.

ii. The residual Cauchy stresses within the plaque in both directions are the most critical location because the observed high residual stress always exceeds all rupture criteria. However, the stretch of the plaque remains under safety region. This result suggests that the eccentric plaque obstruction with the large lipid core and the thin fibrous cap is a reason of the rupture.

iii. For the plaque geometry studied here (the large lipid core, thin fibrous cap, and eccentric plaque obstruction), the residual Cauchy stresses in both directions are comparable. The reversed result was observed on the intact of the arterial wall opposite the plaque.

5.6 STUDY LIMITATION AND FUTURE WORKS

This study adopted the isotropic material model in the analyses. Many researchers suggest to consider the anisotropic material model in the FE studies on the atherosclerotic diseases [31][46][51][55]. Therefore, an advanced study adopted the anisotropic material model in this case should be performed in the future. According to Schmidt et al., a simple adjustment can be made to compare the simulation results between the isotropic and anisotropic material model, so one could interpret the result of the anisotropic model from the isotropic model. Nevertheless, the specific-location comparative data is still necessity, i.e. for the human carotid artery.

Considering the direction of balloon expansion that directly opposes the plaque, another direction of balloon expansion, i.e. against the intact of arterial wall, becomes a further investigation because the rupture criterion of the intact of arterial wall is higher than the plaque. Moreover, the calcification of vulnerable plaque that harden fibrous cap layer, is ignored in this study. Finally, the position of the critical plaque vulnerability and the arterial wall rupture are correlated with the changes in stent surface roughness because it is trigger to a larger problem as suggested by the author [56].

References

[1] Ambrose et al., 1985. Angiographic morphology and the pathogenesis of unstable angina pectoris. Journal of American College of Cardiology 5, 609–616.

[2] Richardson, P.D. et al., 1989. Influence of plaque configuration and stress distribution on fissuring of coronary atherosclerotic plaques. Archives of Pathology & Laboratory Medicine 334, 941–944.

[3] Waller, B.F., 1989. The eccentric coronary atherosclerotic plaque: morphologic observations and clinical relevance. Clinical Cardiology 12, 14–20.

[4] Yamagishi, M. et al., 2000. Morphology of vulnerable coronary plaque: Insights from follow-up of patients examined by intravascular ultrasound before an acute coronary syndrome. Journal of the American College of Cardiology 35, 106–111.

[5] Iannaccone, F. et al., 2014. The influence of vascular anatomy on carotid artery stenting: A parametric study for damage assessment. Journal of Biomechanics 47, 890–898.

[6] Carr, S. et al., 1996. Atherosclerotic plaque rupture in symptomatic carotid artery stenosis. Journal of Vascular Surgery 23, 755–766.

[7] Carr, S. et al., 1997. Activated inflammatory cells are associated with plaque rupture in carotid artery stenosis. Surgery 122, 754–757.

[8] Teng, Z. et al., 2014. Material properties of components in human carotid atherosclerotic plaques: A uniaxial extension study, Acta Biomaterialia 10, 5055–5063.

[9] Karimi, A. et al., 2013. Measurement of the uniaxial mechanical properties of healthy and atherosclerotic human coronary arteries. Journal of Materials Science and Engineering C 33, 2550–2554.

[10] Akyildiz, A.C. et al., 2014. Mechanical properties of human atherosclerotic intima tissue. Journal of Biomechanics 47, 773–783.

[11] Holzapfel, G.A. et al., 2014. Computational approaches for analyzing the mechanics of atherosclerotic plaques: A review. Journal of Biomechanics 47, 859–869.

[12] Li, Z.Y. et al., 2006. Stress analysis of carotid plaque rupture based on in vivo high resolution MRI. Journal of Biomechanics 39, 2611–2622.

[13] Li, Z.Y. et al., 2008. Assessment of carotid plaque vulnerability using structural and geometrical determinants. Circulation Journal 72, 1092–1099.

[14] Kiousis, D.E. et al., 2009. A methodology to analyze changes in lipid core and calcification onto fibrous cap vulnerability: The human atherosclerotic carotid bifurcation as an illustratory example, Journal of Biomechanical Engineering 131, 121002.

[15] Sadat, U. et al., 2010. Finite element analysis of vulnerable atherosclerotic plaques: a comparison of mechanical stresses within carotid plaques of acute and recently symptomatic patients with carotid artery disease. Journal of Neurology, Neurosurgery & Psychiatry 81, 286–289.

[16] Auricchio, F. et al., 2011. Carotid artery stenting simulation: From patient-specific images to finite element analysis. Medical Engineering and Physics 33, 281–289.

[17] Gasser, T.C. and Holzapfel, G.A., 2007. Finite element modeling of balloon angioplasty by considering overstretch of remnant non-diseased tissues in lesions. Computational Mechanics 40, 47–60.

[18] Ohayon, J. et al., 2007. Influence of residual stress/strain on the biomechanical stability of vulnerable coronary plaques : potential impact for evaluating the risk of plaque rupture. American Journal of Physiology - Heart and Circulatory 293, 1987–1996.

[19] Cilla, M. et al., 2012. 3D computational parametric analysis of eccentric atheroma plaque: Influence of axial and circumferential residual stresses. Biomechanics and Modeling in Mechanobiology 11, 1001–1013.

[20] Karimi, A. et al., 2014. A finite element study of balloon expandable stent for plaque and arterial wall vulnerability assessment, Journal of Applied Physics 116, 044701 (1–7).

[21] Riyahi-Alam, S. et al., 2015, Preoperative in silico analysis of atherosclerotic calcification vulnerability in carotid artery stenting using Finite Element Analysis. IFMBE Proceeding 51, 881–884.

[22] Saab, M.A., 2000. Application of high-pressure balloons in the medical device industry, Medical Device & Diagnostic Industry, accessed on January 17, 2014.

[23] Ju, F. et al., 2008. On the finite element modelling of balloon-expandable stents, Journal of Mechanical Behavior of Biomedical Materials 1, 86–95.

[24] Libby, P., 1995. Molecular Bases of the Acute Coronary Syndromes. Circulation 91, 2844–2850.

[25] Bentzon, J.F. et al., 2014. Mechanisms of plaque formation and rupture. Circulation Research 114, 1852–1866.

[26] Cai, J.M. et al., 2002. Classification of human carotid atherosclerotic lesions with in vivo multi contrast magnetic resonance imaging. Circulation 106, 1368–1373.

[27] Li, Z.Y. et al., 2006. How critical is fibrous cap thickness to carotid plaque stability? A flow-plaque interaction model. Stroke. 37, 1195–1199.

[28] Yonetsu, T. et al., 2011. In vivo critical fibrous cap thickness for rupture-prone coronary plaques assessed by optical coherence tomography. European Heart Journal 32, 1251–1259.

[29] Peterson, S.J. and Okamoto, R.J., 2000. Effect of residual stress and heterogeneity on circumferential stress in the arterial wall. Journal of Biomechanical Engineering 122, 454–456.

[30] Raghavan, M.L. et al, 2004. Three-dimensional finite element analysis of residual stress in arteries. Annals of Biomedical Engineering 32, 257–263.

[31] Holzapfel, G.A. et al., 2007. Layer-specific 3D residual deformations of human aortas with non-atherosclerotic intimal thickening. Annals of Biomedical Engineering 35, 530–545.

[32] Sommer, G. et al., 2010. Biaxial mechanical properties of intact and layer-dissected human carotid arteries at physiological and supraphysiological loadings. American Journal of Physiology: Heart and Circulatory Physiology 298, 898–912.

[33] ANSYS Mechanical APDL Theory Reference. ANSYS Inc., U.S.A., pp. 134–137.

[34] ANSYS Helps 15.0. Hyperelastic material curve fitting. ANSYS Inc., U.S.A.

[35] ANSYS Helps 15.0. Coupling and constraint equations. ANSYS Inc., U.S.A.

[36] Huang, H. et al, 2001. The impact of calcification on the biomechanical stability of atherosclerotic plaques. Circulation 103, 1051–1056.

[37] Williamson, S.D. et al., 2003. On the sensitivity of wall stresses in diseased arteries to variable material properties. Journal of Biomechanical Engineering 125, 147–155.

[38] Tang, D. et al., 2005. Quantifying effects of plaque structure and material properties on stress distributions in human atherosclerotic plaques using 3D FSI models. Journal of Biomechanical Engineering 127, 1185–119.

[39] Gasser, T.C. and Holzapfel, G.A., 2007. Modeling plaque fissuring and dissection during balloon angioplasty intervention. Annals of Biomedical Engineering 35, 711–723.

[40] Kock, S.A. et al., 2008. Mechanical stresses in carotid plaques using MRI-based fluid–structure interaction models. Journal of Biomechanics 41, 1651–1658.

[41] Kaazempur-Mofrad, M.R. et al., 2003. Cyclic strain in human carotid bifurcation and its potential correlation to atherogenesis: idealized and anatomically-realistic models. Journal of Engineering Mathematics 47, 299–314.

[42] Humphrey, J.D. and Holzapfel, G.A., 2012. Mechanics, mechanobiology, and modeling of human abdominal aorta and aneurysms. Journal of Biomechanics 45, 805–814

[43] Kock, S.A. et al., 2008. Mechanical stresses in carotid plaques using MRI-based fluid–structure interaction models. Journal of Biomechanics 41, 1651–1658.

[44] Cheng, G.C. et al., 1993. Distribution of circumferential stress in ruptured and stable atherosclerotic lesions. A structural analysis with histopathological correlation. Circulation 87, 1179–1187.

[45] Herisson, F. et al., 2011. Carotid and femoral atherosclerotic plaques show different morphology. Atherosclerosis 216, 348–354.

[46] Schriefl, A.J. et al., 2012. Determination of the layer-specific distributed collagen fiber orientations in human thoracic and abdominal aortas and common iliac arteries. Journal of The Royal Society Interface 9, 1275–1286.

[47] Maher, E. et al., 2012. Site specific inelasticity of arterial tissue. Journal of Biomechanics 45, 1393–1399.

[48] Teng, Z. et al., 2009. An experimental study on the ultimate strength of the adventitia and media of human atherosclerotic carotid arteries in circumferential and axial directions. Journal of Biomechanics 42, 2535–2539.

[49] Schmermund, A. and Erbel, R., 2001. Current perspective unstable coronary plaque and its relation to coronary calcium, Circulation 104, 1682–1687.

[50] Mulvihill, J.J. et al., 2013. Mechanical, biological and structural characterization of in vitro ruptured human carotid plaque tissue. Acta Biomaterialia 9, 9027–9035.

[51] Holzapfel, G.A et al., 2004. Anisotropic mechanical properties of tissue components in human atherosclerotic plaques. Journal of Biomechanical Engineering 126, 657–665.

[52] Maldonado, N. et al., 2012. A mechanistic analysis of the role of microcalcifications in atherosclerotic plaque stability: potential implications for plaque rupture. The American Journal of Physiology - Heart and Circulatory Physiology 303, 619–628.

[53] Cheng, G.C. et al., 1993. Distribution of circumferential stress in ruptured and stable atherosclerotic lesions. A structural analysis with histopathological correlation. Circulation 87, 1179–1187.

[54] Huang, H. et al., 2001. The impact of calcification on the biomechanical stability of atherosclerotic plaques. Circulation 103, 1051–1060.

[55] Schmidt, T. et al., 2015. Influence of isotropic and anisotropic material models on the mechanical response in arterial walls as a result of supra-physiological loadings. Mechanics Research Communications 64, 29–37.

[56] Syaifudin, A., 2013. Deformation analysis of balloon-expandable stents considering its surface roughness and viscoplasticity. Master Thesis of Graduate School of Engineering, Hokkaido University.

6 GENERAL CONCLUSIONS AND OUTLOOK

6.1 General Conclusions

Stent, a tiny mesh tube that is well known to treat narrow or blocked artery due to the plaque obstruction, remains relevant to investigate after decades of the development. Researchers are still trying to solve the problems, such as in-stent restenosis, vessel wall inflammation, and plaque rupture. Prior to the stent investigation, review of literatures to map the problems surrounding the stent deployment is a non-negligible stage of the study. Numerous developments have been conducted to reveal the mechanism of the stent expansion, and the mesh structure of the stent geometry. In the case of the balloon expandable stent (BES), there is a possibility of the development related to both the material properties and the cost. Therefore, BES is the main choice of the treatment around the world. Nowadays, the development of BES should be conducted considering the results of the clinical trials and/or the experimental data. From the clinical trials, the deep injury of arterial tissue is a more potent stimulus for neointima formation than stretch. From this point of view, the author presumes that the stent developments considering the specific plaque type and the appropriate material model of the arterial tissue are effective to minimize the vascular injury.

The physical properties of the stent surface influence the effectiveness of the vascular disease treatment after stent deployment. During the expanding process, the stent subjected to the high-level deformation that alters both the microstructure and the magnitude of the surface roughness. In this paper, the structural transient dynamic analysis was performed using ANSYS R15.0 to identify the deformation after the stent is placed in a blood vessel. Two types of bare metal stents are studied: a Palmaz type and a Sinusoidal type. The relationship between the plaque length and the changes in surface roughness was investigated by utilizing three different length of plaque; plaque length longer than the stent, shorter than the stent, and the same length as the stent. In order to reduce computational time, the 3D cyclical and translational symmetry were implemented into the FE model. The material models were defined as a multilinear isotropic for the stent and hyperelastic for the balloon, plaque, and vessel wall. The correlation between the plastic deformation and the changes in surface roughness was obtained by the intermittent pure tensile test. The plastic strain obtained by the FE simulation can be used to estimate the surface roughness of the expanded stent using the relationship between the plastic deformation and the changes in the surface roughness. The study showed that the plaque size significantly influenced the changes in the surface roughness. It was also found that the stent having the same length as the plaque is preferable because of the small surface roughness after expansion.

Both the stent and balloon types are key factors in the stenting process. In the treatment of the eccentric plaque obstruction, the symmetric expansion of the stent generates non-uniform stress distribution,

which may aggravate the fibrous cap that is prone to rupture. In chapter 4, a non-symmetric structural geometry of stent is constructed to obtain a reasonable stress distribution. To derive the novel structural geometry, the Sinusoidal stent is modified by varying the struts length and width, adding bridges and varying the curvature width of struts. An end ring of stent struts was also modified to eliminate the dogboning phenomenon and to reduce the Ectropion angle. Two balloon types were used to deploy the stent, i.e. the ordinary cylindrical and the offset balloon. Analyses of the deformation characteristics, surface roughness changes, and induced stresses within intact arterial layer were subsequently examined using a structural transient dynamic analysis in ANSYS R15.0. Interaction between the stent and vessel wall was implemented considering the surface roughness changes and stress distribution analyses. The Palmaz and Sinusoidal stent were used for comparative study. This study indicated that the Asymmetric stent type has effect on reducing the central radial recoiling and the dog-boning phenomenon. As for the surface roughness changes and stresses, the Asymmetric stent results were similar to those of the Sinusoidal stent.

Mechanical characteristic assessment of the new stent design is important to improve the performance during the stenting process. Stent with good performance in geometric assessment should pass several tests in the unexpanded and expanded condition. The FEM assessment is expected to replace the actual mechanical assessment to save the cost and time of the manufacturing. In section 4, the FEM assessment is conducted using the structural nonlinear analyses in ANSYS R15.0. Four assessments are included in this study: two flexibility tests on the unexpanded condition (single-load and multi-load) and the other tests on the expanded condition (single-load and multi-load). The stent type used in the simulation is the Asymmetric stent and the Sinusoidal stent. The analysis results showed that Asymmetric stent has lower flexibility comparing with Sinusoidal stent in the unexpanded configurations. In the case of Asymmetric stent, its inflated-side is more flexible than the fixed-side.

Section 5 focused on the plaque obstruction, which mainly appears in an eccentric shape, should be treated carefully to avoid severe vascular injury. As a series of the new stent development, the rupture analysis after the stent deployment was conducted. Namely, the structural transient nonlinear analysis was constructed in ANSYS R15.0 to investigate the plaque vulnerability and arterial tissue rupture. An idealized human carotid artery and the eccentric fibroatheroma plaque type are chosen as a FEM model. The large lipid pool and the fibrous cap are accommodated in the plaque model to simulate the rupture. Arterial tissue with multilayer material parameters, including intima, media and adventitia, was modeled as the isotropic hyperelastic material. All material parameters for the arterial tissue are extracted from the experimental data using the hyperelastic curve fitting in ANSYS R15.0. Sinusoidal stent was included in the simulation to be used as a comparative tool in analyses. For the expansion mechanism, the cylindrical and the offset balloon types were incorporated to inflate the stents alternately. The simulation results show that the four expansions combination did not produce the

residual stress and stretch within the diseased adventitia, diseased media, and the fibrous plaque cap. The residual stress affected on the intact of arterial wall opposite of the plaque. The fibrous plaque cap brakes due to the critical residual stress though the stretch remains under safety region.

This study indicated the importance of choosing appropriate stent type and length in the treatment of the atherosclerotic diseases. This result also supports the idea that a specific stent type cannot be used for all atherosclerotic plaque shape.

6.2 Outlook

This investigation presents a finite element analysis of predicting the changes in surface roughness due to the different length of concentric plaque. In actual conditions, the shape of the plaque is both circumferentially and the axially eccentric, which causes the plastic strain deformation in any part of the stent surface and alter the surface roughness. In addition, the experimental data was not obtained from the actual Palmaz or Sinusoidal stent; however, it came from a test piece of tensile test specimen. There is only one directional stress acting in the tensile test specimen, i.e. the axial stress. However, in the expanding and deflating process of stent, the radial pressure loading generates three directional stresses acting in the stent, i.e. the radial, axial, and circumferential stress. Though stents have the same material properties, the elevated stress level causes the different grain boundary elongation, which ultimately affects the magnitude of the plastic strain and the changes in surface roughness comprehensively. More sophisticated expansion model should be discussed in future works.

This study adopted the isotropic material model in the analyses. Many researchers suggest considering the anisotropic material model in the FE studies on the atherosclerotic diseases. The study of the anisotropic model for the stent-arterial layer interaction was conducted firstly by Holzapfel et al. Thereafter, the necessity of the anisotropic model in the simulation of the stent-arterial layer interaction is still a debate among researchers because of its complexity in FEM application. On the other hand, though the anisotropic model of plaque or arterial layer is necessary and critical during supra-physiological loading, the results of the simulation with the isotropic model remains able to be considered as comparative study. According to Schmidt et al., a simple adjustment can be made to compare the simulation results between isotropic and anisotropic material model. The result can also interpret the result of anisotropic model from isotropic model. Nevertheless, considering the anisotropic material model in the analysis of the plaque rupture or vessel wall inflammation may be a better method to observe Asymmetric stent in the future.

Considering direction of the balloon expansion that directly opposes the plaque, another direction of the balloon expansion, i.e. against the intact of the arterial wall becomes a further investigation, because the rupture criterion of the intact of the arterial wall is higher than the plaque. Moreover, the

calcification of vulnerable plaque that harden fibrous cap layer is ignored in this study. Finally, the position of critical plaque vulnerability and arterial wall rupture should be correlated with the changes in the stent surface roughness because it could be trigger to a larger problem.